1989

Interpretation of Solid State Deuterium NMR Spectroscopic Parameters.

Kermin Guo
Louisiana State University and Agricultural & Mechanical College

Order Number 9002144

Interpretation of solid-state deuterium NMR spectroscopic parameters

Guo, Kermin, Ph.D.

The Louisiana State University and Agricultural and Mechanical Col., 1989

U·M·I
300 N. Zeeb Rd.
Ann Arbor, MI 48106

INTERPRETATION OF SOLID-STATE DEUTERIUM NMR SPECTROSCOPIC PARAMETERS

A Dissertation

Submitted to the Graduate Faculty of the

Louisiana State University and

Agricultural and Mechanical College

in partial fulfillment of the

requirements for the degree of

Doctor of Philosophy

in

The Department of Chemistry

by

Kermin Guo

B.S., Fu-Jen Catholic University, Taipei, Taiwan, 1979

M.S., Cleveland State University, Ohio, 1985

May 1989

Acknowledgements

First, I would like to thank Professor Leslie G. Butler for his enlightening guidance and support in my research and his direction on all the aspects in the solid-state NMR. I especially want to thank Margo Jackisch, Maria Altbach and William Jarrett for their friendships and many enthusiastic suggestions. I would also like to thank Professor Neil Kestner for helpful advice and criticism in using GAUSSIAN 82 molecular orbital calculation program, Professor Steven Watkins for allowing us to use the microVax computer and its peripheral facilities, Professor Paul Russo for the assistance with the CONTIN data fitting program. I want to thank Professor John L. Ragle at the University of Massachusetts for providing us the spectral simulation program. In addition, I like to thank Bob Zinn for his generous assistance in using the TSO on IBM-3084/3900 mainframe, Marcus Nauman for his assistance with NMR spectroscopy, Jane Metcalf for the data transfer over Ethernet cluster and the C programming language.

The financial support from the National Science Fundation, the Petroleum Research Fund as administered by the American Chemical Society, the LSU Center for Energy Studies, and the Louisiana Board of Regents through the Louisiana Educational Quality Support Fund are gratefully acknowledged. I also wish to thank the financial assistance from the Charles E. Coates Memorial Fund in preparing this dissertation.

Finally, I would like to extend my deepest appreciation to my wife and my parents for their love, support, and encouragement.

To Yenping, my dearest wife – who provided me all the love and strength, was always proud of me, always treated my *follies* with humour and patience – I dedicate this volume.

Table of Contents

List of Figures

List of Tables

Abstract

Solid-state deuterium NMR spectroscopic parameters including the deuterium quadrupole coupling constant and asymmetry parameter are interpreted in both theoretical and experimental aspects. Ab initio molecular orbital calculations were performed on the alkali metal hydrides, toluene, thymine, acetic acid dimer, and phenylacetic acid molecules with different conformations. In the alkali metal hydrides, the electric field gradient at the hydrogen atom site was calculated in three model systems: terminal metal hydride, bridging metal hydride, and dihydrogen adducts. The effect of metal hydride geometry on the deuterium quadrupole coupling constant was examined. The results can be used in the assignment and interpretation of solid-state deuterium NMR spectra of metal-hydrogen bonds in organometallic complexes. In the carbon-bound deuterium system, the orientation of the C–^{2}H bond vector in different conformers was varied with respect to either (or both, in the case of phenylacetic acid molecule) the phenyl ring or the carboxylic acid group. The correlation between the calculated NMR parameters and the conformational change was found, and fitted into Karplus-type equations. The deuterium quadrupole coupling constant obtained from ADLF spectroscopy and the torsion angles from X-ray structural data for substituted arylacetic acids were used to obtain the coefficient values in the Karplus–type equations. The application of the Karplus-type equation to measure the solid-state local structural effect in substituted arylacetic acids is discussed in detail.

CHAPTER ONE

General Introduction

Introduction

The primary objectives of the research presented in this dissertation are to obtain a detailed understanding of the solid-state nuclear magnetic resonance (NMR) parameters, including the quadrupole coupling constant and the asymmetry parameter, for deuterium nuclei in a variety of bonding situations in metal hydrides and to develop and apply the solid-state NMR spectroscopic method to the determination of the static structures of a series of substituted acetic acid compounds in the crystalline state.

Metal-hydrogen bonds are of great interest in organometallic chemistry because their structures can be quite varied.[1] A large range of geometric variability usually appears in homogeneous transition metal complexes[2] and on catalytic surfaces[3] with different bonding modes, ranging from terminal to bridging and sometimes dihydrogen-addition.[4]

We have found that solid-state deuterium NMR spectroscopy is a valuable technique for the study of both structural and electronic features of metal-hydride bonds . The deuterium quadrupole coupling constant arises from the interaction between the deuteron nuclear electric quadrupole moment and the electric field gradient around the nuclear site. Since the electric field gradient is a sensitive function of molecular charge distribution in the close vicinity of the deuterium nucleus,[5] a correlation exists between the bonding geometry and the electric field gradient. Through the electric field gradient calculated from an ab initio molecular orbital program for different model systems, the results of solid-state deuterium NMR experiments can be better interpreted.

For a static aliphatic structure, where the electric field gradient tensor usually is axially symmetric for a deuteron bound to carbon and with the major axis of the tensor aligned along the C–^{2}H bond, the deuterium quadrupole coupling constant has a typical non-motionally averaged value of 173 kHz.[6] Any reduction in the apparent quadrupole coupling constant observed in the high-field deuterium solid-state powder NMR experiments had been presumed to be caused by the reorientation of C–^{2}H bonds with

respect to the applied magnetic field due to molecular motion.[7] However, Hiyama *et al.* noted that the solid-state deuterium powder pattern of thymine–*methyl*–d_3 has an unusual asymmetry that can be traced to the exocyclic oxygen atom adjacent to the rapidly–rotating methyl group.[8] This discovery showed that static structural effects are additive to dynamical averaging. As a result, this work led to a further study in our group of a series of substituted acetic acids. We found two distinct deuterium sites with different static quadrupole coupling constants at the deuterons of the methylene group in several substituted acetic acids; molecular orbital calculations for an acetic acid dimer also revealed that the deuterium quadrupole coupling constant and asymmetry parameter depend on the ^2H–C_{alpha}–C_{acid}–OH torsion angle.[9] Inequivalent sites in C^2H_2 units have also been observed in α-glycine,[10,11] γ-glycine,[11] and succinic acid.[12]

The adiabatic demagnetization in the laboratory frame (ADLF) method has proven to be a useful technique in determining the static quadrupole coupling constant and asymmetry parameter at 77 K. Further development of this technique should yield an important tool in the study of molecular motion and structural elucidation for bulk and surface analysis.

1.1 Quadrupolar Interaction

For all nuclei with a nuclear spin quantum number greater than 1/2, there exists a nuclear electric quadrupole moment, eQ, due to the asymmetric distribution of nuclear charge. In the absence of an external magnetic field, the degeneracy of the nuclear spin states in a quadrupolar nucleus is lifted by the presence of the quadrupolar interaction. The nuclear quadrupolar interaction is defined as the interaction of the nuclear electric quadrupole moment with the electric field gradient, $\partial^2V/\partial r^2$. The classical electrostatic interaction energy between a nucleus with nuclear charge density distribution ρ(r), in cgs unit of esu/cm^3, and an electric potential V(r), in esu/cm, from electrons around the nucleus can be expressed as[13,15]

$$E_e = \int \rho(r)V(r)\, d\tau. \qquad (1.1)$$

If we take the nuclear center of mass as the origin, the potential V(r) may be expanded in a Taylor series in any arbitrarily oriented Cartesian coordinate system,

$$V(r) = V(0) + \sum_{\alpha=1}^{3} X_\alpha \left[\frac{\partial V}{\partial X_\alpha}\right]_{r=0} + \frac{1}{2!}\sum_{\alpha,\beta=1}^{3} X_\alpha X_\beta \left[\frac{\partial^2 V}{\partial X_\alpha \partial X_\beta}\right]_{r=0} + \ldots., (1.2)$$

where X_α, X_β are over the coordinates of x, y, and z axes.

The expansion of the electrostatic energy is

$$\begin{aligned} E_e &= V(0)\int \rho d\tau + \sum_{\alpha=1}^{3} \left[\frac{\partial V}{\partial X_\alpha}\right]_{r=0}\int X_\alpha \rho d\tau + \frac{1}{2!}\sum_{\alpha,\beta=1}^{3} \left[\frac{\partial^2 V}{\partial X_\alpha \partial X_\beta}\right]_{r=0}\int X_\alpha X_\beta \rho d\tau + \ldots \\ &= V(0)\int \rho d\tau + \sum_{\alpha=1}^{3} V_\alpha \int X_\alpha \rho d\tau + \frac{1}{2!}\sum_{\alpha,\beta=1}^{3} V_{\alpha\beta}\int X_\alpha X_\beta \rho d\tau + \ldots, (1.3) \end{aligned}$$

where $V_\alpha = \partial V/\partial X_\alpha$ and $V_{\alpha\beta} = \partial^2 V/\partial X_\alpha \partial X_\beta$. The first term is the Coulomb electrostatic energy due to a nucleus with point charge. The second term involves the nuclear electric dipole moment interacting with the electric field, V_α, at the nuclear site. Provided that a definite parity exists in all nuclear states, then nuclei cannot have electric dipole moments because of the time reversal symmetry requirement for a nuclear wavefunctions.[14] Even if the nuclear electric dipole moment did exist, their effect would not be observable because, at a nuclear site, the averaged electric field is usually close to zero; any electric field would exert a force determined by the product of the nuclear charge and the electric field to accelerate the nucleus to a region of zero electric field.

The third term is the nuclear electrical quadrupolar interaction energy term, E_e^Q. We

introduce a quantity $Q_{\alpha\beta}$, defined as

$$Q_{\alpha\beta} = \int \left(3X_\alpha X_\beta - \delta_{\alpha\beta} r^2\right)\rho(r) d\tau, \tag{1.4}$$

where the Kronecker function is defined as $\delta_{\alpha\beta}=1$ for $\alpha=\beta$ and vanishes otherwise. The quadrupolar interaction energy term then becomes

$$E_e^Q = \frac{1}{6}\sum_{\alpha\beta}^{3}\left[V_{\alpha\beta}Q_{\alpha\beta} + V_{\alpha\beta}\delta_{\alpha\beta}\int r^2\rho d\tau\right]. \tag{1.5}$$

The most important feature in equation 1.5 is that both $V_{\alpha\beta}$ and $Q_{\alpha\beta}$ are quantities that can be described by a symmetric three dimensional covariant tensor of second rank. If we choose an appropriate coordinate system, all the above tensors may be converted to diagonal form. The electric field gradient tensor, $V_{\alpha\beta}$, represented in the principal axis system has only the three diagonal components, V_{zz}, V_{yy}, and V_{xx}, where all of the off-diagonal terms vanish. In addition, since it is assumed that electrons penetrating into the nucleus can be ignored, V will satisfy Laplace's equation $\nabla^2 V = 0$. This makes the electric field gradient a traceless tensor with $V_{xx} + V_{yy} + V_{zz} = 0$. Thus all of the terms in the second half of equation 1.5 vanish, leaving the quadrupolar interaction energy term as

$$E_e^Q = \frac{1}{6}\sum_{\alpha\beta}^{3} V_{\alpha\beta}Q_{\alpha\beta} \tag{1.6}$$

For a nucleus located at a site with at least cubic symmetry, $V_{xx} = V_{yy} = V_{zz}=0$ and thus the value of E_e^Q is zero. An example where the quadrupolar interaction energy term is zero is a deuterium nucleus in solid sodium hydride which has a face-centered cubic crystal

structure. The condition of cubic symmetry is also effectively satisfied in an isotropically tumbling molecule with a correlation time short compared to the inverse of the quadrupolar interaction energy term (expressed in frequency units), as in the case of the nitrogen-14 nucleus in the ammonium ion in solution.

The charges in the nucleus precess rapidly about the nuclear spin axis which gives a cylindrical symmetry to the nuclear charge distribution function; thus, the time–averaged nuclear electric quadrupole moment tensor is also symmetric and traceless. Taking z as the symmetry axis, then we have $Q_{xx} = Q_{yy} = (-1/2)Q_{zz}$. In order to describe the energy change upon nuclear reorientation with respect to an electric field gradient external to the nucleus, the scalar nuclear electric quadrupole moment, eQ, can be defined as the difference between the expectation values of the charge distribution for orientations parallel and transverse to the z axis. Classically the nuclear electric quadrupole moment can be expressed as

$$eQ = \int 2(z^2 - x^2)\rho(r)d\tau = \int (2z^2 - x^2 - y^2)\rho(r)d\tau = \int (3z^2 - r^2)\rho(r)d\tau . \qquad (1.7)$$

After replacing the classical $\rho(r)$ in equation 1.7 by the quantum mechanical operator and applying it to equation 1.6, we have the quantum expression for the quadrupole Hamiltonian[15]

$$H_Q = \frac{eQ}{6I(2I-1)} \sum_{\alpha\beta}^{3} V_{\alpha\beta} \left[\frac{3}{2} \left(\hat{I}_\alpha \hat{I}_\beta + \hat{I}_\beta \hat{I}_\alpha \right) - \delta_{\alpha\beta} \hat{I}^2 \right], \qquad (1.8)$$

where I is the spin quantum number of the nuclear spin state and $\hat{I}$ is the spin angular momentum operator. Only one nuclear constant, eQ, is required here to represent the nine components of the original nuclear quadrupole tensor $Q_{\alpha\beta}$.

1.2 Description of the Electric Field Gradient Tensor Elements and Asymmetry Parameter

The electric field gradient at the nucleus, arising from the electronic and nuclear charge distribution outside the nucleus, can be described by a symmetric traceless tensor with five independent components. The number of independent components is reduced from five to two after the electric field gradient tensor is transformed to the principal axis system. By convention, two parameters, eq_{zz} and η, are used to describe the electric field gradient tensor in the principal axis system and are defined as

$$eq_{zz} = V_{zz}, \quad \eta = \frac{V_{xx} - V_{yy}}{V_{zz}} \quad (0 \le \eta \le 1), \tag{1.9}$$

with the axes labeled so that $|V_{zz}| \ge |V_{yy}| \ge |V_{xx}|$. The orientation of the principal axes of the electric field gradient tensor is determined by the eigenvectors used for the diagonalization in the laboratory frame. By convention, the orientation is defined in a right-handed coordinate system.

In the principal axis system, we can then rewrite equation 1.8 in terms of the symbols eq_{zz} and η as

$$\begin{aligned} H_Q &= \frac{eQ}{6I(2I-1)}\left[V_{xx}\left(3\hat{I}_x^2 - \hat{I}^2\right) + V_{yy}\left(3\hat{I}_y^2 - \hat{I}^2\right) + V_{zz}\left(3\hat{I}_z^2 - \hat{I}^2\right)\right] \\ &= \frac{eQ}{4I(2I-1)}\left[V_{zz}\left(3\hat{I}_z^2 - \hat{I}^2\right) + (V_{xx} - V_{yy})\left(\hat{I}_x^2 - \hat{I}_y^2\right)\right] \\ &= \frac{e^2 q_{zz} Q}{4I(2I-1)}\left[\left(3\hat{I}_z^2 - \hat{I}^2\right) + \eta\left(\hat{I}_x^2 - \hat{I}_y^2\right)\right] \\ &= \frac{e^2 q_{zz} Q}{4I(2I-1)}\left[\left(3\hat{I}_z^2 - \hat{I}^2\right) + \frac{\eta}{2}\left(\hat{I}_+^2 + \hat{I}_-^2\right)\right]. \end{aligned} \tag{1.10}$$

The magnitude of the electric field gradient is referred to as the quadrupole coupling

constant, $e^2q_{zz}Q/h$, and is usually given in frequency units. The asymmetry parameter is dimensionless, ranging in value from 0 to 1, and is used to measure the departure of the field gradient from cylindrical symmetry. If the field gradient is axially symmetric, as in the case of methane-d_1, with the symmetric environment around the bond connecting carbon to the deuterium nucleus, then $V_{xx} = V_{yy}$, and we have an asymmetry parameter value of zero.

1.3 Measurement of the Deuterium Quadrupole Coupling Constant and Asymmetry Parameter

The smallest spin quantum number that exhibits a quadrupolar interaction is I=1, as for deuterium, which gives a three-level energy system. We use the spin angular momentum matrix formalism for the I=1 system:[16]

$$\hat{I}_x = \frac{1}{2}\begin{pmatrix} 0 & \sqrt{2} & 0 \\ \sqrt{2} & 0 & \sqrt{2} \\ 0 & \sqrt{2} & 0 \end{pmatrix}, \quad \hat{I}_y = \frac{i}{2}\begin{pmatrix} 0 & -\sqrt{2} & 0 \\ \sqrt{2} & 0 & -\sqrt{2} \\ 0 & \sqrt{2} & 0 \end{pmatrix}, \quad \hat{I}_z = \begin{pmatrix} 1 & 0 & 0 \\ 0 & 0 & 0 \\ 0 & 0 & -1 \end{pmatrix}, \tag{1.11}$$

and $\hat{I}^2 = \hat{I}_x^2 + \hat{I}_y^2 + \hat{I}_z^2$; then the quadrupole Hamiltonian in the principal axis system, equation 1.10, with I = 1, has the form of

$$H_Q = \frac{e^2q_{zz}Q}{4}\begin{pmatrix} 1 & 0 & \eta \\ 0 & -2 & 0 \\ \eta & 0 & 1 \end{pmatrix}. \tag{1.12}$$

Thus a set of eigenvalues of equation 1.12 can be given for the energy levels E_m as follows (see Figure 1.1)

$$E_0 = -\frac{e^2q_{zz}Q}{2}, \quad E_{\pm 1} = \frac{e^2q_{zz}Q}{4}(1 \pm \eta). \tag{1.13}$$

If a small Zeeman perturbation from an external magnetic field, H_0, is applied along the z axis of the principal axis system, the energy levels for $E_{\pm 1}$ will be shifted while E_0 is unchanged, and the perturbed energy levels are

$$E_0 = -A, \quad E_{\pm 1} = \frac{A}{2} \pm \sqrt{\frac{1}{4}A^2\eta^2 + g_N^2\beta_N^2 H_0^2}, \tag{1.14}$$

where $A = e^2 q_{zz} Q/2$, g_N is the dimensionless Lande factor for deuterium, 0.857387, and β_N is the nuclear magneton, 5.0508×10^{-24} erg/Gauss. The dependence of the energy levels on the applied magnetic field strength is shown in Figure 1.2. At low magnetic field strengths, $|g_N\beta_N H_0| \ll |A\eta|$; expansion of the square root indicates that each energy level shift depends quadratically on the applied field, whereas for very high magnetic field strengths, the shift becomes linear in the field. In the case of an asymmetry parameter of zero and a high magnetic field applied along the z' axis (differing from the z axis by an angle of θ), the first order quadrupolar energy levels have the general form[17]

$$E_m = -\gamma_n \hbar H_0 m + \frac{e^2 q_{zz} Q}{4I(2I-1)}\left(\frac{3\cos^2\theta - 1}{2}\right)[3m^2 - I(I+1)], \tag{1.15}$$

with E_m in ergs, γ_n as the nuclear gyromagnetic ratio for deuterium, 4106.4 rad/s-Gauss, and $\hbar$ as Planck's constant, 1.0546×10^{-27} erg-s/rad.

For pure quadrupole resonance in this three-level system at zero applied magnetic field, the allowed transitions $|\Psi_i\rangle \rightarrow |\Psi_j\rangle$ are those for which $|i| - |j| = 0, \pm 1$. These transition frequencies are assigned as ν_- and ν_+, corresponding to transitions between the levels $|0\rangle \rightarrow |-1\rangle$ and $|0\rangle \rightarrow |+1\rangle$, and ν_0 for $|-1\rangle \rightarrow |+1\rangle$, and are given in Hertz as

$$\nu_\pm = \frac{e^2 q_{zz} Q}{4h}(3 \pm \eta), \quad \nu_0 = (\nu_+ - \nu_-) = \frac{e^2 q_{zz} Q}{2h}\eta. \tag{1.16}$$

Since the electric field gradient tensor is traceless, the quadrupolar interaction does not change the center of gravity of the spin system. Thus, only two of the three allowed transitions are needed to completely describe these energy states and the corresponding electric field gradient tensor elements. Experimentally, we measure the ν_- and ν_+ transitions and report the deuterium quadrupole coupling constant and asymmetry parameter according to the equations:

$$\frac{e^2 q_{zz} Q}{h} = \frac{2}{3}(\nu_+ + \nu_-), \quad \eta = \frac{2h}{e^2 q_{zz} Q}(\nu_+ - \nu_-). \tag{1.17}$$

For the deuterium dipolar coupled system with two spin sites close to each other, it is possible to detect the double transition quadrupole resonance in which a single radio-frequency photon is absorbed with the simultaneous transition of two dipolar coupled deuterons.[5,18] Interaction between the dipolar-coupled deuterium spin pairs results in a complicated spectrum which is commonly observed in hydrates,[19] amines,[19,20] and in intermolecular hydrogen bonded systems.[21] Such double transition quadrupole resonance is a powerful aid in the assignment of particular spectral lines to nuclei in particular crystalline sites.[19b]

1.4 Calculation of Electric Field Gradients

At the nuclear site, the potential V(r) arises from the surrounding charges of both nuclei and electrons. For a unit point charge e that is located at a point (x,y,z) from the origin will produce an electric field gradient along the z axis at the origin,

$$V_{zz} = \frac{e(3z^2 - r^2)}{r^5} = \frac{e(3\cos^2\theta - 1)}{r^3}, \tag{1.18}$$

where $r^2 = x^2 + y^2 + z^2$. Due to the $\frac{1}{r^3}$ dependence, charges close to the origin have greatest effect on the electric field gradient. However, for an electron occupying a spherically symmetric orbital about the origin, such as an s-electron, the spatially-averaged electric field gradient contribution is zero at the origin. Hence, a p-electron will have a significant contribution to the electric field gradient at the nucleus provided that it is in an open shell. This makes deuterium a unique quadrupolar species since it has only a single 1s electron in its ground state, so that the electric field gradient at a deuterium nuclear site is mainly due to the charges (nuclear and electronic) of neighboring atoms near the deuterium. In general, the major component of an electric field gradient tensor, eq_{zz}, is a sum of nuclear and electronic contributions, expressed in cgs units of esu/cm^3 as

$$eq_{zz} = \sum_n K_n \frac{3z_n^2 - r_n^2}{r_n^5} - e\left\langle \Psi^* \middle| \sum_i \frac{3z_i^2 - r_i^2}{r_i^5} \middle| \Psi \right\rangle, \qquad (1.19)$$

where e is the absolute value of the electronic charge, 4.80325x10^{-10} esu/electron, the index n is over the other atoms in the molecule with nuclear charge K_n, and the index i is over the electrons of the molecule.[22] Only the occupied molecular orbitals contribute to the electric field gradient;[23] the absence of excited-state contributions makes the molecular orbital calculation of eq_{zz} much easier than is the case for chemical shifts and scalar coupling constants which do involve excited states.[24]

For deuterium in a simple terminal C–^{2}H bond, the orientation of eq_{zz} at a deuterium is aligned closely with the bond vector.[5,22] The value of eq_{zz} is roughly proportional to the product of C–^{2}H bond distance to the inverse third power and the nuclear charge at the carbon atom to the first power.[5] Since the vibrational force constant of a C–^{2}H bond is also correlated with the C–^{2}H bond length, the force constant can be used to estimate the electric field gradient at the deuterium site.[25] By comparing the deuterium quadrupole coupling constant for a C–^{2}H site with a reference compound and its C–^{2}H site, the

relative charge on a carbon atom can also be determined.[26]

1.5 Theory of ADLF Spectroscopy

Adiabatic demagnetization in the laboratory frame (ADLF) spectroscopy is a useful technique to measure the nuclear quadrupole coupling constant and the asymmetry parameter of quadrupolar nuclei in the presence of another sensitive nuclear spin in the nearby region.[6,27] In this method, the quadrupole transitions at zero field of the less abundant nuclei, such as deuterium, are detected by monitoring the recovered magnetization of the more sensitive or more abundant nuclei, such as protons, in high field after a field cycling process, where a level-crossing take place between these two nuclear spin states. We show the experimental cycle as a function of time together with the changes of energy levels for both proton and deuteron nuclear spin states in Figure 1.3, and describe it as follows: A sample containing both nuclei was first placed in the high field region (A) where an equilibrium magnetization of proton spin state has been established after a period on the order of T_1, the proton spin-lattice relaxation time. Then it was transported to the zero field region (B) where we applied a specific deuterium search frequency with known rf energy to the sample for a short period on a time scale of T_{1d}, the deuterium zero-field spin-lattice relaxation time. Then the sample was moved back to the high field region (C) where we used a pulse sequence to measure the proton recovered magnetization in the sample. If the time required for the sample to move in and out of zero field is short compared to T_1, there is no spin redistribution among the nuclear energy states, and it is therefore an adiabatic process. During the sample transport period a level crossing occurs between the proton and deuteron nuclear spin systems; the two spins systems exchange magnetization through thermal contact of the two nuclear energy states. When the search frequency irradiating the sample in zero field matches one of the deuterium zero-field quadrupole transition frequencies, the spin populations of the corresponding deuterium

energy levels become saturated due to the rf induced transition. As a consequence, when the second level-crossing takes place on going to high field, magnetization of the proton spin system will be transferred to the deuterium spin system, and the amount of magnetization remaining in the proton spin system is measured immediately after the sample is returned to the high field region. The field cycle process is repeated for each increment of search frequency irradiation in zero field.

A plot of the resulting spectrum for perdeuterated adamantane acquired at 77 K is shown in Figure 1.4. Two resolved peaks are centered at 129 and 130.5 kHz. A double transition frequency at 261 kHz (not shown) indicated that peak at 130.5 kHz may be assigned to the ν_+ transition of the secondary deuteron sites with an asymmetry parameter of 0.017. The transition involving tertiary deuterons is not resolved, possibly due to its low population relative to the methylene sites (12:4), but it is expected to be a single peak with asymmetry parameter of zero due to the C_3 symmetry at this deuteron site. The ν_0 transition for deuterium is usually not observable due to interference from the proton dipolar bath.[6] In addition, a small magnetic field can be applied in the zero-field region during the irradiation period so that the detected ν_+ and ν_- frequencies shifts in opposite directions (Figure 1.2). This technique can be helpful in the assignment of unresolved or overlapping transitions.[28] If two deuterons are in close proximity (about 4 Å), then it is possible to detect the double transitions due to simultaneous transitions of the two adjacent dipolar-coupled deuterons with absorption of a single rf photon.

There are certain limitation to this technique: the deuterium transitions are detectable only when the sample has a proton relaxation time T_1 and deuteron relaxation time T_{1d} greater than 1 s. A sample with rapid internal vibration or rotation, such as an organometallic complex with rapidly rotating cyclopentadienyl rings, will generally have a short T_1, on the order of milliseconds even at 77 K.[29] For this reason, a new version of the ADLF spectrometer is currently under construction in which the magnetic field is

switched within 30 ms by a high speed DC power amplifier between 0 and 0.18 Tesla (corresponding to a proton resonance frequency of 8.1 MHz).[30] With this fast-field-switching version of the ADLF spectrometer, it will be possible to analyze samples with very short spin-lattice relaxation times; hence, the instrument will be used for surface analysis in the near future.

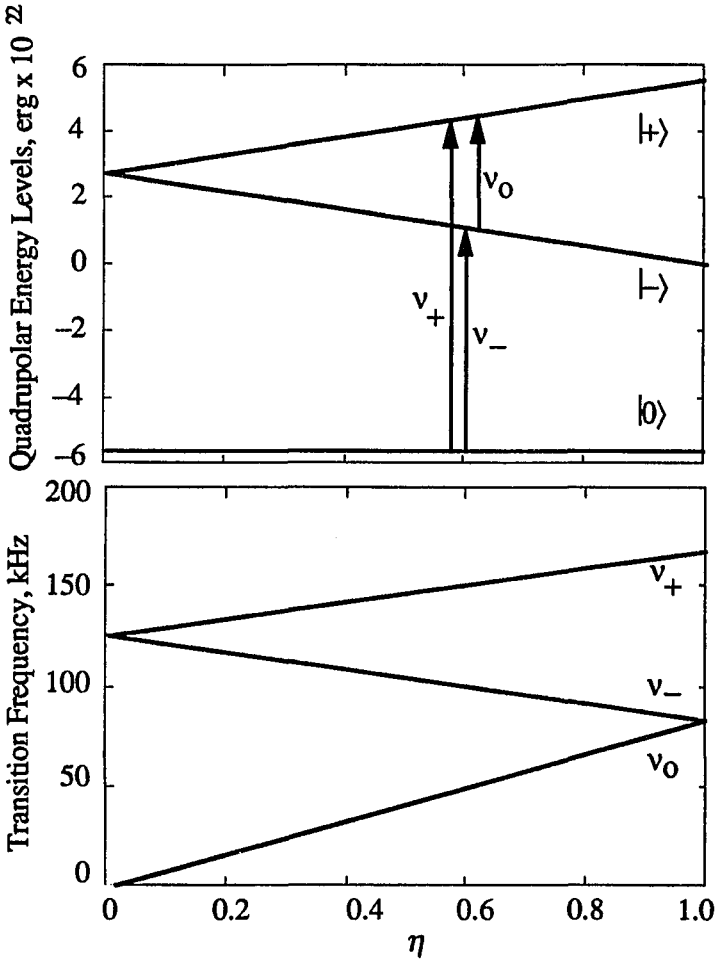

Figure 1.1 Zero-field quadrupole splitting for an I = 1 spin system as a function of the asymmetry parameter. The m = 0, ±1 nuclear energy levels and the transition frequencies are given in units of erg and kHz respectively.

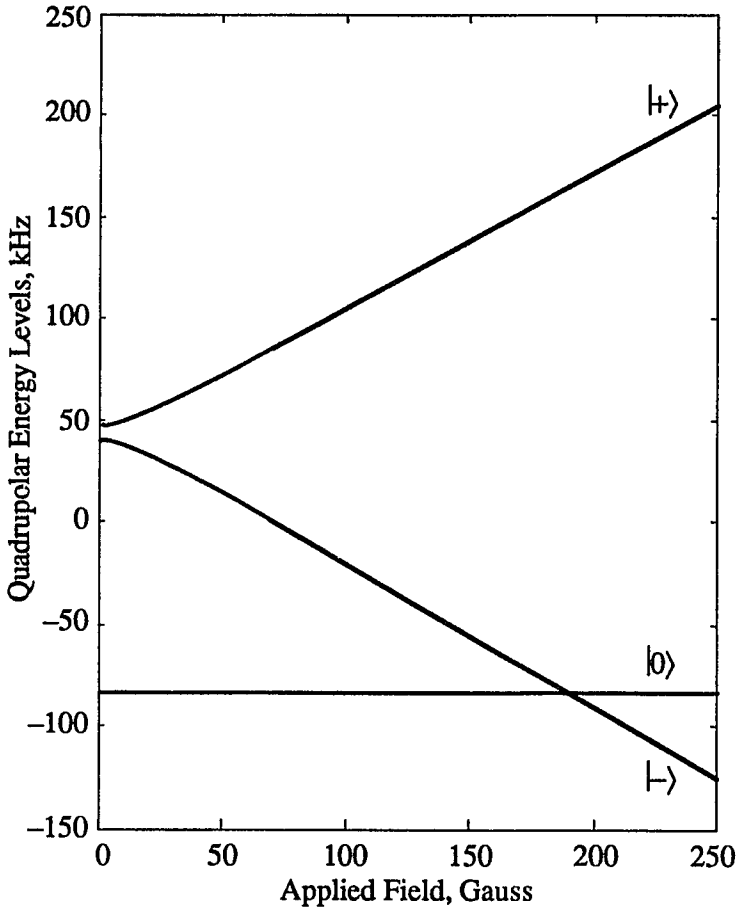

Figure 1.2 The effect of a small Zeeman perturbation on the deuterium quadrupolar energy levels with applied magnetic field parallel to the direction of principal axis z. The calculation is based on equation 1.14 with $e^2q_{zz}Q/h = 168$ kHz, $\eta = 0.1$.

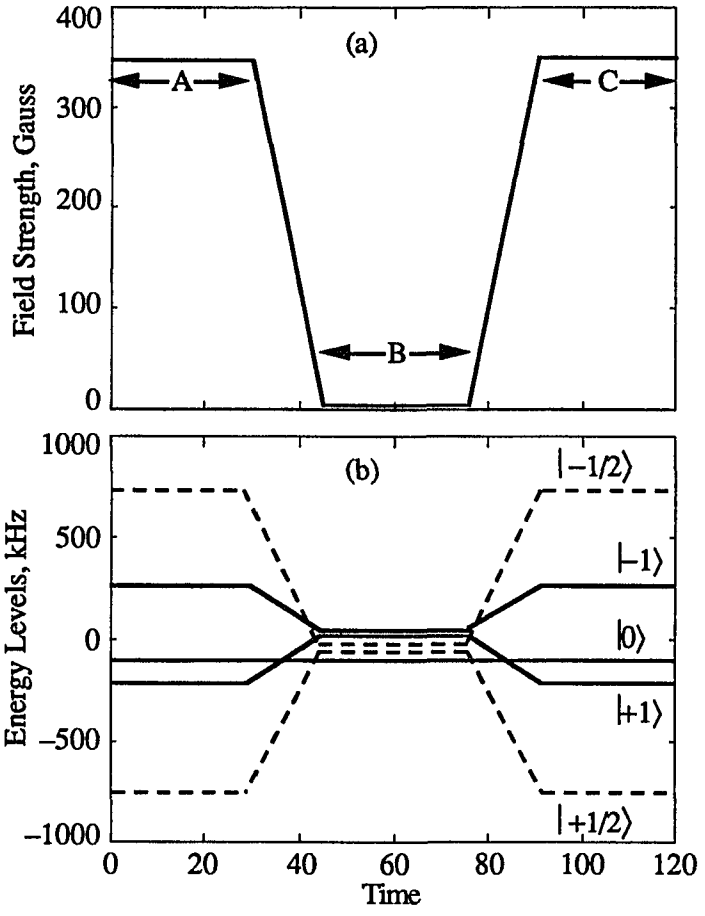

Figure 1.3 (a) ADLF field cycle, as explained in the text, and (b) the corresponding energy levels splitting for proton (- -) and deuteron (–) systems. In order to representing the detail of level splitting at zero-field, the high- and low-field strengths shown here are 352 gauss (corresponding to a resonance frequency of 1.5 MHz for proton) and 5 gauss respectively.

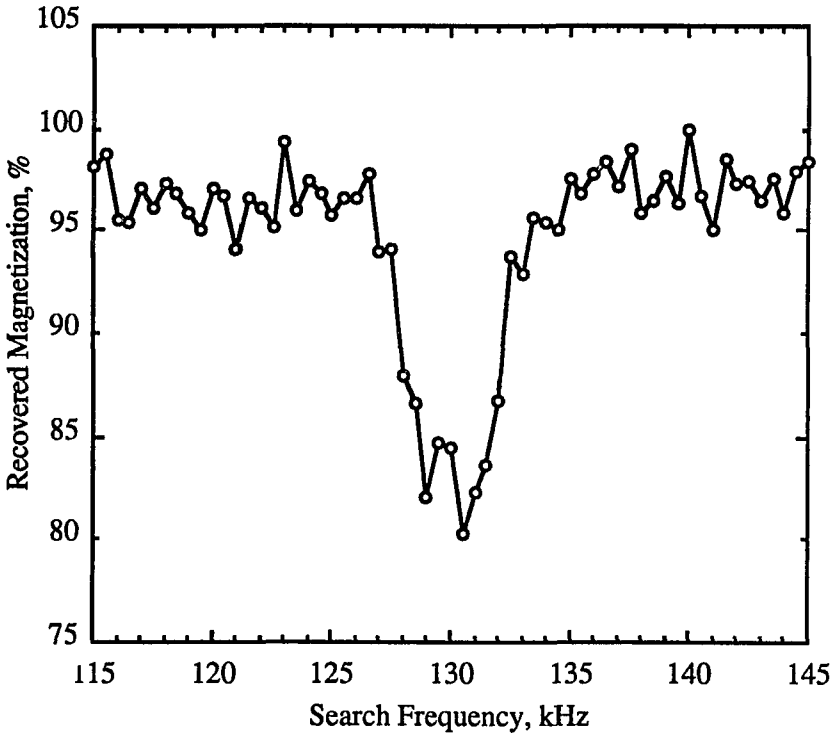

Figure 1.4 ADLF spectrum for perdeuterated adamantane (~33%; recrystallized with perprotonated adamantane in 1:2 ratio) acquired at 77 K and an applied perturbation field of 0 gauss. The high- and zero-field delays were 120 and 2 seconds, respectively. The zero-field irradiation amplitude was 26 milliGauss. The sample was prepared by Dr. Maria I. Altbach.

References

1. Bau, R. Teller, R. G.; Kirtley, S. W.; Koetzle, T. F. *Accts. Chem. Res.* **1979**, *12*, 176-183.
2. *Transition Metal Hydrides*; Muetterties, E. L., Ed.; Marcel Dekker: New York, 1971.
3. Gavin, Jr., R. M.; Reutt, J.; Muetterties, E. L. *Proc. Natl. Acad. Sci. USA*, **1981**, *78*, 3981-3985.
4. (a) Kubas, G. J.; Unkefer, C. J.; Swanson, B. I.; Fukushima, E.; *J. Am. Chem. Soc.* **1986** *108* 7000-7009.(b) Collman, J. P; Hegedus, L. S. *Principles and Applications of Organotransition Metal Chemistry*; University Science: Mill Valley, CA, 1980.
5. Huber, H. *J. Chem. Phys.* **1985**, *83*, 4591-4598.
6. Edmonds, D. T. *Phys. Reports C* **1977**, *29*, 233-290.
7. Jelinski, L. W. *Ann. Rev. Mater. Sci.* **1985**, *15*, 359-377.
8. Hiyama, Y.; Roy, S.; Guo, K.; Butler, L. G.; Torchia, D. A. *J. Am. Chem. Soc.* **1987**, *109*, 2525-2526.
9. Jackisch, M. A.; Jarrett, W. L.; Guo, K.; Fronczek, F.; Butler, L. G. *J. Am. Chem. Soc.* **1988**, *110*, 343-347.
10. Edmonds, D. T.; Summers, C. P. *Chem. Phys. Lett.* **1976**, *41*, 482-485.
11. Hartzell, C. J.; Kwiram, A. L. *J. Magn. Reson.* **1987**, *73*, 315-322.
12. Boroske, E.; Mayas, L.; Mobius, K. *J. Magn. Reson.* **1979**, *35*, 231-246.
13. (a) Lucken, E. A. C. *Nuclear Quadrupole Coupling Constants* Academic: New York, 1969. (b) Cohen, M. H.; Reif, F. *Solid State Physics* **1957**, *5*, 321-438.
14. Preston, M. A. *Physics of the Nucleus* Addison-Wesley: New York, 1962.
15. Slichter, C. P. *Principles of Magnetic Resonance* 2nd ed., Springer-Verlag: Berlin, 1978, Chapter 9.
16. Poole, C. P., Jr.; Farach, H. A. *Theory of Magnetic Resonance* 2nd ed., Wiley: New

York, 1987, Chapters 2 and 8.

17. Abragam, A. *The Principales of Nuclear Magnetism*, Oxford: London 1961, Chapter VII. p 233.

18. Hadipour, N.; Ragle, J. L. *Z. Naturforsch. A: Phys., Phys. Chem., Kosmophys.* **1985**, *40A*, 355-360.

19. (a) Edmonds, D. T.; Hunt, M. J.; Mackay, A. L. *J. Magn. Reson.* **1975**, *20*, 505–514. (b) Edmonds, D. T.; White, A. A. L. *J. Magn. Reson.* **1978**, *31*, 149–159.

20. (a) D. T. Edmonds, M. J. Hunt, and A. L. Mackay, *J. Magn. Reson.* **1973**, *11*, 77–82. (b) d'Avignon, D. A.; Brown, T. L. *J. Phys. Chem.* **1981**, *85*, 4073-4079.

21. Day, R. O.; Hadipour, N.; Ragle, J. L. *J. Magn. Reson.* **1984**, *57*, 369-384.

22 Snyder, L. C. *J. Chem. Phys.* **1978**, *68*, 291-294. also see Synder L. C.; Basch, H. *Molecular Wave Functions and Properties*, Wiley: New York, 1972.

23. (a) Gready, J. E. *J. Am. Chem. Soc.* **1981**, *103*, 3682-3691. (b) Townes, C. H.; Dailey, B. P. *J. Chem. Phys.* **1949**, *17*, 782-796. (c) Butler, L. G.; Brown, T. L. *J. Am. Chem. Soc.* **1981**, *103*, 6541-6549.

24. Ando, I. and Webb, G. A. *Theory of NMR Parameters* Academic: New York, 1983.

25. (a) Salem, L. *J. Chem. Phys.* **1963**, *38*, 1227-1236. (b) Merchant, S. Z.; Fung, B. M. *J. Chem. Phys.* **1969**, *50*, 2265-2267. (c) Fung, B. M.; Wei, I. Y. *J. Am. Chem. Soc.* **1970**, *92*, 1497-1501. (d) Wei, I. Y.; Fung, B. M. *J. Chem. Phys.* **1971**, *55*, 1486-1487. (e) Mokarram, M.; Ragle, J. L. *J. Chem. Phys.* **1973**, *59*, 2770-2771. (f) McDugle, W. G., Jr.; Schreiner, A. F.; Brown, T. L. *J. Am. Chem. Soc.* **1967**, *89*, 3111-3114. (g) Kukolich, S. G. *Mol. Phys.* **1975**, *29*, 249-255.

26. Altbach, M. I.; Hiyama, Y.; Gerson, D.; Butler, L. G. *J. Am. Chem. Soc.* **1987**, *109*, 5529-5531.

27. Noack, F. *Prog. NMR Spectroscopy* **1986**, *18*, 171-276.

28. Jarrett, W. L., Jr.; Guo, K.; Jackisch, M. J.; Butler, L. G. *J. Magn. Reson.* **1989**, *82*, 76-85.

29. Altbach, M. I. Ph.D. Dissertation, Louisiana State University, 1988.

30. Ader, R.; Shporer, M. *J. Magn. Reson.* **1982**, *47*, 483-489.

(to be submitted to the *Rev. of Sci. Instrum.*, May, 1989)

CHAPTER TWO

A Field-Cycling NMR Spectrometer: An Application of CAMAC Modules and the LabVIEW Programming Language.

by

Kermin Guo, William L. Jarrett, Maria I. Altbach,

Brannon C. Perilloux, David Barksdale, and Leslie G. Butler*

Contribution from the

Department of Chemistry

Louisiana State University

Baton Rouge, LA 70803

---

*To whom correspondence should be addressed.

Accurate values of the deuterium quadrupole coupling constant and asymmetry parameter can be used to infer a variety of electronic and geometrical features in powdered or amorphous materials: measuring the relative charge on carbon in a bridging methylene metal dimer,[1] determining hydrogen bond lengths,[2] measuring a ^{2}H–C–C–X torsion angle,[3] and identifying terminal and bridging metal hydride sites.[4] High-field deuterium NMR spectroscopy is used to measure the deuterium quadrupole coupling constant,[5] but difficulties with overlapping powder patterns are encountered for multiple deuterium sites.[4] Thus, zero magnetic field techniques are necessary to resolve multiple deuterium sites in polycrystalline or amorphous materials. To date, most zero field deuterium spectra have been obtained with adiabatic demagnetization in the laboratory frame (ADLF) spectroscopy with level crossing between an abundant proton spin system and the deuterium spin system.[6] Descriptions of several instruments and key components have been published over the past twenty years.[6-15] A related technique, zero field NMR spectroscopy, has been described recently.[16] The ADLF instrument described herein differs significantly from the other instruments[8,9] in that CAMAC-based hardware is used together with a Macintosh II computer running a control program written in the LabVIEW programming language. The advantages we have found with the CAMAC/Macintosh/LabVIEW combination may be of use to others constructing their own instruments.

An ADLF instrument consists of three major components: (1) a solid-state ^{1}H NMR spectrometer for measuring the ^{1}H spin magnetization; (2) a gated, automatically tuned, variable frequency rf system for selective irradiation of the zero field ^{2}H transitions; and (3) a mechanism for alternately placing the sample in regions of high and zero (or near zero) magnetic field strength. Typically, the sample is physically moved from the center of an electromagnet to a nearby region of zero or near zero magnetic field strength.

Figure 2.1 schematically shows the ADLF spectrometer. Details of the components are given in Table 2.1. The CAMAC crate contains modules for all three components of

the ADLF spectrometer: the pulse programmer and signal averagers for the solid-state ^{1}H NMR spectrometer, the sample position and zero field shim power supply controllers, and the TTL control signals for the relays used in the capacitor tuning unit of the zero field rf irradiation unit.[15] While CAMAC technology has been recommended for NMR apparatus,[17] this is one of the few applications known to us. There is one novel feature about the ^{1}H NMR unit for a homebuilt spectrometer; the digitizers are externally clocked, enabling efficient measurement of the 128 spin echo from an Ostroff-Waugh pulse sequence is used to generate 128 spin echoes. The pulse programmer is essentially a word generator with a 12-bit word coming from a 1K memory with a readout rate of 10 MHz. The address counter in the pulse programmer has one level of looping so that some long pulse sequences can be generated. One bit of the 12-bit word is used as the clock signal for the signal averagers. Thus, the echoes are selectively digitized, usually with four analog-to-digital conversions per echo per signal averager.

A very important component of the instrument is the controlling software, written in the LabVIEW programming language,[18] and run on a Macintosh II computer. A NuBus card installed in the Macintosh II provides an interface to the IEEE-488 bus;[19,20] a software driver is included in the LabVIEW programming language.[21] LabVIEW (version 1.2) is an interpretive, graphical programming language specific to the Macintosh computer family. LabVIEW is radically different from the other languages we have used: Intel 8085 machine code; DEC PDP-11/03 assembly language and FORTRAN; IBM Instruments CS9000 Pascal. Because of the unique character of the LabVIEW programming language, one of the subroutines is described herein.

Table 2.1. Major Components of the ADLF Spectrometer.

Label	Description
Magnet	Varian XL100 electromagnet; shim coils and flux stabilizer removed; 0.36 Tesla.
Freq Syn	Syntest, model SI-105, 1-32 MHz.[a]
Transceiver	Novex, Novaspec series wideband transceiver.[b]
Amp	Novex; 15 MHz, 400 W.
Preamp	Novex preamplifier.
Master Timer	Kinetic Systems model 3655, 8-channel timing pulse generator.[c]
Pulse Programmer	Custom built; 12-bit wide by 1K long 10 MHz readout word generator, programmable halt, external resume and reset.
Sample Position	CAMAC kluge card; contains OR gate and manual pushbutton.
20 MHz Signal Ave.	DSP model 2108; 8-bit digitizer with 24-bit wide by 8K long acquisition memory; internal and external clocks.[d]
Binary to DVS	Kinetic Systems model 3072-A1C; dual 24-bit TTL output registers.
Binary to Capacitors	Kinetic Systems model 3072-A1C; dual 24-bit TTL output registers.
Interface Display	Interface Standards DTM series diagnostic module.[e]
CAMAC Controller	Kinetic Systems model 3988-G3A, IEEE-488 crate controller.
Frequency Synthesizer	Hewlett-Packard model 3314A frequency, function, and waveform synthesizer; 1 mHz to 20 MHz, programmable amplitude.[f]
Amp 50W	ENI model 240L, 20 kHz to 10 MHz, 40 W.[g]
DMM	Fluke model 8840A multimeter.[h]
Current Detector	Toroidal transformer in zero-field LC circuit, output rectified and RC filtered.
Tuning Caps	Array of relay-switched capacitors, see ref 15.
Air Piston	1.5" bore by 27.5" stroke air piston, 5-way air valve for positive drive in both directions.
DVS	Hewlett-Packard model 6131C binary logic; ±100 V, ±0.5 A.
CAMAC Crate	DSP model Optima-850, 60A powered CAMAC crate.

a. Syntest Corp., 40 Locke Drive, Marlboro, MA 01752.

b. Novex, Inc., PO Box 3006 Gaithersburg, MD 20760.

c. Kinetic Systems Corp., 11 Maryknoll Dr., Lockport, IL 60441.

d. DSP Technology, Inc., 48500 Kato Road, Fremont, CA 94548-7338.

e. Interface Standards, 45845-A Warm Springs Blvd., Fremont, CA 94539.

f. Hewlett-Packard Co., 5161 Lankershim Blvd., North Hollywood, CA 91601.

g. ENI, Inc., 100 Highpower Road, Rochester, NY 14623-3498.

h. John Fluke Mfg. Co., Inc., PO Box C9090, Everett, WA 98206.

A digital voltage source (HP 6131C, circa 1973, recovered from a defunct mass spectrometer) energizes the zero field shim coils. In the ADLF spectroscopy of deuterium, it is useful to obtain spectra at zero to five Gauss applied magnetic field.[22] The digital voltage source (DVS) has a simple, but non-standard computer interface. Thus it is a convenient example to illustrate the CAMAC crate and the LabVIEW programming language.

Fifteen data lines encode the voltage magnitude, ranging from 0.5 mV (LSB) to 8.192 mV (MSB) in what is called "computer binary code" in the HP 6131C manual. Positive voltages are straight binary and range from 0 to +16.3835 V; negative voltages are in 2's complement and range from –0.5 mV to –16.384 V. The sign bit is considered separate from the voltage magnitude data, possibly because of the lack of sophistication of the users when the DVS was built. A gate input initiates storage and processing of the data 10 μs after the positive edge of the gate pulse. Additional programming information is supplied for a X10 voltage output (up to ±100 V, 1 data line) and a current limit (3 data lines).

At this point, the interface between the DVS and the CAMAC must be specified. A Kinetics System 3072-A1C dual 24-bit TTL output module is the interface to the DVS. One 24-bit register (CAMAC subaddress A=0) is wired to the voltage data lines; the other register (A=1) is wired to the sign (bit 0), gate (bit 1), current limit data lines (bits 2, 3, 4) and X10 voltage output (bit 5).

Figure 2.2 shows the "front panel" of the DVS program. The slide control for voltage can be operated with the mouse or numerical values can be entered into the windows above the controls. Current limit is an arbitrarily labeled index control; the value of the index is used in the program. The CAUTION: High Range indicator darkens whenever the user requests a voltage outside a preset limit contained within the program. Figures 2.3 and 2.4 show the actual program, termed the "diagram". The sequence

structure is used to define the three major steps of the program. In sequence 0, the requested voltage is compared to preset limits; notice the manner in which data flow is indicated from the source to the comparison icon, the b≤x≤a operator. A line, termed a "wire", connects the source of the data to the operator which uses the data. This is the graphical analog of a variable x in a conventional language. The other icon in sequence 0, NAF–Write–High.Middle.Low, performs a CAMAC operation which prepares the crate controller to receive information in three 8-bit bytes (the other common data transfer mode is for transferring a large number of bytes to or from a CAMAC module). Sequence 1 in Figure 2.3 shows the manipulation of a negative voltage from the source icon to the CAMAC three byte write icon set to address N=15, subaddress A=0 (the F=16 is a mode command to the CAMAC module to store incoming data from the CAMAC bus). Sequence 1 uses a comparison operator (voltage less than zero), a true-false case statement where the true condition is shown, and several numeric operations. The numeric operation shown here is not the most direct route for setting the control lines; rather, it represents the closest approach to programming the device as given in the Hewlett-Packard manual. An absolute value operator is used to extract the voltage magnitude, multiplication by 2000 converts 0.5 mV (LSB) to one. The 1's complement of the 15-bit number is obtained by subtraction from 32767 and 2's complement by adding 1. The 15-bit number is separated into a low order 8-bit numbers and high order 8-bit numbers by division by 256; the integer quotient, IQ, is the high-order byte and the remainder R is rounded to give the low-order byte. The output of the particular CAMAC module used to control the DVS has negative true logic; thus the 1's complement is taken again for each byte. The two bytes are then written to the CAMAC module. The value of the sign bit is one for a negative number; this constant is generated in the case statement and the value transferred to an intermediate variable denoted by the arrow at the bottom of sequence 1.

Sequence 2 is shown in Figure 2.4. The X10 voltage output, the current limit from

the front panel, and the sign bit from the sequence 1 are combined into a single integer. Since the output module does not have a strobe line, the gate signal is sent with the data. To make the gate pulse, three writes are done sequentially with gate equal to 0, 1, and 0. The three write statements are contained in a subsequence as shown in Figure 2.4. Finally, Figure 2.4 also contains the other case statement used for positive voltages in sequence 1.

To this point, the DVS program has been treated as a stand-alone program. However, it can be called from another routine. The icon and connector pane shown in Figure 2.2 are used to activate this program and to pass parameters. The connector pane specifies the locations on the icon and the corresponding controls and indicators. For example, locations 0 and 2 are for the Current and Voltages inputs, respectively, and location 1 is for the CAUTION: High Range output. The details of parameter passing, whether Boolean, string, real, or arrays, are indicated by different wire styles. Also, the problem of parameters out of range can be handled in two useful manners: stop, or coerce into range and proceed. The attribute detailing out of range handling is not shown.

There are two features of the LabVIEW programming that we have not used. First, there is a formula icon for math functions that are too cumbersome to write in graphical form. Second, routines written in the C language can be called from LabVIEW. This option is mainly intended for procedures that must be done rapidly. In spite of the many separate procedures in the field cycling experiment, neither of these features has been needed; all instrument control procedures are written in LabVIEW.

The performance of the instrument can be assessed roughly by comparison to conventional high-field solid-state deuterium NMR methods.[5] In the search for a method for measuring molecular conformations in the solid state, a series of arylacetic acids deuteriated at the carbon alpha to the carboxylic group have been studied.[3,22] Shown in Figure 2.5 are spectra taken with the ADLF spectrometer and with a Bruker MSL300 NMR spectrometer. In conclusion, CAMAC hardware, driven by a graphical programming

language like LabVIEW, provides a powerful, flexible means of developing home-built instruments for use in a wild variety of experiments.

Acknowledgement

The support of the donors of the Petroleum Research Fund, administered by the American Chemical Society, the Louisiana Board of Regents through the Louisiana Educational Quality Support Fund, and by the National Science Foundation under Grant CHE-8715517 is gratefully acknowledged.

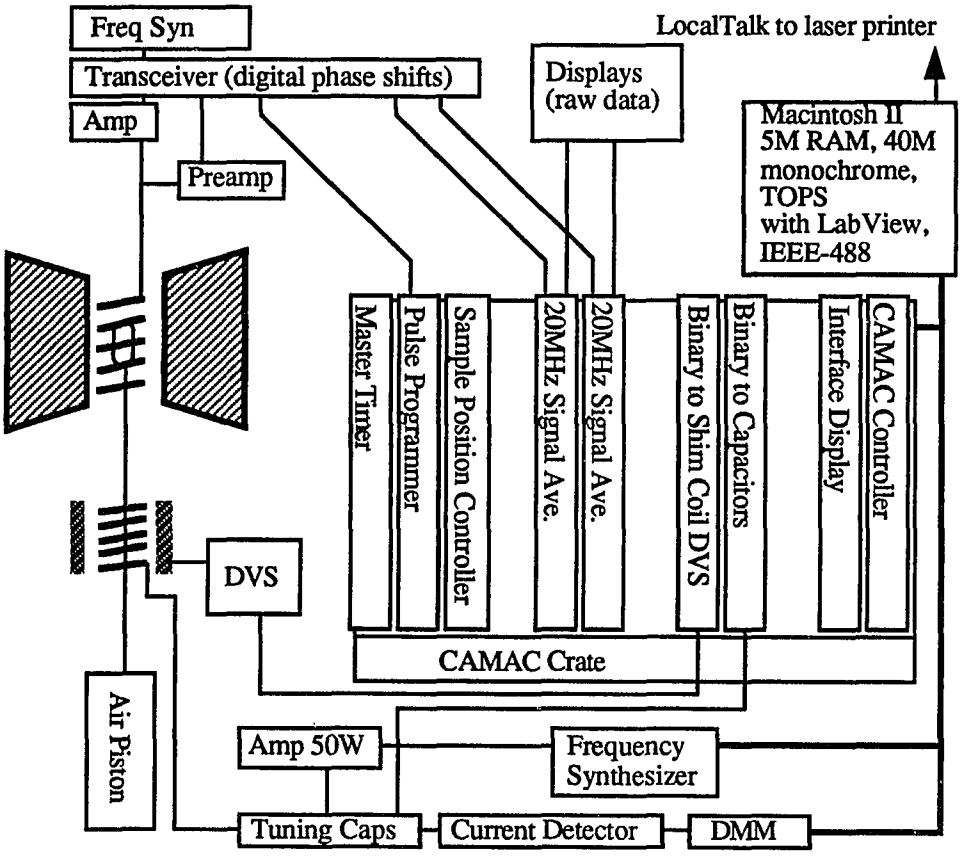

Figure 2.1 Schematic diagram of the ADLF spectrometer. Not shown on the diagram is a silvered-glass, long-tail liquid nitrogen dewar.

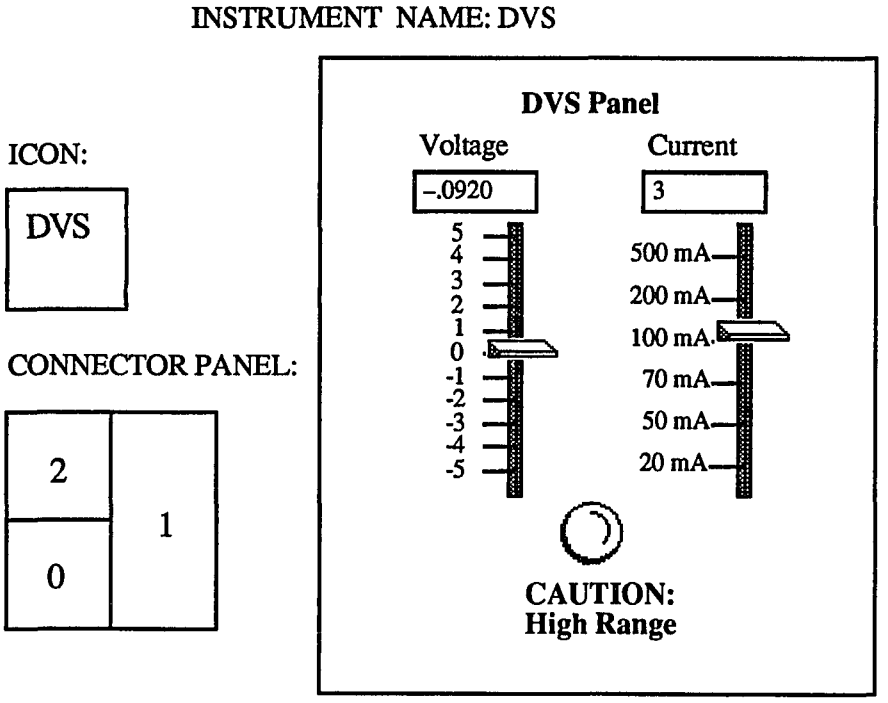

Figure 2.2 Front panel of the DVS program written in LabVIEW. The DVS program can be called by other programs. Then, parameters are passed to the DVS routine through the icon; the connector pane shows the wiring pattern. The location code is: 0=Current input, 1=CAUTION output, and 2=Voltage input.

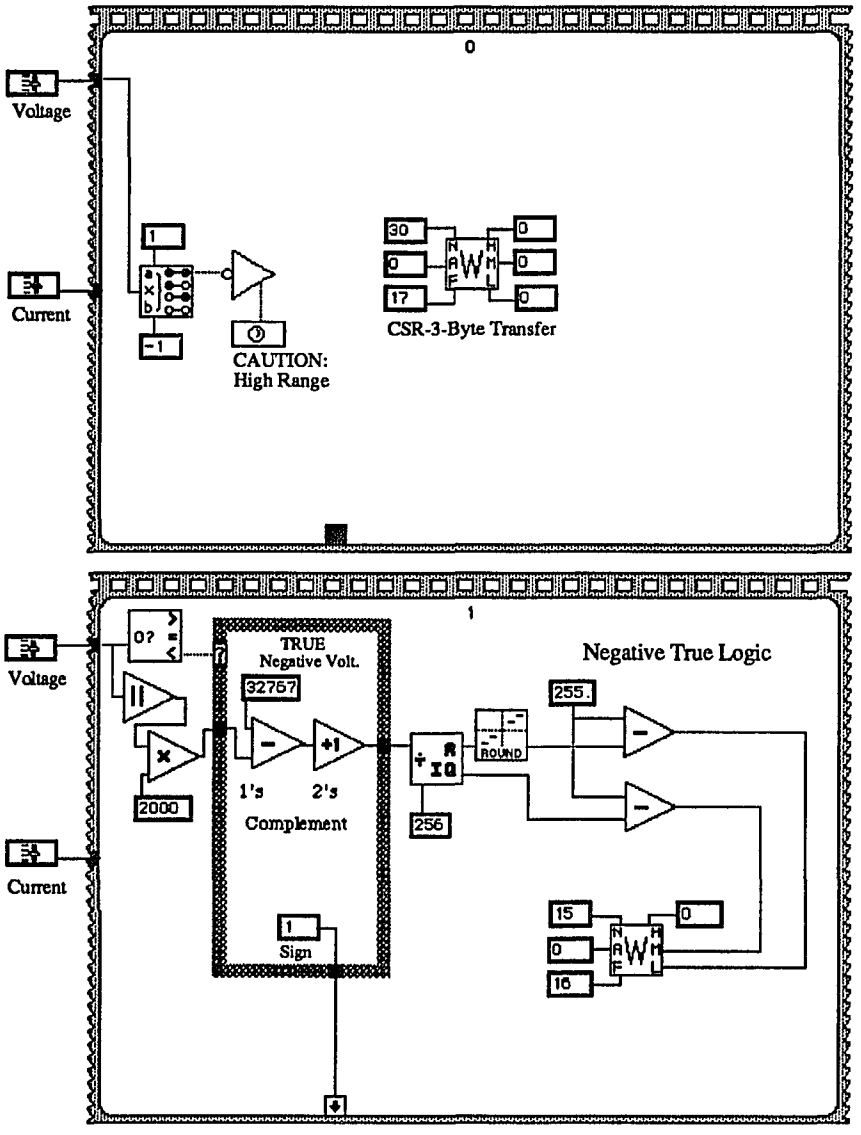

Figure 2.3 Sequence 0 and 1 of the DVS program. In sequence 0, the range checking is done and the CAMAC crate controller is initialized for three–byte transfers. In sequence 1, the magnitude of the voltage is written to one of the 24-bit output registers (A=0).

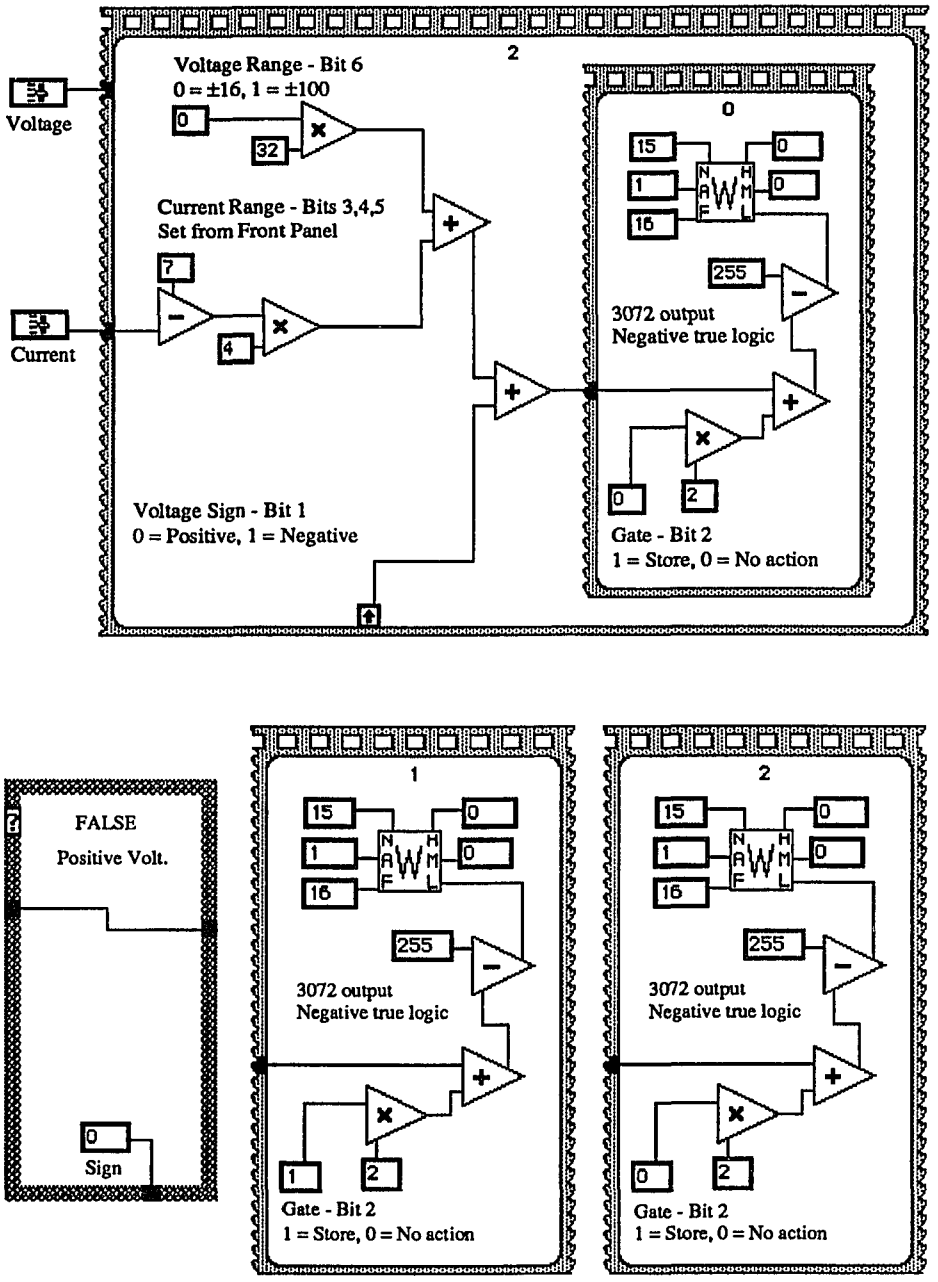

Figure 2.4 Sequence 2 shows preparation of the voltage range, current limit, voltage sign, and gate pulses and the sub-sequences used to perform three write operations to strobe the data into the DVS.

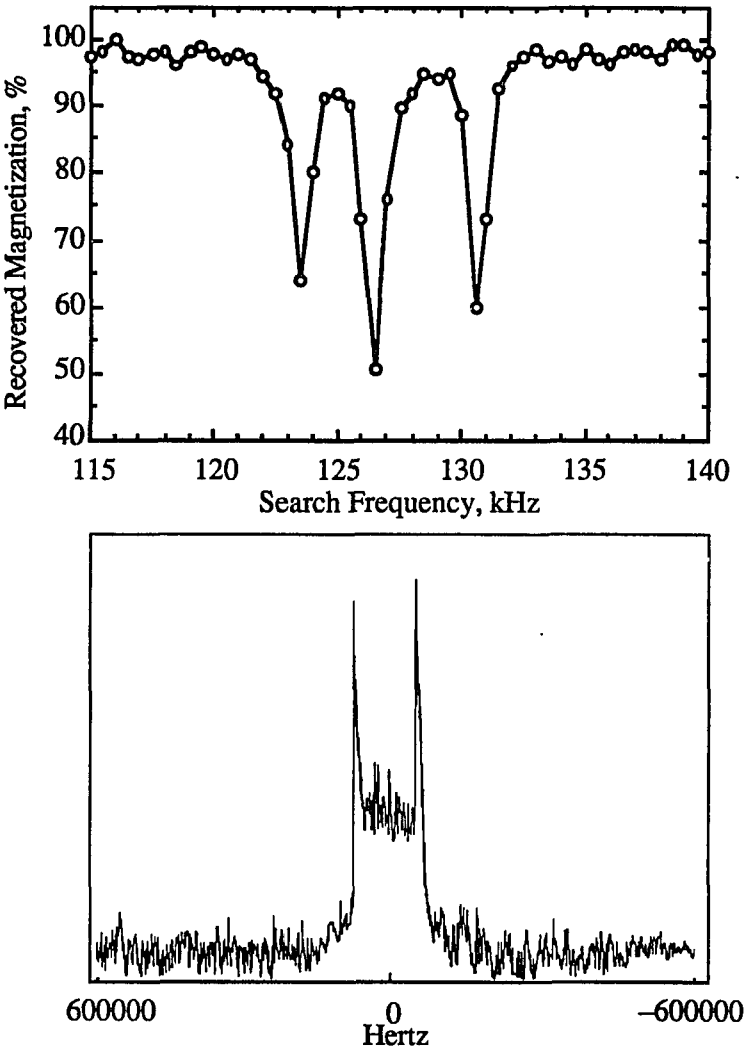

Figure 2.5 Relative performance of ADLF spectroscopy and high-field solid-state deuterium NMR spectroscopy for the study of 2-(4-nitrophenyl)[2,2-$^{2}H_{2}$]acetic acid. The ADLF spectrum in the upper trace required 200 mg of sample and 24 hours. The solid-state deuterium NMR in the bottom trace required 100 mg of sample and 24 hours.

References

1. Altbach, M. I.; Hiyama, Y.; Gerson, D. J.; Butler, L. G. *J. Am. Chem. Soc.* **1987**, *109*, 5529-5531.
2. Butler, L. G.; Brown, T. L. *J. Am. Chem. Soc.* **1981**, *103*, 6541-6549.
3. Jackisch, M. A.; Jarrett, W. L.; Guo, K.; Fronczek, F.; Butler, L. G. *J. Am. Chem. Soc.* **1988**, *110*, 343-347.
4. Jarrett, W. L.; Farlee, R. D.; Butler, L. G. *Inorg. Chem.* **1987**, *25*, 1381-1383.
5. Hentschel, R.; Spiess, H. W. *J. Magn. Reson.* **1979**, *35*, 157-162.
6. Edmonds, D. T. *Phys. Rep. C* **1977**, *29*, 233-290.
7. Slusher, R. E.; Hahn, E. L. *Phys. Rev.* **1968**, *166*, 332-347.
8. Edmonds, D. T.; Mailer, J. P. G. *J. Phys. E* **1977**, *10*, 868-871.
9. Cheng, C. P.; Brown, T. L. *J. Am. Chem. Soc.* **1979**, *101*, 2327-2334.
10. Goldstein, N.; Ragle, J. L. *J. Chem. Phys.* **1979**, *70*, 5072-5075.
11. Shporer, M.; Achlama, A. M. *J. Chem. Phys.* **1976**, *65*, 3657-3664.
12. Seliger, J.; Zagar, V.; Blinc, R.; Novak, A. *J. Chem. Phys.* **1986**, *84*, 5857-5861.
13. Lotz, A; Oliges, J.; Voitlander, J. *Chem. Phys. Lett.* **1982**, *93*, 560-563.
14. Ader, R.; Shporer, M. *J. Magn. Reson.* **1982**, *47*, 483-489.
15. Butler, L. G.; Reiner, C. A.; Brown, T. L. *Rev. Sci. Instrum.* **1982**, *53*, 984-988.
16. Bielecki, A.; Zax, D. B.; Zilm, K. W.; Pines, A. *Rev. Sci. Instrum.* **1986**, *57*, 393–403.
17. Fukushima, E.; Roeder, S. B. W. *Experimental Pulse NMR, A Nuts and Bolts Approach*; Addison-Wesley: Reading, MA., 1981.
18. LabVIEW Software System, National Instruments Corp., 12109 Technology Blvd., Austin, TX 78727-6204.
19. Newrock, R. S. *Microsystems* **1983**, April, 34-61.
20. Andresen, P. L. *Microsystems* **1984**, September, 88-104.

21. NB-DMA-8-G, National Instruments Corp., 12109 Technology Blvd., Austin, TX 78727-6204.

22. Jarrett, W. L.; Guo, K.; Jackisch, M. A.; Butler, L. G. *J. Magn. Reson.* **1989**, *82*, 76-85.

(Reprinted with permission from *Inorganic Chemistry* **1987**, *26*, 3001-3004.

CHAPTER THREE

Deuterium Quadrupole Coupling Constants and Asymmetry Parameters in Metal Hydrides: Calculations of Model Systems Representing Three Modes of Metal-Hydrogen Bonding.

by

Kermin Guo, William L. Jarrett and Leslie G. Butler*

Received March 16, 1987

Contribution from the

Department of Chemistry

Louisiana State University, Baton Rouge, LA 70803

*To whom correspondence should be addressed.

LSU
Department of Chemistry
LOUISIANA STATE UNIVERSITY AND AGRICULTURAL AND MECHANICAL COLLEGE
BATON ROUGE · LOUISIANA · 70803-1804
504/388-3361

Sat, Dec 10, 1988

Executive Secretary
Inorganic Chemistry
ACS Journal Department
Columbus, OH 43210

Dear Sir:

I am writing to you in reference to the article "The Deuterium Quadruple Coupling Constants and Asymmetry Parameters in Metal Hydrides: Calculations of Model Systems Representing Three Modes of Metal-Hydrogen Bonding." published in Inorganic Chemistry **1987**, *26*, 3001-4. I am the first author of this paper and I would like to use a manuscript in my Ph.D. dissertation.

Please, forward permission to reprint the manuscript. I will appreciate your prompt reply.

Sincerely,

Kermin Guo

Kermin Guo
Box B-18, Department of Chemistry
Louisiana State University
Baton Rouge, LA 70803

Abstract

The electric field gradient at the hydrogen atom site has been calculated in three model systems: M–H (M = Li, Na, K, Rb, and Cs), $[Na–H–Na]^+$, $[Na–H_2]^+$, and $[Rb–H_2]^+$. The effect of metal hydride geometry on the deuterium quadrupole coupling constant was examined with an extended basis set by using restricted Hartree-Fock methods. For the terminal M–H bonds (M = K, Rb, and Cs), the deuterium quadrupole coupling constant is about 20 kHz. Formation of a bridging metal-hydrogen bond reduces the value of quadrupole coupling constant; nonlinearity reduces the quadrupole coupling constant further. For the $[M–H_2]^+$ system, the value of the deuterium quadrupole coupling constant is strongly affected by H–H bonding. These results can be used in the assignment and interpretation of solid-state deuterium NMR spectra of metal-hydrogen bonds in organometallic complexes.

3.1 Introduction

Recent solid-state deuterium NMR experiments have shown that the deuterium quadrupole coupling constant, $e^2q_{zz}Q/h$, is a sensitive function of the metal-hydride bond geometry, with characteristics similar to those observed in the solid-state deuterium NMR spectra of O–D···O bonds. An amorphous polymeric solid, bis(cyclopentadienyl) zirconium dideuteride, has two inequivalent deuterium sites.[1] On the basis of the solid-state deuterium NMR spectrum, the existence of a terminal metal hydride and a bridging metal hydride was deduced; integration of the peak areas quantified the results.

The interpretation of solid-state deuterium NMR spectra has been aided by the results of molecular orbital calculations done on model systems. With use of extended Gaussian basis sets, relationships between molecular geometry and the electric field gradient at deuterium have been established. In small molecules, C–H, N–H, and O–H bonds have been studied and the dependence noted between the deuterium quadrupole coupling constant and the atom to which deuterium is bound and the bond length.[2,3] Variations in the hydrogen bond length or angle(O–H···O bonds) affect the deuterium quadrupole coupling constant and asymmetry parameters; ab initio molecular orbital calculations were used to study the causal factors. The assignment of major factors has been confirmed by solid-state deuterium NMR and ADLF spectroscopy.[4]

Structural information comes about from the fact that, in the solid state, the deuterium NMR spectrum is determined by the electric field gradient at the deuterium nuclear site. The electric field gradient is a tensor quantity with a trace of zero. When solid-state deuterium NMR data are reported, the common convention is to identify an axis system that diagonalizes the electric field gradient tensor; the largest diagonal element of the tensor, eq_{zz}, gives the quadrupole coupling constant, $e^2q_{zz}Q/h$. The quadrupole coupling constant is a direct function of the charge distribution in the close vicinity (within about 3 Å) of the deuterium nucleus, as shown in equation 3.1. Note that only occupied

$$eq_{zz} = \sum_n K_n \frac{3z_n^2 - r_n^2}{r_n^5} - e\left\langle \Psi^* \left| \sum_i \frac{3z_i^2 - r_i^2}{r_i^5} \right| \Psi \right\rangle \qquad (3.1)$$

molecular orbitals contribute to the electric field gradient; the absence of contributions from excited states greatly simplifies the calculations required to compute quadrupole coupling constants by using ab initio molecular orbital calculations. The other major elements of the electric field gradient tensor, eq_{xx} and eq_{yy}, are obtained by a similar summation of neighboring charge with a $1/r^3$ distance dependence. Also specified in the solid-state deuterium NMR is the asymmetry parameter, η, of the electric field gradient tensor:

$$\eta = \frac{eq_{xx} - eq_{yy}}{eq_{zz}} \qquad (3.2)$$

The asymmetry parameter is useful since a terminal X–^{2}H or linear X···^{2}H–Y bond should have a near-zero value for η; non-zero values are characteristic of nonlinear X···^{2}H–Y bonds.

Solid-state deuterium NMR spectroscopy can be applied to a large range of metal hydride chemistry. In homogeneous transition-metal complexes,[5-8] and on catalytic surfaces,[9,10] structures of metal-hydrogen bonds are quite varied, ranging from terminal metal-hydride bonds to several types of bridging geometries. One method of synthesizing transition-metal hydrides proceeds by the oxidative addition of dihydrogen to a coordinatively unsaturated metal center. The addition process is presumed to involve, at some point along the reaction pathway, nonclassical coordination of the dihydrogen molecule to the metal center.[11] Recently, sterically constrained metal complexes have been isolated that contain weakly coordinated dihydrogen molecules.[12]

Herein, we report the results of three series of calculations. Terminal metal deuterides are modeled by diatomic metal deuterides. Bridging metal hydrides are modeled

by a $[Na–H–Na]^+$ system. Finally, the interaction of dihydrogen with a metal center has been followed with $[Na–H_2]^+$ and $[Rb–H_2]^+$ complexes.

3.2 Calculations

GAUSSIAN 82 and the associated properties package was used for all SCF-HF calculations.[13] The cesium metal atom basis set was taken from the compilation of Huzinaga and consisted of the nominal basis set enhanced with a two-membered p-type polarization function.[14] For the purpose of comparing results between the alkali-metal hydrides, the basis sets for lithium, sodium, potassium, and rubidium were restricted to the same form as available for cesium. The hydrogen atom basis set was (1s2p1d).[15] In this work, we have taken the deuterium nuclear quadrupole moment, Q, as 2.86×10^{-27} cm^2.[16] The convention used herein for reporting the electric field gradient is $|q_{zz}| \geq |q_{yy}| \geq |q_{xx}|$.[17]

For the terminal metal deuterides, the M–H bond distances and vibrational stretching force constants were taken from Herzberg.[18] In the linear bridging metal hydride model $[Na–H–Na]^+$, the hydride was constrained to be symmetrically situated between the metal atoms. In the nonlinear bridging hydride model, the Na–H distance was fixed at 2.0 Å. For the $[M–H_2]^+$ systems, all geometries were optimized by using as input the M–(H_2 centroid) distance.

No corrections for vibrational effects were made to the calculated electric field gradients. In the cases when calculated electric field gradients have been corrected for vibration, the general effect is to slightly reduce the magnitude of the electric field gradient tensor elements.[19]

3.3 Results and Discussion

3.3.1 Terminal Metal Hydrides. The quality of the basis set was evaluated by

comparing the results obtained here for LiH with other calculations and with the results of gas-phase microwave spectroscopy. Hameka and co-worker have evaluated the effect of basis set on the electronic contribution to the electric field gradient, q_{el}, for the hydride site in LiH, $q_{el} = -0.1642$ (this work) and $q_{el} = -0.1615$ (Hameka et al.).[20,21] Adding to the electric field gradient tensor the positive contribution due to the lithium nucleus, we calculate a deuterium quadrupole coupling constant, $e^2q_{zz}Q/h$, of 36.8 kHz, in good agreement with the experimental value of 33(1) kHz.[22] Unfortunately, experimental values of the deuterium quadrupole coupling constant are not available for the other alkali-metal hydrides. However, a correlation has been noted between the vibrational stretching force constant, k, and the deuterium quadrupole coupling constant;[23-27] the correlation is used here to show that the calculated deuterium quadrupole coupling constants, especially for larger metals, do not suffer from any gross errors. The ratio e^2q_{zz}/k, should be near unity,[23,27] as is found for all of the alkali-metal hydrides reported herein. Table 3.1 lists the M–H distance, the vibrational force constant, the nuclear contribution to the deuterium quadrupole coupling constant., the calculated deuterium quadrupole coupling constant, and the ratio e^2q_{zz}/k for the alkali-metal hydrides.

The results shown in Table 3.1 lead to two important conclusions. First, for terminal metal hydrides, the smallest value of the deuterium quadrupole coupling constant is on the order of 20 kHz. Since the alkali-metal hydrides KH, RbH, and CsH have smaller vibrational force constants than typical organometallic transition-metal hydrides,[26,28,29] 20 kHz represents a lower bound for the deuterium quadrupole coupling constant. In a recent survey of organometallic hydrides, the smallest value yet found is 46.7(5) kHz.[1] Second, as one proceeds from lithium to cesium, the alkali-metal core electrons are quite effective at shielding the increased nuclear charge from contributing to the total electric field gradient at the hydride site. This second conclusion has been previously discussed in a different format on the basis of a comparison of the similar origins for vibrational force constants

and electric field gradients in hydrides.[23]

Table 3.1. The Deuterium Quadrupole Coupling Constants for Alkali-Metal Deuterides and Comparison to Vibration Force Constants.

atom	M–H, Å[a]	k,[b] 10^5 dyn/cm	$e^2q_{nucl}Q/h$, kHz	$e^2q_{zz}Q/h$, kHz[c]	e^2q_{zz}/k[d]
Li	1.595	1.02	147.16	36.80	0.8298
Na	1.887	0.78	325.89	24.84	0.7351
K	2.244	0.56	334.88	20.60	0.8486
Rb	2.376	0.51	549.37	19.74	0.8867
Cs	2.494	0.46	680.44	21.04	1.0410

[a]From ref 18. [b]k is calculated from ω_e values.[18] [c]Values from the results of the GAUSSIAN 82 calculations. [d]Calculated by following the procedure of ref 27.

3.3.2 Bridging Metal Hydrides. The model bridging metal hydride $[Na–H–Na]^+$ was studied over a range of Na–Na distances, ranging from 3 to 4.6 Å; at all points, equal Na–H bond distances were maintained. While generally satisfactory in most features, the $[Na–H–Na]^+$ model, because of the net positive charge, yields values for the deuterium quadrupole coupling constants that are forced to be more positive than would be expected for an organometallic complex. A point charge model, with +0.5 e charge situated at each sodium nuclear site, was used to correct the calculated deuterium quadrupole coupling constants. The $[Na–H–Na]^+$ data are plotted in Figure 3.1 with the corrected deuterium quadrupole coupling constants.

The most notable feature in Figure 3.1 is the large reduction in the value of the deuterium quadrupole coupling constant with increasing metal-metal distance. The reduction is caused by the decreasing nuclear contribution to the electric field gradient and is exactly analogous to the reduction calculated and observed in symmetric O–H–O bonds.[4a,30] Also noted on the graph is the Na–H bond distance for the neutral diatomic hydride. Since formation of a bridging hydride bond causes an increase in the Na–H distance, from Figure 3.1 we would predict that bridging metal hydrides should have a deuterium quadrupole coupling constant smaller than that of a comparable terminal metal hydride.

The deuterium quadrupole coupling constants of nonlinear bridging metal hydrides were investigated with a fixed Na–H bond distance of 2.0 Å. Fixed O–H distances were also used in a study of O–H···O bond angles and the correlation with deuterium quadrupole coupling constants.[4a] Figure 3.2 shows the effect bending the bridging metal-hydride bonds has upon the deuterium electric field gradient. Relative to the case for a linear system, bent metal-hydride bonds have a reduced deuterium quadrupole coupling constant. Also, the asymmetry parameter becomes large upon bending; the relative orientation of the electric field gradient principal axis system is shown in Figure 3.2.

The solid-state deuterium NMR spectrum of bis(cyclopentadienyl)zirconium dideuteride shows two deuterium sites with deuterium quadrupole coupling constants of 46.7(5) and 32.7(20) kHz.[1] The site with the smaller value for the deuterium quadrupole coupling constant was assigned, partly on the basis of the known trends for O–H···O bonds, to a bridging metal hydride site.

3.3.3 Dihydrogen Adducts. In this model, a dihydrogen molecule is brought near an alkali-metal ion that is acting as a Lewis acid.[11i] As the dihydrogen molecule is brought closer to the metal, the H–H bond is broken and two new M–H bonds are formed. In this work the geometry of the complex was determined by an energy minimization process. The principal coordinates of the complex are as follows: (1) the M–(H_2) distance,

the distance between the metal and the centroid of the dihydrogen system, and (2) the H–H distance, the distance between the two hydrogen atoms. For example, little interaction between the metal ion and the dihydrogen molecule occurs with d(M–(H_2)) = 4 Å and d(H–H) = 0.85 Å . At the other extreme, a linear $[H–M–H]^+$ complex corresponds to d(M–(H_2)) = 0 Å and d(H–H) = 4.2236 Å, the sum of the two M–H bond distances. Figure 3.3 shows representations of the electron density in the $[Rb–(H_2)]^+$ complex for three M–(H_2) distances in the region where the H–H bond is being broken.

In spite of the complexity of the dihydrogen addition process, it is possible to describe, in relatively simple terms, the evolution of the deuterium quadrupole coupling constant and asymmetry parameter. In the dihydrogen molecule prior to interaction with a metal, the deuterium quadrupole coupling constant is +225 kHz and is dominated by the relatively unshield neighboring hydrogen nucleus only 0.79 Å distant. After an alkali-metal-hydride bond is formed, the deuterium quadrupole coupling constant is on the order of 20 kHz but is still positive and is dominated by the nuclear charge of the alkali-metal atom. Having established the limiting cases, one would expect intermediate regions of the dihydrogen addition process to show a smooth evolution of deuterium quadrupole coupling constant and reorientation of the electric field gradient major axis. The arrow in Figure 3.3 shows the orientation of the electric field gradient major axis; Figure 3.4 shows the evolution of the deuterium quadrupole coupling constant and asymmetry parameters. The $[Rb–(H_2)]^+$data are summarized in Table 3.2. The $[Na–(H_2)]^+$ system behaved similarily to $[Rb–(H_2)]^+$, differing mainly in having a shorter M–(H_2) distance in the M–H bond-breaking region.

The evolution of the minor axes of the electric field gradient tensor is not as predictable as for the major axis. For Rb–(H_2) distances of 1.75 Å and greater, q_{yy} is normal to the Rb–(H_2) plane. After the H–H bond is broken, q_{yy} lies in the Rb–(H_2) plane.

Table 3.2. The Deuterium Quadrupole Coupling Constants and Asymmetry Parameters for $[Rb–H_2]^+$.

Rb–(H_2), Å	H–H, Å	θ, deg[a]	η	e^2qQ/h, kHz
4.00	0.8500	0.103	0.0250	181.770
3.00	0.8492	0.378	0.0627	179.965
2.50	0.8452	1.061	0.1250	178.867
2.00	0.8386	4.665	0.3372	171.082
1.75	0.8450	12.905	0.6228	155.373
1.50	3.9545	36.733	0.0170	14.775
1.40	4.2200	32.931	0.0080	13.565
1.30	4.3840	29.974	0.0046	13.156
1.20	4.4912	27.393	0.0031	13.123
1.10	4.5582	25.019	0.0022	13.343
1.00	4.5936	22.769	0.0017	13.779
0.50	4.4346	12.003	0.0007	19.634
0.00	4.2236	0.000	0.0000	26.902

[a]Angle between the H–H vector and the major axis of the electric field gradient tensor (z axis).

The solid-state deuterium NMR spectrum of a tungsten dihydrogen complex gives a deuterium quadrupole coupling constant of about 124 kHz,[12c] in good agreement with the trends found herein. Due to motional averaging, the asymmetry parameter could not be

obtained from the spectrum but would be expected to be non-zero.

3.4 Conclusions

Terminal Metal Hydrides. From the calculations on the alkali-metal hydrides and subsequent comparison to vibrational stretching force constants, two general statements can be made:

1. A lower limit for the deuterium quadrupole coupling constant in organometallic hydrides is 20 kHz.

2. Metal core electrons effectively shield the deuteron from the electric field gradient generated by large nuclear charges.

Bridging Metal Hydrides. Formation of a bridging metal-hydride bond causes a reduction in the deuterium quadrupole coupling constant relative to the value found for a terminal metal-hydride bond to the same metal.

Dihydrogen Adducts. In the adduction of dihydrogen to a d^0 metal center, the major features of the electric field gradient at the hydrogen site evolve in a straightforward manner.

1. The value of the deuterium quadrupole coupling constant is reduced, with the most rapid reduction occurring as the H–H bond is being broken.

2. The orientation of the electric field gradient major axis, aligned along the H–H bond in the dihydrogen molecule, rotates toward alignment with the M–H bond as the H–H bond is broken.

3. At structures corresponding to intermediate H–H and M–H bonds, the asymmetry parameter is non-zero.

Given the occasional experimental difficulties in acquiring solid-state deuterium NMR spectra, it can be highly beneficial to the spectroscopist to optimize the instrumental parameters on the basis of estimates of the deuterium quadrupole coupling constant and the

asymmetry parameter. Also, there is a clear and definitive connection between the observed solid-state deuterium NMR spectrum and structural features of the metal-hydrogen bond, making solid-state deuterium NMR spectroscopy a potentially unique and valuable asset for physical organometallic chemistry.

Acknowledgement. We thank Professor Neil Kestner for his astute comments and Bob Zinn for assistance with the GAUSSIAN 82 program. The support of the Research Corp., the donors of the Petroleum Research Fund, administered by the American Chemical Society, the LSU Council on Research, and the LSU Center for Energy Studies is gratefully acknowledged.

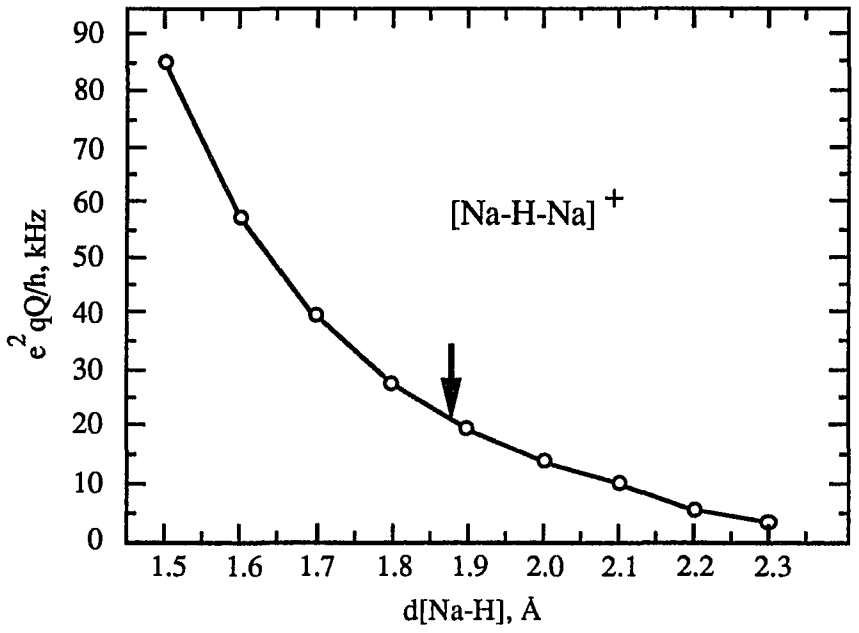

Figure 3.1. Deuterium quadrupole coupling constants in the bridging metal hydride, $[Na–H–Na]^+$. Also shown(arrow) is the Na–H bond distance for the neutral diatomic hydride. The values shown for the deuterium quadrupole coupling constants are corrected for the net positive charge on the model complex by using a point charge model.

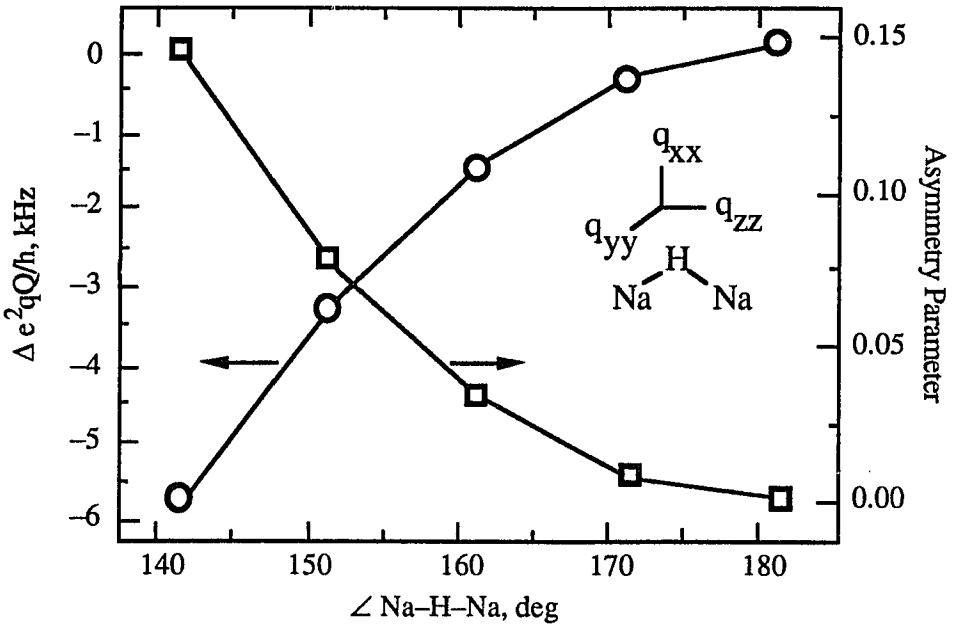

Figure 3.2. Effect of a nonlinear bond on the deuterium quadrupole coupling constants and asymmetry parameters in $[Na–H–Na]^+$. The Na–H distance is held constant at 2 Å. The orientation of the electric field gradient tensor principal axis system relative to that of the molecular system is shown with the convention $|q_{zz}| \geq |q_{yy}| \geq |q_{xx}|$. The deuterium quadrupole coupling constants are shown to the calculated value at ∠Na–H–Na = 180°.

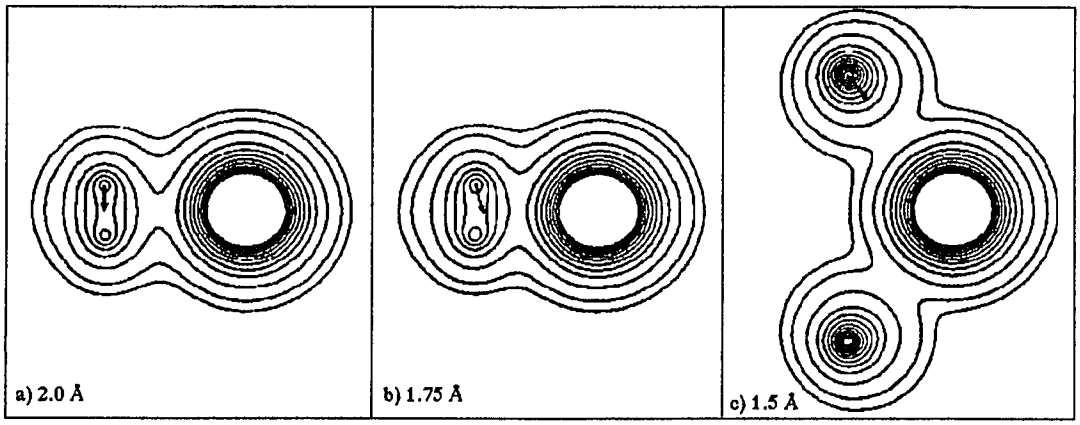

Figure 3.3. Plot representing the electron density (contour) and orientation (arrow) of the electric field gradient major axis for $[Rb–H_2]^+$. Rb–(H_2) distance are (a) 1.50, (b) 1.75, and (c) 2.00 Å. The outermost contour shown is at 0.01 e/Å^3; the next contour is at 0.02 e/Å^3, and the next 10 contours start at 0.05 e/Å^3 with 0.05 e/Å^3 steps.

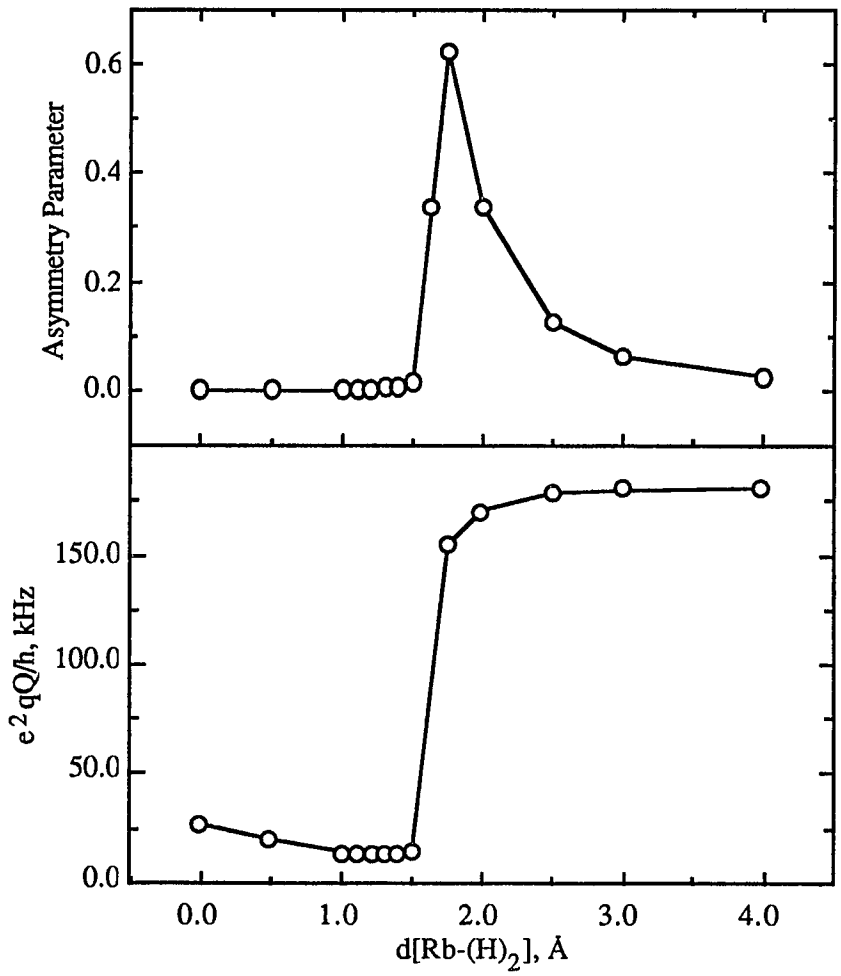

Figure 3.4. Evolution of the deuterium quadrupole coupling constant and asymmetry parameter in the addition of dihydrogen to a Rb^+ center.

References

1. Jarrett, W. L.; Farlee, R. D.; Butler, L. G. *Inorg. Chem.* **1987**, *25*, 1381-1383.
2. Synder, L. C. *J. Chem. Phys.* **1974**, *61*, 5032-5034.
3. Synder, L. C. *J. Chem. Phys.* **1978**, *68*, 291-294.
4. (a) Butler, L. G.; Brown, T. L. *J. Am. Chem. Soc.* **1981**, *103*, 6541-6549. (b) Brown, T. L.; Butler, L. G.; Curtin, D. Y.; Hiyama, Y.; Paul, J. C.; Wilson, R. G. *J. Am. Chem. Soc.* **1982**, *104*, 1172-1177.
5. (a) *Transition Metal Hydrides*; Muetterties, E. L., Ed.; Marcel Dekker: New York, 1971. (b) Kaesz, H. D.; Saillant, R. B. *Chem. Rev.* **1972**, *72*, 231-282.
6. Collman, J. P.; Hegedus, L. S. *Principles and Applications of Organotransition Metal Chemistry*; University Science: Mill Valley, CA, 1980.
7. (a) Bau, R.; Teller, R. G.; Kirtley, S. W.; Koetzle, T. F. *Accts. Chem. Res.* **1979**, *12*, 176-183. (b) Teller, R. G.; Bau, R. *Struct. Bonding (Berlin)* **1981**, *44*, 1-82.
8 Hart, D. W.; Bau, R.; Koetzle, T. F. *Organometallics* **1985**, *4*, 1590-1594.
9. Gavin, R. M., Jr.; Reutt, J.; Muetterties, E. L. *Proc. Natl. Acad. Sci. USA*, **1981**, *78*, 3981-3989.
10. Zaera, F.; Gellman, A. J.; Somorjai, A. *Accts. Chem. Res.* **1986**, *19*, 24-31.
11. (a) Steigerwald, M. L.; Goddard, W. A., III. *J. Am. Chem. Soc.* **1984**, *106*, 308–311. (b) Low, J. J.; Goddard, W. A., III. *J. Am. Chem. Soc.* **1984**, *106*, 6928-6937. (c) Low, J. J.; Goddard, W. A., III. *Organometallics* **1986**, *5*, 609–621. (d) Nakatsuji, H.; Hada, M. *J. Am. Chem. Soc.* **1985**, *107*, 8264-8268. (e) Obara, S.; Kitaura, K.; Morokuma, K. *J. Am. Chem. Soc.* **1984**, *106*, 7482–7492. (f) Ruette, F.; Blyholder, G.; Head, J. *J. Chem. Phys.* **1984**, *80*, 2042-2048. (g) Jarque, C.; Novaro, O.; Ruiz, M. E.; Garcia-Prieto, J. *J. Am. Chem. Soc.* **1986**, *108*, 3507-3509. (h) Novaro, O.; Garcia-Prieto, J.; Poulain, E.; Ruiz, M. E. *THEOCHEM* **1986**, *135*, 79-91. (i) Rabaa, H.; Saillard, J. -Y.; Hoffman, R.

J. Am. Chem. Soc. **1986**, *108*, 4327-4333.

12. (a) Kubas, G. J.; Ryan, R. R.; Swanson, B. I.; Vergamini, P. J.; Wasserman, H. J. *J. Am. Chem. Soc.* **1984**, *106*, 451-454. (b) Crabtree, R. H.; Lavin, M. *J. Chem. Soc. Chem. Commun.* **1985**, *12*, 794-795. (c) Kubas, G. J.; Unkefer, C. J.; Swanson, B. I.; Fukushima, E.; *J. Am. Chem. Soc.* **1986**, *108*, 7000-7009. (d) Crabtree, R. H.; Hamilton, P. G. *J. Am. Chem. Soc.* **1986**, *108*, 3124-3128. (e) Sweany, R. L. *Organometallics* **1986**, *5*, 387-388.
13. GAUSSIAN 82 by J. S. Binkley; M. J. Frisch; D. J. DeFrees; K. Raghavachari; R. A. Whitesides; H. B. Schelgel; E. M. Fluder; and J. A. Pople (copyright 1984, Carneige-Mellon University).
14. *Gaussian Basis Sets for Molecular Calculations*; Huzinaga, S.; Andzelm, J.; Klobukowski, M.; Radzio-Andzelm, E.; Sakai, Y.; Tatewaki, H., Eds.; Elsevier: New York, 1984. The basis sets are as follows: Li, [7s,2p] contracted to (2s,2p); Na, [10s,6p] contracted to (3s,3p); K, [13s,9p] contracted to (4s,4p); Rb, [16s,12p,4d] contracted to (5s,5p,1d); Cs, [18s,14p,6d] contracted to (6s,6p,2d).
15 Andzelm, J.; Klobukowski, M.; Radzio–Andzelm, E. *J. Comput. Chem.* **1984**, *5*, 146. This basis set was supplemented with a d function having an exponential coefficient of 1 to give [4s,2p,1d] contracted to (1s,2p,1d).
16. Reid, R. V., Jr.; Vaida, M. L. *Phys. Rev. Lett.* **1975**, *34*, 1064.
17. Poole, C. P., Jr.; Farach, H. A. *The Theory of Magnetic Resonance*; Wiley: New York, 1972.
18. Herzberg, G. *Molecular Spectra and Molecular Structure. Infrared Spectra of Diatomic Molecules*, 2nd ed.; Van Nostrand Reinhold: New York, 1960.
19. Kern, C. W.; Matcha, R. L. *J. Chem. Phys.* **1968**, *49*, 2081-2091.
20. Pietrovito, A. J.; Hameka, H. F.; Zeroka, D. *J. Chem. Phys.* **1984**, *81*, 1960-1965.
21. Barfield, M. Gottlieb, H. P. W.; Doddrell, D. M. *J. Chem. Phys.* **1978**, *69*,

4504–4515.

22. Wharton, L.; Gold, L. P.; Klemperer, W. *J. Chem. Phys.* **1962**, *37*, 2149-2150.

23. Salem, L. *J. Chem. Phys.* **1963**, *38*, 1227-1236.

24. (a) Merchant, S. Z.; Fung, B. M. *J. Chem. Phys.* **1969**, *50*, 2265-2267. (b) Fung, B. M.; Wei, I. Y. *J. Am. Chem. Soc.* **1970**, *92*, 1497-1487. (c) Wei, I. Y.; Fung, B. M. *J. Chem. Phys.* **1971**, *55*, 1486-1487.

25. Mokarram, M.; Ragle, J. L. *J. Chem. Phys.* **1973**, *59*, 2770-2771.

26. McDugle, W. G., Jr.; Schreiner, A. F.; Brown, T. L. *J. Am. Chem. Soc.* **1967**, *89*, 3111-3114.

27. Kukolich, S. G. *Mol. Phys.* **1975**, *29*, 249-255.

28. McDugle, W. G., Jr.; Brown, T. L. *J. Am. Chem. Soc.* **1967**, *89*, 3111-3114.

29. Maslowsky, E., Jr. *Vibrational Spectra of Organometallic Compounds*; Wiley-Interscience: New York, 1977.

30. Chiba, T. *J. Chem. Phys.* **1963**, *39*, 947-950.

(Reprinted in part with permission from the *J. Am. Chem. Soc.* **1987**, *109*, 2525–2526.

CHAPTER FOUR

Unusual Asymmetry of Methyl ^{2}H EFG in Thymine: Solid State Deuterium NMR and ab Initio MO Study

Yukio Hiyama, Siddhartha Roy, Kermin Guo,
Leslie G. Butler,* and Dennis Torchia*

Received September 26, 1986

Contribution from

Bone Research Branch, National Institute of Dental Research
Clinical Pharmacology Branch, National Cancer Institute
National Institutes of Health
Bethesda, Maryland 20892

Department of Chemistry
Louisiana State University, Baton Rouge, LA 70803

*To whom correspondence should be addressed.

Department of Chemistry
LOUISIANA STATE UNIVERSITY AND AGRICULTURAL AND MECHANICAL COLLEGE
BATON ROUGE · LOUISIANA · 70803-1804
504/388-3361

Wed, Mar 15, 1989

Copyright Administrator
Books & Journals Division
American Chemical Society
1155 16th Street, N.W.
Washington, D. C. 20036

Dear Sir:

I am writing to you in reference to the communication:"Unusual Asymmetry of Methyl ^2H EFG in Thymine: A Solid State Deuterium NMR and ab Initio MO Study" published in the Journal of the American Chemical Society, 1987, *109*, 2525-2526. I am a contributing author of this communication. Two of the coauthor, Dennis A. Torchia and Leslie G. Butler, (both listed as "To whom correspondence should be addressed" on the title page of the manuscript) have given me permission to use the relevant portions of the manuscript in my Ph.D. dissertation. The relevant excerpts are: (1) an introduction to the problem, (2) my contribution to the collaborative research effort, and (3) the conclusion reached in this work.

Please forward permission to reprint the relevant excerpts of the manuscript. I will appreciate your prompt reply.

Sincerely,

Kermin Guo
Box B-18, Department of Chemistry
Louisiana State University
Baton Rouge, LA 70803

PERMISSION TO REPRINT IS GRANTED BY THE AMERICAN CHEMICAL SOCIETY

ACS COPYRIGHT CREDIT LINE REQUIRED. Please follow this sample: Reprinted with permission from (full journal reference). Copyright (year) American Chemical Society.

& in part

BOOKS & JOURNALS DIVISION

1155 - 16th St., N.W.
Washington, D.C. 20036

3-28-89

Copyright Administrator

Coauthor, Leslie G. Butler

Coauthor, Dennis A. Torchia

Solid-state ^2H NMR spectroscopy is a powerful method of studying molecular motion in the solid state.[1-4] The power of this technique derives from the facts that quadrupole coupling is the dominant interaction and the electric field gradient (EFG) tensor is usually axially symmetric for a deuteron bonded to carbon, with the unique axis along the C–D bond. In the case of a methyl group, rapid 3-fold rotation yields an averaged EFG whose symmetry axis is along the rotation axis, and the corresponding powder pattern is axially symmetric ($\eta \leq 0.01$) with a quadrupole splitting of ca. 40 kHz.[5]

Hiyama and coworkers are interested in obtaining spectra of thymidine and ribothymidine, deuteriated at the methyl position, to study motion of nucleotide bases in DNA and tRNA, respectively. In their initial work they are studying the dynamics of the model compound, thymine–*methyl–d*$_3$.[6] Inversion-recovery ^2H NMR spectra of this compound clearly showed the T_1 anisotropy predicted for 3–fold methyl jumps.[5,7] The linear Arrhenius plot of correlation time, τ_c, against $1/T$ (where $\tau_c = \tau_o \circ \exp(E/RT)$) yielded an apparent activation energy of 6.9 kJ/mol and a preexponential factor, τ_o, of 2×10^{-13} s. These results show that the ^2H spin-lattice relaxation is determined by the 3–fold methyl motion. However, this motion does not account for the asymmetry in the observed line shape. A computer simulation of this lineshape showed that the asymmetry parameter was 0.07–0.08, unusually large for a methyl deuteron, while the splitting, 36 kHz, was several kilohertz less than expected. The goal of the work reported herein was to determine the cause of this unusual methyl line shape.

We performed ab initio molecular orbital calculations[8] to see if the calculated static ^2H EFG tensors of thymine–*methyl–d*$_3$ could explain the large asymmetry parameter. The static EFG tensors of toluene–*methyl–d*$_3$ were also calculated, because the methyl group is also adjacent to an aromatic ring, but the observed asymmetry parameter, in contrast to that of thymine, is very small (less than 0.02).[9]

Figure 4.1 shows the calculated angular dependence of the deuterium quadrupole

coupling constant (QCC) with respect to methyl group orientation for thymine and toluene. We note that for thymine with a dihedral angle of zero, the deuteron-exocyclic oxygen internuclear distance is only 2.436 Å. The Mulliken atomic charge on the exocyclic oxygen is 0.59 e^-. This value is in good agreement with UPS results[10] and other ab initio calculations.[11] The angle between the vector along the deuteron-excyclic oxygen atom and the C–^{2}H bond vector is 103.46° at a dihedral angle of zero. From a point charge model, the partially shielded nuclear charge at the oxygen site creates an EFG component of –5.8 kHz/charge along the C–H bond vector of the thymine methyl group. As seen in the electron density map shown in Figure 4.3, a point charge model does not fully account for the electron density in the oxygen p-orbitals that lie close to the methyl deuteron site. A more exact calculation involving integration over all occupied molecular orbitals of the thymine molecule gives the deuterium QCCs shown in Figure 4.1. The 8–kHz reduction in QCC is noteworthy for the deuterium closest to the exocyclic oxygen site, i.e., $\emptyset = 0°$. The effect of the exocyclic oxygen on the EFG is also seen in the orientation of the *z*–axis, as shown in Figure 4.2. We note that the aromatic π-electrons do not affect the deuterium QCC or the *z*–axis orientation in toluene to nearly the same extent as the exocyclic oxygen of thymine. The calculated asymmetry parameters of the static EFG tensors of both thymine and toluene are about 0.05. Following the convention $|q_{zz}| \geq |q_{yy}| \geq |q_{xx}|$, the calculations showed, for both molecules, that the *y*–axis of the deuterium EFG is normal to the C_{ring}–C_{methyl}–D plane while the *x*–axis lies in the C_{ring}–C_{methyl}–D plane.

Since the hydrogen positions of the methyl group are unknown in the thymine crystal,[12] the space-averaged (C_3 jumps) ^{2}H EFG tensor is calculated based upon the ab initio results (Figures 4.1 and 4.2), varying the dihedral angle $\emptyset$ from 0° to 60°. At $\emptyset = 0°$, 20°, 40°, and 60°, the calculated values of the asymmetry parameter are 7%, 5%, 4%, and 3%, respectively. So a dihedral angle of less than 20° in thymine explains the experimentally obtained asymmetry parameter. On the other hand the calculated asymmetry

parameters of the space-averaged ^2H EFG tensor for toluene are always less than 1% because the static EFG is nearly independent of Ø. We believe that because a large asymmetry parameter is calculated over a large range of dihedral angle, that axially asymmetric spectra of the thymine moiety will be commonly seen.[15]

This study illustrates that reliable analysis of ^2H line shapes requires careful consideration of both the dynamic and static factors that affect the EFG tensor. In the case of thymine–*methyl*–d_3, the large ^2H methyl asymmetry parameter is caused by the partially shielded nuclear charge density on the exocyclic oxygen, rather than motional narrowing.

Acknowledgement. Computational support was provided by the Louisiana State University. We also thank one of the referees for bringing the hexamethylbenzene results[16] to our attention.

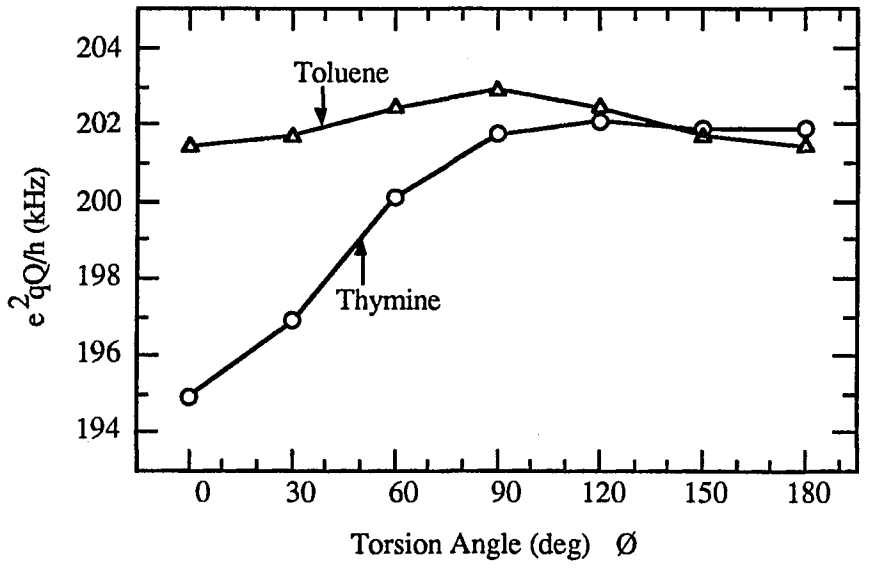

Figure 4.1. Calculated deuterium quadrupole coupling constant for C–^{2}H in methyl group of thymine (o) and toluene (Δ) vs. Ø.. Torsion angle, Ø, is defined by the atoms $C_{carbonyl}$–C_{ring}–C_{methyl}–D.

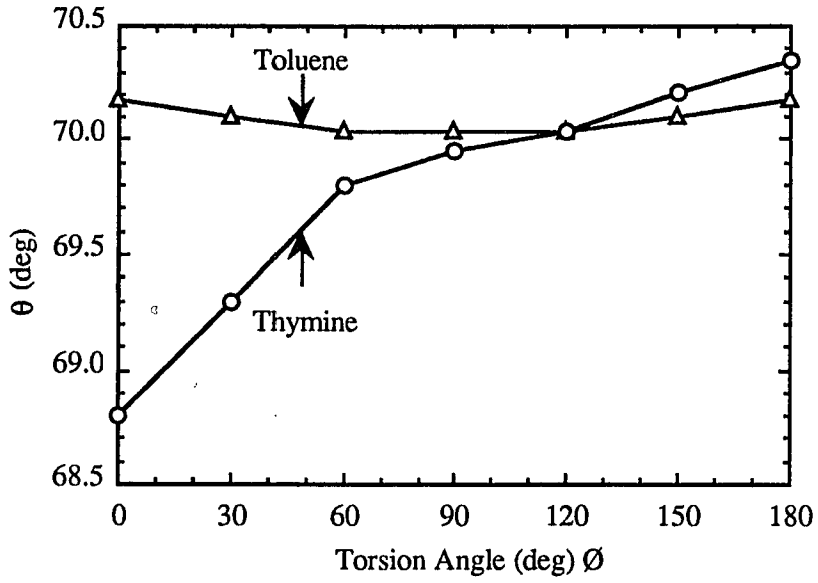

Figure 4.2 The orientation of the z–axis, θ, of calculated deuterium electric field gradient tensor for C–^{2}H in methyl group of thymine (o) and toluene (Δ) with respect to the C_3 rotation axis. Torsion angle, Ø, is defined by the atoms $C_{carbonyl}$–C_{ring}–C_{methyl}–D.

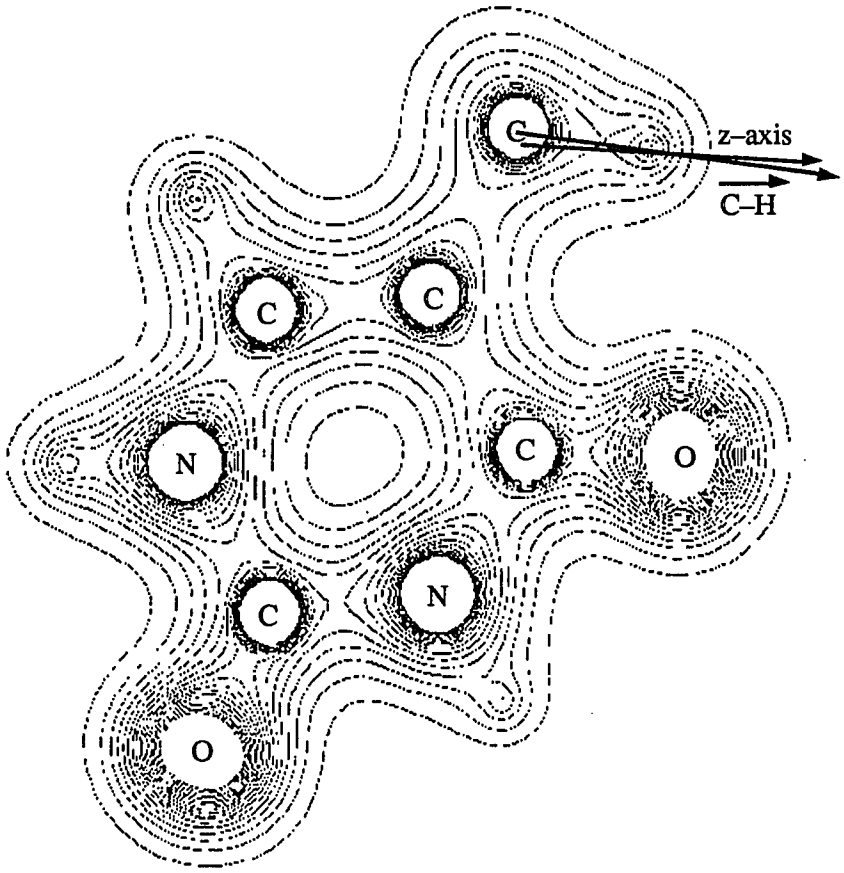

Figure 4.3 Electron density map of thymine from the ab initio MO calculation. Note that the z–axis is about 2° out of the C–H bond direction when Ø = 0°. Contours at 0.05 e/ $Å^3$; maximum contour at 1.0 e/ $Å^3$.

References

1. Spiess, H. W. *Adv. Polym. Sci.* **1985**, *66*, 23-58.
2. Vold, R. R.; Brandes, R.; Tsang, P.; Kearns, D. R.; Vold, R. L. *J. Am. Chem. Soc.* **1986**, *108*, 302-305.
3. Torchia, D. A. *Ann. Rev. Biophy. Bioeng.* **1984**, *13*, 125-144.
4. Eckman, R.; Vega, A. J. *J. Am. Chem. Soc.* **1983**, *105*, 4841-4842.
5. Batchelder, L. S.; Niu, C. H.; Torchia, D. A. *J. Am. Chem. Soc.* **1983**, *105*, 2228–2234.
6. Thymine–*methyl*–d_3 was purchased from Merck Co. ND-deuteriated thymine was prepared by dissolving thymine in warm D_2O and lyophilizing. Deuteriation was checked by ^1H NMR and found to be at least 85% deuteriated. Solid-state ^2H NMR spectra obtained at 38.45 MHz can be found in original paper (Figure 1).
7. Torchia, D. A.; Szabo, A. *J. Magn. Reson.* **1982**, *49*, 107-121.
8. GAUSSIAN 82 and the associated properties package was used to calculate the ^2H EFG in molecular and principal axis systems.[13] An interactive matrice manipulation program (Speakeasy) was used for determining the orientation of the EFG tensor. A Gaussian basis set (6–31G) was used for the results reported here. One calculation of toluene was done with p- and d-orbitals on the methyl hydrogen atoms; relative to (6–31G) basis set results, all electric field gradients were reduced by roughly the same factor, 0.9, while the orientation of the EFG tensor was unchanged. No correction were made for C–H stretching vibrational effects.[14]
9. Eckman, R. *J. Chem. Phys.* **1983**, *79*, 524-525.
10. Palmer, M. H.; Wheeler, J. R.; Kwiatowski, J. S.; Lesyng, B. *J. Mol. Struct.* **1983**, 92, 283-302.
11. Scanlan, M. J.; Hillier, I. H.; MacDowell, A. A. *J. Am. Chem. Soc.* **1983**, *105*, 3568-3571.

12. Ozeki, K.; Sakabe, N.; Tanaka, J. *Acta Crystallogr., Sect. B* **1969**, *25*, 1038-1045.

13. GAUSSIAN 82 by: Binkley, J. S.; Frisch, M. J.; DeFrees, D. J.; Raghavachari, K.; Whitesides, R. A.; Schelgel, H. B.; Fluder, E. M.; and Pople, J. A., Carneige-Mellon University, 1984.

14. Kern, C. W.; Matcha, R. L. *J. Chem. Phys.* **1968**, *49*, 2081-2091.

15. An axially asymmetric ^2H powder pattern has been reported[16] for hexamethylbenzene at 130 K. Ab initio and point charge model calculations show that the static ^2H EFG in *o*–xylene is reduced by ca. 4 kHz because of the 0.16 e^+ charge on the nearest hydrogen of neighboring methyl group. We therefore suggest that charge density on neighboring hydrogens is in part responsible for the asymmetric powder pattern observed[16] for hexamethylbenzene. It is also possible that rapid small-amplitude motions of the molecule may contribute to the anisotropy of the EFG in this case.

16. Schwartz, L. J.; Meirovitch, E.; Ripmeester, J. A.; Freed, J. H. *J. Phys. Chem.* **1983**, *87*, 4453-4461.

(Reprinted in part with permission from the *J. Am. Chem. Soc.*, **1988**, *110*, 343–347.

CHAPTER FIVE

Karplus-Type Relationship for Quadrupole Coupling Constants and Asymmetry Parameters for Substituted Acetic Acids

Margo A. Jackisch, William L. Jarrett, Kermin Guo, Frank R. Fronczek,

and Leslie G. Butler*

Received April 13, 1987

Contribution from the

Macromolecular Studies Group

Department of Chemistry

Louisiana State University, Baton Rouge, LA 70803

*To whom correspondence should be addressed.

Department of Chemistry
LOUISIANA STATE UNIVERSITY AND AGRICULTURAL AND MECHANICAL COLLEGE
BATON ROUGE · LOUISIANA · 70803-1804
504/388-3361

Wed, Mar 15, 1989

Copyright Administrator
Books & Journals Division
American Chemical Society
1155 16th Street, N.W.
Washington, D. C. 20036

Dear Sir:

I am writing to you in reference to the article:"Karplus–Type Relationship for Quadruple Coupling Constants and Asymmetry Parameters for Substituted Acetic Acids." that published in the Journal of the American Chemical Society, **1989**, *110*, 343-347. I am a contributing author of this paper. My coauthors, Leslie G. Butler, (listed as "To whom correspondence should be addressed" on the title page of the manuscript), Margo A. Jackisch,William L. Jarrett and Frank R. Fronczek have given me permission to use the relevant excerpts of the manuscript in my Ph.D. dissertation. The relevant excerpts are: (1) an introduction to the problem, (2) my contriburion to the collaborative research effort, and (3) the conclusion reached in this work.

Please forward permission to reprint the relevant excerpts of the manuscript. I will appreciate your prompt reply.

Sincerely,

Kermin Guo

Kermin Guo
Box B-18, Department of Chemistry
Louisiana State University
Baton Rouge, LA 70803

Leslie G. Butler

Coauthor, Leslie G. Butler

Margo A. Jackisch

Coauthor, Margo A. Jackisch

Frank R. Fronczek

Coauthor, Frank R. Fronczek

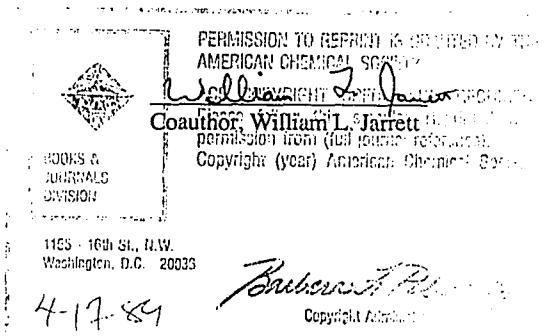

Coauthor, William L. Jarrett

Abstract:

The deuterium quadrupole coupling constant for the methyl group in the acetic acid dimer was calculated as a function of the torsion angle about the carbon-carbon bond. The results show that when a deuteron approaches either of the negatively charged oxygen atoms, the quadrupole coupling constant for the deuteron is reduced by as much as 4.2 kHz. Both the calculated quadrupole coupling constant, $e^2q_{zz}Q/h$, and asymmetry parameter, η, are fitted with a Karplus-type equation: $e^2q_{zz}Q/h = A - 0.5491\ \cos\theta - 1.7859\ \cos 2\theta$; $\eta = 0.0491 + 0.0058\ \cos\theta - 0.0081\ \cos 2\theta$. Adiabatic demagnetization in the laboratory frame spectroscopy at 77 K for (4-chlorophenyl)[2,2-$^2H_2$]acetic acid showed two inequivalent deuteron sites that, on the basis of deuterium double transitions, are demonstrated to be due to two deuterium sites bound to the same carbon atom. The solid-state structure of (4–chlorophenyl)acetic acid was determined by single-crystal X-ray diffraction. The ADLF and structural data for (4-chlorophenyl)[2,2-$^2H_2$]acetic acid were used to obtain a preliminary value for the *A* parameter of 170.767 kHz.

5.1 Introduction

Solid-state deuterium NMR spectroscopy is mainly used to study molecular motions[1-7] but rarely to determine solid-state structures. There are relatively few methods for utilizing solid-state deuterium NMR spectra to measure structural parameters. In 1964, Chiba reported a correlation between deuterium quadrupole coupling constants and hydrogen bond lengths between oxygen donors and acceptors.[8] The deuterium asymmetry parameter has also been used to assign distances in hydrogen bonds.[9,10] This work has been extended to include nitrogen donors and acceptors.[11] However, there are no reported correlations between carbon-bound deuterium quadrupole coupling constants and solid-state structural features. Herein, we report preliminary results for a Karplus-type relationship[12,13] for measuring torsion angles involving C–^{2}H sites α to a carboxyl group. This is the first report of an expression that allows one to convert solid-state deuterium NMR data into structural information for a C–^{2}H bond adjacent to some functional group. The possible areas of application are as varied as the current use of solid-state deuterium NMR, ranging from polymers to biomaterials to surface-adsorbed species.

It is generally assumed that, in the aliphatic C–^{2}H bond, there is a characteristic value for the static deuterium quadrupole coupling constant. Furthermore, in the high-field solid-state deuterium NMR experiment, all observed reductions in the apparent quadrupole coupling constant have been attributed to molecular motions that reorient the C–^{2}H bond with respect to the applied magnetic field. However, Hiyama et al. found that in thymine–*methyl–d*$_3$ the methyl group deuteron resonances are affected by an adjacent exocyclic oxygen atom.[14] Also of note, the C^{2}H$_2$ units in succinic acid,[15] α–glycine,[16] and DL–serine[17] have at least two distinct values for the deuterium quadrupole coupling constant. In this work, we report the high-resolution adiabatic demagnetization in the laboratory frame (ADLF) spectrum of (4-chlorophenyl)[2,2-^{2}H$_2$]acetic acid, which reveals inequivalent deuterium sites. The origin of the inequivalency is traced to the carboxylic

oxygen atoms adjacent to the C^2H_2 unit.

In solid-state deuterium NMR spectroscopy, structural information comes about from the fact that the deuterium NMR spectrum is determined by the electric field gradient at the deuterium nuclear site. The electric field gradient is a tensor quantity with a trace of zero.[18] In reports of solid-state deuterium NMR data, the common convention is to refer to an axis system that diagonalizes the electric field gradient tensor; the largest diagonal element of the tensor, eq_{zz}, gives the quadrupole coupling constant, $e^2q_{zz}Q/h$.[19] The quadrupole coupling constant is a direct function of the charge distribution in the close vicinity of the deuterium nucleus, as shown in equation 5.1.

$$eq_{zz} = \sum_n K_n \frac{3z_n^2 - r_n^2}{r_n^5} - e\left\langle \Psi^* \middle| \sum_i \frac{3z_i^2 - r_i^2}{r_i^5} \middle| \Psi \right\rangle \qquad (5.1)$$

Note that only occupied molecular orbitals, ignoring electron correlation, contribute to the electric field gradient; the absence of contributions from excited states greatly simplifies the calculations required to compute quadrupole coupling constants. This is in contrast to the situation for chemical shift calculations. The other major elements of the electric field gradient tensor, eq_{xx} and eq_{yy}, are obtained by a similar summation of neighboring charge with a $1/r^3$ distance dependence. Also specified in reports of solid-state deuterium NMR spectra is the asymmetry parameter, η, of the electric field gradient tensor (equation 5.2).

$$\eta = (eq_{xx} - eq_{yy})/eq_{zz} \qquad (5.2)$$

We note that C–^{2}H bonds, with local axial symmetry, should have asymmetry parameters close to zero.

This report consists of four components: (1) The results of an ab initio molecular

orbital calculation of an acetic acid dimer, in which the methyl group orientation is varied with respect to the oxygen atoms of the carboxylic group, are fitted to Karplus-type equations. (2) A single-crystal X-ray diffraction experiment of (4-chlorophenyl)acetic acid shows two distinct C–H sites α to the carboxyl group. (3) The ADLF spectrum of (4–chlorophenyl)[2,2-$^2H_2$]acetic acid shows two inequivalent deuterium sites. (4) Analysis of the ADLF double transitions proves that the two inequivalent deuterium sites are bound to the same carbon atom.

5.2 Molecular Orbital Calculations

The electric field gradient tensors at the methyl hydrogen sites in acetic acid were obtained from ab initio molecular orbital calculations with the GAUSSIAN 82 program and a 6–31G** basis set.[20,21] In this work, we have taken the deuterium nuclear quadrupole moment as 2.86×10^{-27} cm^2.[22] The convention used herein for reporting the electric field gradient is $|q_{zz}| \geq |q_{yy}| \geq |q_{xx}|$.[19] The acetic acid dimer geometry was taken from the literature;[23] all conformations of the dimer had at least a center of symmetry. As a brief check of superposition error, some conformations of the dimer were studied with a 6–31G basis set, while some monomer conformations were examined with both 6–31G and 6–31G** basis sets.[24] Minor changes in the deuterium quadrupole coupling constant and asymmetry parameter were found with the smaller basis set, but, most importantly, the orientation of the electric field gradient tensor was not affected. No corrections were made for vibrational effects that are expected to slightly reduce the magnitude of the electric field gradient tensor elements.[25]

5.3 Experimental Section

The ADLF spectra of (4-chlorophenyl)[2,2-$^2H_2$]acetic acid were obtained on a home-built spectrometer.[26,27] All spectra were obtained at 77 K. The high-field strength

was 0.3 T, corresponding to a frequency of 15 MHz (^{1}H). The 90° pulse length for ^{1}H was 4 μs with a probe ringdown time of approximately 10 μs. The signal was acquired with an Ostroff-Waugh pulse sequence set to generate 128 spin echoes;[28] each echo is individually digitized. The zero-field rf amplitude was 0.034 G peak for single quantum spectra and 1.9 G peak for the double-transition spectra.

The deuterium fine structure[29-35] in the ADLF spectrum was analyzed with Ragle's program.[35] The electric field gradient tensor orientation with respect to the molecular coordinate system was taken from an acetic acid dimer calculation with a conformation set to yield the same torsion angles as found in the crystal structure of (4–chlorophenyl)acetic acid. The calculated electric field gradient tensor orientations were adjusted to give a right-handed coordinate system prior to using the Ragle program.

5.4 Results and Discussion

On the basis of the significant difference between the C1–O1 and C1–O2 bond distances and on the correlation noted by Dieterich et al.,[36] there appears to be little crystallographic disorder of the type that would result in an interchange of C–OH and C=O sites in the carboxyl group in (4-chlorophenyl)acetic acid. Thus, we conclude that O2 is the hydroxyl oxygen site and O1 the carbonyl. This assignment is supported by the location and refinement of the acid H atom. When we assume tetrahedral geometry at C2, the torsion angles shown in Figure 5.1 are related by an angle of 120° to the O2–C1–C2–C3 torsion angle, 150.6(2)°. Figure 5.1 shows a portion of the $CH_2(C_6H_4Cl)$ unit viewed along the C2–C1 bond and the torsion angles for the two inequivalent methylene hydrogen atoms.

The calculated deuterium quadrupole coupling constant and asymmetry parameters for an acetic acid dimer are shown in Figure 5.2. To minimize the basis set dependence, the acetic acid results are plotted as the change in the deuterium quadrupole coupling constant.

The reference value ($e^2q_{zz}Q/h$= 218.2 kHz) is for a deuterium site rotated so as to give maximum distance from the oxygen atoms to the deuterium site and corresponds to a torsion angle, θ, of 90°. We note that there is a large variation in $\Delta e^2q_{zz}Q/h$ with rotation angle; it reaches a maximum of –4.2 kHz for a deuteron at closest approach to the hydroxyl oxygen site, θ = 0°. The points shown in Figure 5.2 were fitted by Karplus-type equations to give equations 5.3 and 5.4. Because of the tendency

$$e^2q_{zz}Q/h = A - 0.5491\cos\theta - 1.7859\cos2\theta \qquad (5.3)$$

$$\eta = 0.0491 + 0.0058\cos\theta - 0.0081\cos2\theta \qquad (5.4)$$

for calculated deuterium quadrupole coupling constants to be larger than experimental values,[9,37,38] the A parameter of equation 5.3 was determined by use of experimentally derived deuterium quadrupole coupling constants.

On the basis of the torsion angles shown in Figure 5.1 and on the Karplus-type equation, equation 5.3, for predicting the deuterium quadrupole coupling constant, the high resolution, zero-field ADLF spectrum of (4-chlorophenyl)[2,2-$^2H_2$]acetic acid should show two different sets of deuterium ν_- and ν_+ transitions. While four transitions are indeed observed, as shown in Figure 5.3, the assignment is not straightforward. The methods used for spectral interpretation are similar to those applied to other coupled deuterium spin systems: (1) Zeeman-perturbed ADLF spectroscopy and (2) analysis of the deuterium-deuterium induced fine structure and double transitions. Application of small magnetic fields causes the ν_- and ν_+ transitions to be asymmetrically broadened in a characteristic fashion; the ν_- transition is broadened to lower frequency, the ν_+ to higher frequency.[39] By this technique, the peaks at 125.0 (7) and 129.0 (7) kHz are identified as the ν_- transitions and the ones at 127.0 (7) and 132.0 (7) kHz as the ν_+ transitions.

Observations of deuterium-deuterium dipolar coupling induced fine structure and double transitions were used to assign the ν_- transition of a deuteron to its corresponding ν_+ transition. Figure 5.4 shows the observed double-transition spectrum together with the calculated transition frequencies and relative intensities.[29-35] The fine structure shown in

Figure 5.3 (top trace) contributes to the rather large line width, $\Delta v \sim 1.5$ kHz, in the 0–G spectrum. The observation of double transitions conclusively shows that the two deuterium sites are in close proximity, less than several angstroms from each other. Also, the form of the double-transition spectrum is incompatible with other possible explanations for two distinct deuterium sites, for instance, two crystallographic modifications of (4–chlorophenyl)acetic acid.

The deuterium ADLF spectroscopy and structural data for (4-chlorophenyl)[2,2-$^2H_2$]acetic acid are summarized in Table 5.1. The assignment of the site with the larger value of the deuterium quadrupole coupling constant to the deuteron with a torsion angle of 89° is based upon the Karplus-type relationship given in equation 5.3. The "C–^{2}H distant" from an oxygen atom site has a value of the deuterium quadrupole coupling constant that is similar to values found in simple hydrocarbons. For comparison, the C^2H_2 unit in [9,9–$^2H_2$]fluorene has a deuterium quadrupole coupling constant of 173(1) kHz.[40]

In the foregoing analysis, the effect of the phenyl substituent on the C^2H_2 unit has been ignored. This approach is justified on two counts: First, molecular orbital calculations of toluene have shown that there is only a small perturbation of the aliphatic C–^{2}H bonds that is caused by the aromatic π–electrons or the ortho hydrogens.[14] Second, in (4–chlorophenyl)acetic acid, the C1–C2–C3–C4 torsion angle is 94.8 (3)°. This angle is very close to 90°, an orientation that places both methylene hydrogens in equivalent positions with respect to the phenyl ring.

The ADLF and structural data for (4-chlorophenyl)[2,2-$^2H_2$]acetic acid were used to obtain a preliminary value for the *A* parameter of equation 5.3 as 170.767 kHz. All values of the parameters obtained from the acetic acid calculations should be regarded as preliminary until confirmed by experiment as inductive effects from substituents and steric effects may modify the results.

Table 5.1. Deuterium Quadrupole Coupling Constants, Asymmetry Parameters, and Structural Data for (4-Chlorophenyl)[2,2-$^2H_2$]acetic Acid

	C–^{2}H distant	C–^{2}H near
d(O...^{2}H),[a] Å	2.70(3)	2.36(2)
θ,[b] deg	89	31
ν_+	132.0(7)	127.0(7)
ν_-	129.0(7)	125.0(7)
$e^2q_{zz}Q/h$, kHz	174.0(9)	168.0(9)
η	0.034(16)	0.024(17)

[a] Distance from deuteron to nearest oxygen atom. [b] θ is the torsion angle between the hydroxyl oxygen and the deuteron as defined in Figures 5.1 and 5.2.

5.5 Conclusions

Neighboring oxygen atoms can affect the deuterium quadrupole coupling constant of C–^{2}H bonds. In acetic acid and substituted acetic acids, the magnitude of the effect is related to the ^{2}H–C–C–OH torsion angle. A Karplus-type equation fits the calculated values well.

In summary, the oxygen-perturbed C–^{2}H site has a substantially different quadrupole coupling constant than do unperturbed C–^{2}H sites. As noted by Hiyama et al.[14] neighboring oxygen atoms have an unexpected effect on the solid-state deuterium NMR spectrum of deuteriated methyl groups. This work provides further confirmation of their report.

The fact that the calculated deuterium quadrupole coupling constants and asymmetry parameters of acetic acid dimer can be fitted by a Karplus-type equation is very interesting. Heretofore, there were no reported methods for correlating deuterium quadrupole coupling constants with solid-state structural features. Further work is now in progress to refine experimental values for the parameters A, B, and C. It should be straightforward to extend the method to other functional groups, for example, esters, ketones, and sulfones.

Acknowledgement. The support of the Research Corp., the Petroleum Research Fund, administered by the American Chemical Society, and the LSU Center for Energy Studies is gratefully acknowledged. Purchase of 100- and 400-MHz NMR spectrometers was made possible by an NIH shared instrumentation grant (1 S10 RR02459-01). The purchase of the Enraf-Nonius CAD4 diffractometer was made possible by an NSF instrumentation grant (CHE-8500781). We thank Drs. Dennis A. Torchia and Yukio Hiyama for their encouragement with this work and Dr. John L. Ragle for his spectral simulation program.

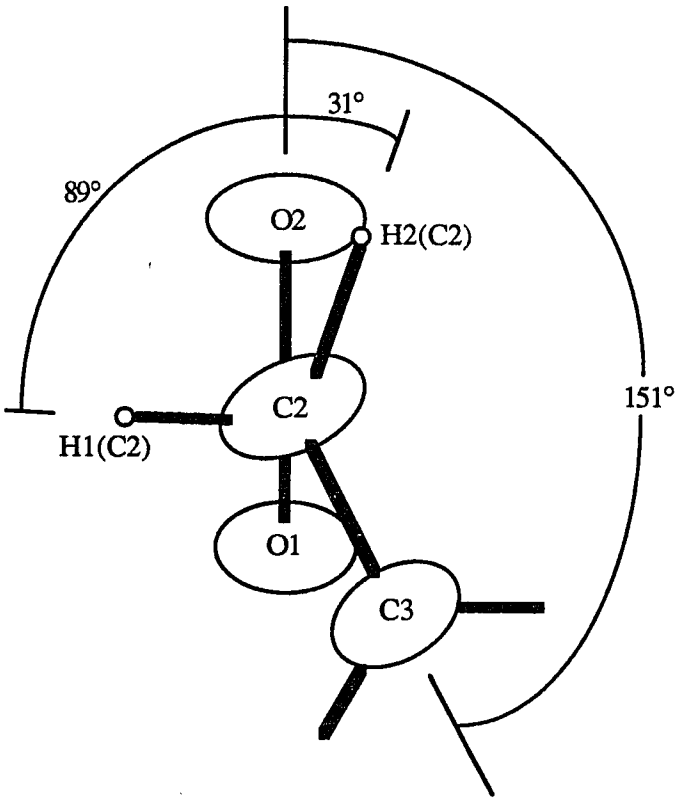

Figure 5.1 Relative orientation of the carboxyl acid group and the CH_2 unit of (4–chlorophenyl)acetic acid. Viewed along the C2–C1 bond. The acid carbon, C1, is hidden from view by C2.

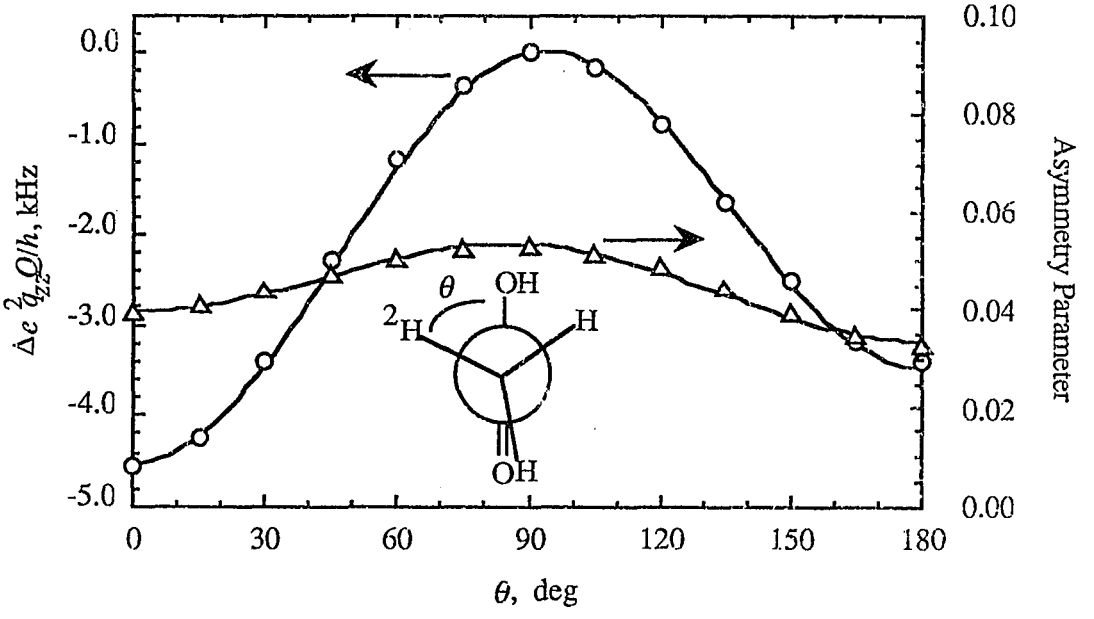

Figure 5.2 Calculated deuterium quadrupole coupling constants and asymmetry parameters for the acetic acid dimer as a function of the ^{2}H–C–C–OH dihedral angle: o, $\Delta e^2 q_{zz} Q/h$; Δ, asymmetry parameter. The solid lines are based on the Karplus-type equations, equations 5.3 and 5.4, given in the text. The average deviations of the fit for $\Delta e^2 q_{zz} Q/h$ and asymmetry parameter are 0.013 and 0.0002 respectively.

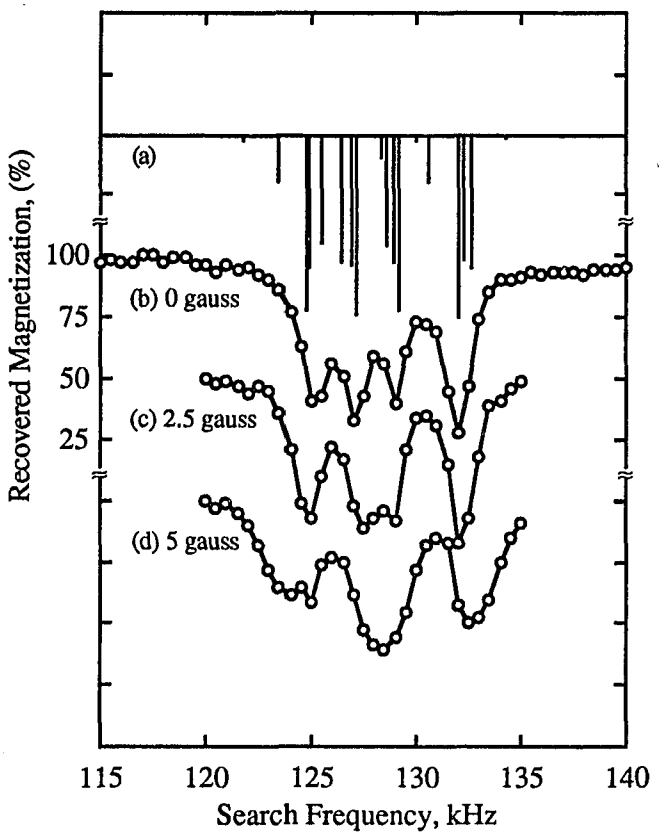

Figure 5.3 Deuterium ADLF spectra of (4-chlorophenyl)[2,2-$^2H_2$]acetic acid taken at 77 K with 0.5-kHz search frequency increments. (a) The calculated fine structure for a C^2H_2 unit. Initial assignment of transitions based upon frequency shifts caused by a small applied magnetic field: (b) 0 G, (c) 2.5 G, (d) 5 G.

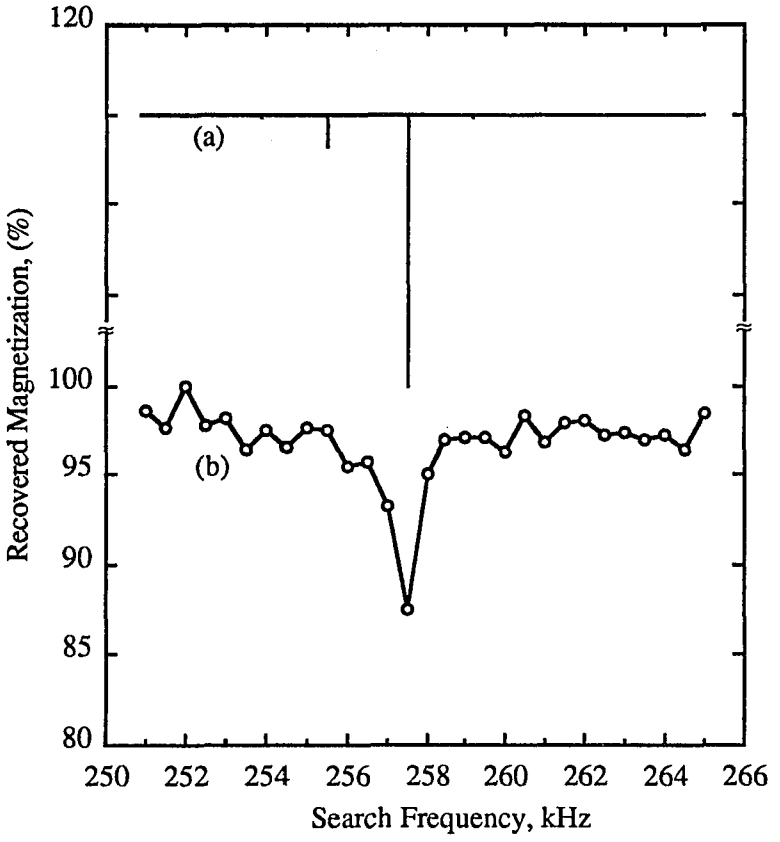

Figure 5.4 Deuterium double-transition ADLF spectra: (a) calculated double-transition spectrum for a C^2H_2 unit; (b) experimental spectrum taken at 77 K with 0.5-kHz search frequency increments.

References

1. Spiess, H. W. *Adv. Polym. Sci.* **1985**, *66*, 23-26.
2. Jelinski, L. W. *Ann. Rev. Mater. Sci.* **1985**, *15*, 359-377.
3. Vold, R. R.; Brandes, R.; Tsang, P.; Kearns, D. R.; Vold, R. L.; Rupprecht, A. *J. Am. Chem. Soc.* **1986**, *108*, 302-303.
4. Torchia, D. A. *Ann. Rev. Biophys. Bioeng.* **1984**, *13*, 125-144.
5. Frey, M. H.; DiVerdi, J. A.; Opella, S. J. *J.* Am. *Chem. Soc.* **1985**, *107*, 7311–7315.
6. Eckman, R.; Vega, A. J. *J. Phys. Chem.* **1986**, *90*, 4679-4683.
7. Major, P. D.; Raidy, T. E.; Ellis, P. R. *J. Am. Chem. Soc.* **1986**, *108*, 8123-8129.
8 Chiba, T. *J. Chem. Phys.* **1964**, *41*, 1352-1358.
9. Butler, L. G.; Brown, T. L. *J. Am. Chem. Soc.*, **1981**, *103*, 6541-6549.
10. Brown, T. L.; Butler, L. G.; Curtin, D. Y.; Hiyama, Y.; Paul, I. C.; Wilson, R. G. *J. Am. Chem. Soc.* **1982**, *104*, 1172-1177.
11. Keiter, E. A. Ph.D. Dissertation, University of Illinois, 1986.
12. Karplus, M. *J. Chem. Phys.* **1959**, *30*, 11-15.
13. Colucci, W. J.; Gandour, R. D.; Mooberry, E. A. *J. Am. Chem. Soc.* **1986**, *108*, 7141-7147.
14. Hiyama, Y.; Roy, S.; Guo, K.; Butler, L. G.; Torchia, D. A. *J. Am. Chem. Soc.* **1987**, *109*, 2525-2526.
15. Boroske, E.; Mayas, L.; Mobius, K. *J. Magn. Reson.* **1979**, *35*, 231-246.
16. Weeding, T.; Kwiram, A. L.; Rawling, D. C.; Davidson, E. R. *J. Chem. Phys.* **1985**, *82*, 3516-3526.
17. Hartzell, C. J.; Kwiram, A. L. *J. Magn. Reson.* **1987**, *73*, 315-322.
18. Flygare, W. H. *Molecular Structure and Dynamics*; Prentice-Hall: Englewood Cliffs, NJ, 1978.

19. Poole, C. P., Jr.; Farach, H. A. *The Theory of Magnetic Resonance*; Wiley-Interscience: New York, 1972.

20. Binkley, J. S.; Frisch, M. J.; DeFrees, D. J.; Raghavachari, K.; Whitesides, R. A.; Schelgel, H. B.; Fluder, E. M.; Pople, J. A. GAUSSIAN 82; Carneige-Mellon University: Pittsburgh, PA, 1984.

21. Hariharan, P. C.; Pople, J. A. *Theor. Chim. Acta* **1973**, *28*, 213-222.

22. Reid, R. V., Jr.; Vaida, M. L. *Phys. Rev. Lett.* **1975**, *34*, 1064.

23. (a) Pross, A.; Radom, L. *J. Am. Chem. Soc.* **1978**, *100*, 6572-6575. (b) Nagaoka, S. I.; Hirota, N.; Matsushita, T.; Nishimoto, K. *Chem. Phys. Lett.* **1982**, *92*, 498–502.

24. Hehre, W. J.; Ditchfield, D.; Pople, J. A. *J. Chem. Phys.* **1972**, *56*, 2257–2261.

25. Kern, C. W.; Matcha, R. L. *J. Chem. Phys.* **1968**, *49*, 2081-2091.

26. A similar, but non-computer-controlled instrument is described in: Cheng, C. P.; Brown, T. L. *J. Am. Chem. Soc.* **1979**, *101*, 2327-2334.

27. Butler, L. G.; Reiner, C. A.; Brown, T. L. *Rev. Sci. Instrum.* **1982**, *63*, 984-988.

28. Ostroff, E. D.; Waugh, J. S. *Phys. Rev. Lett.* **1966**, *16*, 1097-1098.

29. Edmonds, D. T.; Hunt, M. J.; MacKay, A. L. *J. Magn. Reson.* ***1973***, ***11***, 77-82.

30. Edmonds, D. T.; Hunt, M. J.; MacKay, A. L. *J. Magn. Reson.* **1975**, *20*, 505-514.

31. Edmonds, D. T.; White, A. A. L. *J. Magn. Reson.* **1978**, *31*, 149-159.

32. d'Avignon, D. A.; Brown, T. L. *J. Phys. Chem.* **1981**, *85*, 4073-4079.

33. Day, R. O.; Hadipour, N.; Ragle, J. L. *J. Magn. Reson.* **1984**, *57*, 369–384.

34. Day, R. O.; Hadipour, N.; Ragle, J. L. *J. Magn. Reson.* **1984**, *59*, 373–380.

35. Hadipour, N.; Ragle, J. L. *Z. Naturforsch. A: Phys., Phys. Chem., Kosmophys.* **1985**, *40A*, 355-360.

36. Dieterich, D. A.; Paul, I. C.; Curtin, D. Y. *J. Am. Chem. Soc.* **1974**, *96*, 6372–6380.

37. Dunning, T. H., Jr.; Hay, P. J. In *Methods of Electronic Structure Theory*; Schaefer, H. F., III, Ed.; Plenum: New York, 1977.

38. Zamani-Khamiri, O.; Hameka, H. F. *J. Chem. Phys.* **1981**, *75*, 781-786.

39. Edmonds, D. T. *Phys. Rep. C* **1977**, *29*, 233-290.

40. Altbach, M. I.; Hiyama, Y.; Gerson, D. J.; Butler, L. G. *J. Am. Chem. Soc.* **1987**, *109*, 5529-5531.

(Reprint in part with permission from the *J. Magn. Reson.* **1989**, *82*, 76–85.

CHAPTER SIX

A Karplus-Type Relationship for Deuterium Quadrupole Coupling Constants, II: Inequivalent C–^{2}H Sites in Substituted Arylacetic Acids.

William L. Jarrett, Kermin Guo, Margo A. Jackisch,

and Leslie G. Butler*

Received May 12, 1988; revised July 13, 1988

Contribution from the

Macromolecular Studies Group

Department of Chemistry

Louisiana State University, Baton Rouge, LA 70803

---

*To whom correspondence should be addressed.

APR 13 1989

Department of Chemistry
LOUISIANA STATE UNIVERSITY AND AGRICULTURAL AND MECHANICAL COLLEGE
BATON ROUGE · LOUISIANA · 70803-1804
504/388-3361

Fri, Mar 17, 1989

Right and Permission
Academic Press
Production Department
1250 Sixth Avenue.
San Diego, CA 92101

Dear Sir:

I am writing to you in reference to the article that has recently been accepted for publication in the Journal of Magnetic Resonance: "A Karplus–Type Relationship for Deuterium Quadruple Coupling Constants. II. Inequivalent C–^{2}H Sites in Substituted Acetic Acids.". I am a contributing author of this paper. My coauthors, Leslie G. Butler, William L. Jarrett, and Margo A. Jackisch have given me permission to use the relevant excerpts of the manuscript in my Ph.D. dissertation. The relevant excerpts are: (1) an introduction to the problem, (2) my contribution to the collaborative research effort, and (3) the conclusion reached in this work.

Please forward permission to reprint the relevant excerpts of the manuscript. I will appreciate your prompt reply.

Sincerely,

Kermin Guo
Box B-18, Department of Chemistry
Louisiana State University
Baton Rouge, LA 70803

Coauthor, Dr. Leslie G. Butler

William L. Jarrett

Coauthor, Dr. William L. Jarrett

Coauthor, Margo A. Jackisch

PLEASE TURN OVER

April 17, 1989

PERMISSION GRANTED, provided that 1) complete credit is given to the source, including the Academic Press copyright line; 2) the material to be used has appeared in our publication without credit or acknowledgement to another source and 3) if commercial publication should result, you must contact Academic Press again.

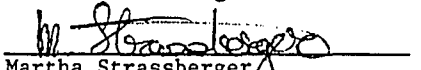

Martha Strassberger
Contracts, Rights and Permissions
ACADEMIC PRESS, INC.
Orlando, Florida 32887

Abstract

Solid-state deuterium NMR spectra have been obtained for several substituted acetic acids. The single quantum and double transition zero-field deuterium spectra for the methylene deuterons in a molecule are shown. Analysis of the spectra indicated that the methylene deuterons can have different quadrupole coupling constants even though they are bound to the same carbon site. The major source of the inequivalency has been traced to the neighboring oxygen atoms of the carboxylic acid group. A useful parameter to describe the geometry of the system is the $^{2}H–C_{alpha}–C_{acid}–OH$ torsion angle. The value of the deuterium quadrupole coupling constant is correlated with the $^{2}H–C_{alpha}–C_{acid}–OH$ torsion angle and is described by a Karplus-type relationship in the form of $A + B\cos(\theta) + C\cos(2\theta)$.

6.1 Introduction

Solid-state deuterium NMR spectroscopy can be a valuable tool in providing dynamic and static structural information. The parameters that are measured, the quadrupolar coupling constant, $e^2q_{zz}Q/h$, and the asymmetry parameter, η, yield information about the distribution of electron density and nuclear charge about the deuterium site. The effect of neighboring atoms on the deuterium quadrupole coupling constant of an X–^{2}H bond has been recognized and utilized: In O–^{2}H···O bonds, the value of the deuterium quadrupole coupling constant is well correlated with the hydrogen bond length;[1-3] and has been extended to include nitrogen donors and acceptors.[4] High-field solid-state deuterium NMR spectroscopy has been used to distinguish between the terminal and bridging metal hydride bonds in polymeric bis(cyclo-pentadienyl)zirconium dideuteride.[5,6] In an organometallic alkyl complex, the values of the carbon-bound deuterium quadrupole coupling constants are compared to an aliphatic reference compound, then the charge on a carbon atom can be determined[7].

Although deuterated carbon sites are common in chemistry, there are no well–established correlations between the value of deuterium quadrupolar coupling constants for carbon-bound deuterons and any feature of the molecular geometry in the solid state. Recently, Hiyama *et al.* noted an unusual asymmetry in the powder pattern for a C–^{2}H site in thymine–*methyl–*d_3 that was traced to a neighboring exocyclic oxygen atom.[8] Subsequently, two distinct deuterium sites with differing quadrupole coupling constants were found in some of the substituted phenyl acetic acid.[9,10] A series of molecular orbital calculations for the acetic acid dimer revealed that the deuterium quadrupole coupling constant and asymmetry parameter depend on the ^{2}H–C$_{alpha}$–C$_{acid}$–OH torsion angle.[10]

Because of the geometry about the carboxylic group in substituted acetic acids, the torsion angle defined by ^{2}H–C$_{alpha}$–C$_{acid}$–OH conveniently describes the relative

orientation of the deuteron sites. The torsion angle, θ, can then be used as the independent parameter in a Karplus-type relationship of the form $e^2q_{zz}Q/h = A + B\cos(\theta) + C\cos(2\theta)$.[11,12] From the results of molecular orbital calculations of the acetic acid dimer (*B* and *C* parameters) and the experimental results for (4-chlorophenyl)[2,2-$^2H_2$]acetic acid (*A* parameter), we have obtained preliminary values for *A*, *B*, and *C*, as shown in equation 6.1, for the value of the deuterium quadrupole coupling constant:[10]

$$e^2q_{zz}Q/h\ (\text{kHz}) = 170.767 - 0.5491\cos(\theta) - 1.7859\cos(2\theta) \quad (6.1)$$

Since these parameters will likely depend on factors other than just the ^2H–C_{alpha}–C_{acid}–OH torsion angle, the notable secondary effects may be associated with the orientation of the aromatic rings bound to the deuterated carbon site,[8,13] and will be the subject of Chapter seven in this dissertation. Herein we report the results of deuterium spectroscopy by adiabatic demagnetization in the laboratory frame (ADLF) for five substituted arylacetic acids: (4-bromophenyl)[2,2-$^2H_2$]acetic acid, 2,2-bis(4-chlorophenyl)[2-^2H]acetic acid, (2-naphthyl)[2,2-$^2H_2$]acetic acid, and (2,2-diphenyl)[2-^2H]acetic acid. Because of the similarity in the orientation of the aromatic ring(s) with respect to the methylene deuterons, the data chosen from the first three compounds, together with previous results for (4-chlorophenyl)[2,2-$^2H_2$]acetic acid,[10] provide support for the proposed relationship between the value of the deuterium quadrupole coupling constant and the ^2H–C_{alpha}–C_{acid}–OH torsion angle in substituted acetic acids. Calculated zero-field spectra for a dipolar-coupled deuterium spin pair are also presented; transitions unique to coupled deuterons are extremely useful in spectral interpretation.

6.2 Experimental

Deuterated substituted acetic acids were prepared by Margo Jackisch in our

laboratory. Substituted arylacetic acids were deuteriated at the *alpha*-carbon site, and the extent of deuteration was followed by integration of the solution ^1H NMR spectra. A complete deuteration of the methylene sites (all sites = C^2H_2) is defined as 100%. Torsion angles were taken from the results of single crystal X–ray diffraction experiments.[14,15] Because of the low scattering factor for hydrogen, the ^2H–C_{alpha}–C_{acid}–OH torsion angle is computed from the C_{phenyl}–C_{alpha}–C_{acid}–OH torsion angle by assuming tetrahedral geometry about C_{alpha}.

ADLF spectra were acquired at 77 K by using the level-crossing technique that has been described in Chapter two of this dissertation. The important experimental parameters conditions were: (1) the zero-field irradiation level typically ranged from 21 to 34 milliGauss peak for single quantum transitions and 1.9 to 4 Gauss peak for double transitions; (2) zero-field irradiation times were between 1.5 and 4 seconds; (3) Zeeman–perturbed zero-field spectra were obtained by continuously energizing a Helmholtz coil about the zero-field region;[16] (4) high-field polarization times were on the order of the proton T_1 (typically, 60 to 300 seconds) at a magnetic field corresponding to a proton Larmor frequency of 15.1 MHz.

In ADLF spectroscopy, dipolar coupling among deuterons[17] gives rise to sets of transitions having numerous sidebands and a set of absorptions labeled "double transitions".[16] Spectral simulations for the highly deuterated samples were calculated by using a program kindly supplied by Prof. J. L. Ragle.[18] As input, the program requires the relative orientation of the deuterium sites and the orientations for the electric field gradient tensors. The internuclear distance used is 1.76 Å and is based on an optimized geometry for the acetic acid dimer.[18] The electric field gradient orientations were taken from molecular orbital calculations for an acetic acid dimer.[10] All of the calculated tensor orientations were adjusted so as to yield a right-handed coordinate system as required by the spectral simulation program.

6.3 Results and Discussion

In the solid state, the deuteron is held in relatively close proximity to the hydroxyl oxygen of the acid group; the nonbonded distance, $d(O\ldots{}^2H)$, is 2.37 Å for 2,2-bis(4-chlorophenyl)[2-^{2}H]acetic acid.[15] The carboxylic acid group may have a significant effect on the electric field gradient at the deuterium site.

Because two deuterium sites can be studied at once, singly substituted acetic acids are preferred over disubstituted acetic acids. However, the spectroscopy of C^2H_2 units is somewhat complicated by the effect of dipolar coupling between the two deuterons. The C^2H_2 systems are unique only in that the two deuterons tend to have more nearly similar, though not identical, electric field gradients. This leads to deuterium spin states that, in zero magnetic field, are nearly degenerate and give rise to a particular form of double transitions and fine structure about the deuterium single quantum transitions.

With regard to nomenclature for discussing C^2H_2 units adjacent to a carboxylic acid group, it usually happens that, in the solid-state, one C–^{2}H site is closer to the hydroxyl oxygen than the other C–^{2}H site. Hence, we will use the terms "Distant" and "Near" to differentiate between deuterium sites bound to the same carbon atom.

The double transition frequencies and the fine structure of the deuterium single quantum transitions can be calculated for the C^2H_2 spin system using as input the ^{2}H–^{2}H internuclear distance, the relative orientations of the two electric field gradient tensors, and the values of the deuterium quadrupole coupling constants and asymmetry parameters. Figure 6.1 shows the calculated single quantum spectra for degenerate and near-degenerate spin states. In this figure, the electric field gradient parameters at one deuteron, the "Distant" site, are held constant: ν_-^D = 128.5 kHz, ν_+^D = 132.0 kHz. At the "Near" site, the quadrupole coupling constant is reduced while the asymmetry parameter is increased so as to maintain a fixed 3.5 kHz separation between the ν_-^N and ν_+^N transitions. As can be seen in Figure 6.1, the most intense transitions in the spectrum of a C^2H_2 unit correspond

closely to the unperturbed ν_+ and ν_- transition frequencies only when the deuterium spin states are well separated in energy, that is, $\nu_+^D - \nu_+^N \geq 3$ kHz. Hence, one would expect that the most accurate values for the deuterium quadrupole coupling constant and asymmetry parameters will be obtained from samples with deuteration levels on the order of 50% or less where C^2H_2 units contribute less than C^1H^2H units to the total spectrum. Finally, the most intense double transition for a C^2H_2 unit occurs 2.63 kHz less than the simple sum of the ν_+^D and ν_+^N transition frequencies; this difference frequency is specific for the EFG orientations and spin state energies used in Figure 6.1.

As a practical matter, the easily accessible deuteration levels, on the order of 50-75%, yield a superposition of spectra due to the presence of both C^1H^2H and C^2H_2 units. In Figure 6.2, the deuterium ADLF spectra of (4-bromophenyl)[2,2-$^2H_2$]acetic acid are shown for four different levels of deuteration. We conclude that, at least for the C^2H_2 systems found in substituted acids, the single-quantum deuterium spectra can be interpreted in a straightforward manner; hence, no corrections for frequency shifts as a function of deuteration have been made for the data listed in Table 6.1.

In deuterium ADLF spectroscopy, Zeeman perturbation has proven to be a consistently useful method to identify a transition as either ν_- or ν_+.[17d,20,21] Small magnetic fields cause the ν_- transition to shift to lower frequency whereas the ν_+ transition is shifted to higher frequency. Figure 6.3 shows the spectrum of (4-bromophenyl)[2,2-$^2H_2$]acetic acid taken at three different magnetic field strengths while being irradiated with the rf search frequency. The assignments of the four transitions, as shown in the figure, are a direct result of this experiment. The frequency shifts due to Zeeman perturbation, to at least 75% deuteration, do not appear to be significantly dependent upon the extent of deuteration; similar results were obtained for samples at 50% deuteration. Spectra for (2-naphthyl)[2,2-$^2H_2$]acetic acid, 2,2-bis(4-chlorophenyl)[2-^2H]acetic acid, and (2,2-diphenyl)[2-^2H]acetic acid are given in Figures 6.4, 6.5, and 6.6, respectively.

Table 6.1. Quadrupole Coupling Constants, Asymmetry Parameters, and Structural Data for Deuterium Bound to Carbon

Parameter	C–^{2}H distant[a]	C–^{2}H near[a]
(4-Chlorophenyl)[2,2-$^2H_2$]acetic acid[b]		
ν_+, ν_-, kHz	132.0(7), 129.0(7)	127.0(7), 125.0(7)
$e^2q_{zz}Q/h$, kHz	174.0(9)	168.0(9)
η	0.034(16)	0.024(17)
d(O...^{2}H), Å	2.70	2.36
θ,[c] deg	89.4	30.6
(4-Bromophenyl)[2,2-$^2H_2$]acetic acid		
ν_+, ν_-, kHz	132.0(7), 129.0(7)	127.5(7), 125.5(7)
$e^2q_{zz}Q/h$, kHz	174.0(9)	168.7(9)
η	0.034(17)	0.024(17)
d(O...^{2}H), Å	2.76(3)[d]	2.39(2)[d]
θ, deg	91.3	28.7
(2-Naphthyl)[2,2-$^2H_2$]acetic acid		
ν_+, ν_-, kHz	128.5(5), 127.5(10)	126.5(10), 124.5(5)
$e^2q_{zz}Q/h$, kHz	170.7(10)	167.3(10)
η	0.012(12)	0.024(18)
d(O...^{2}H), Å	2.66[d]	2.43[d]
θ, deg	76.7(14)	43.3(14)
2,2-Bis(4-chlorophenyl)[2-^{2}H]acetic acid		
ν_+, ν_-, kHz		127.0(5), 126.0(5)
$e^2q_{zz}Q/h$, kHz		168.7(7)
η		0.012(12)
d(O...^{2}H), Å		2.37[e]
θ, deg		18.6
(2,2-Diphenyl)[2-^{2}H]acetic acid		
ν_+, ν_-, kHz		124.5(5), 123.0(5)
$e^2q_{zz}Q/h$, kHz		165.0(7)
η		0.02(1)
d(O...^{2}H), Å		2.463[d]
θ, deg		48.80(15)

[a] "Distant" and "near" qualitatively refer to the nonbonded hydroxyl oxygen-deuteron distance, labeled d(O...^{2}H). [b] Deuterium and structure data from ref 10. [c] The ^{2}H–C_{alpha}–C_{alpha}–OH torsion angle. [d] Structure data from ref 14. [e] Structure data from ref 15.

At this point in the work, accurate transition frequencies have been obtained and individual transitions identified as either ν_- or ν_+. The next step is to pairwise combine ν_- and ν_+ transitions. The most straightforward method is to observe the ν_0 transitions; additivity rules then dictate the appropriate pairwise combinations. However, in ADLF spectroscopy, deuterium ν_0 transitions are seldom observed because of direct proton spin bath heating by the rf search frequency; time-evolution zero-field NMR spectroscopy avoids this problem.[22] An alternative to the observation of ν_0 transitions is the detection of double transitions for the C^2H_2 unit. In fact, the double transition serves two roles: (1) the double transition frequency corresponds to the sum of ν_+^D and ν_+^N, less 1.5 kHz; (2) observation of a double transition, shown in Figure 6.7, unambiguously proves that the two different deuterium sites must be in close proximity, that is, bound to the same carbon atom. Extremely high rf fields may excite intermolecular double transitions between adjacent molecules. This effect has been seen for both ^{10}B and ^{11}B isotopes.[23] Nevertheless, for all of the compounds studied herein, there is only one molecule in the crystallographic asymmetric unit. In these cases, the observation of either inter- or intramolecular double transitions requires that two different deuterium sites be bound to the same carbon atom. Therefore, many alternative spectral interpretations for the four-line pattern, such as two different crystallographic environments, can be ruled out. The four-line pattern shown in Figure 6.2 must be due to two different deuterium sites bound to the same carbon atom. The quadrupole coupling constants and asymmetry parameters for (4-bromophenyl)[2,2-$^2H_2$]acetic acid and (2-naphthyl)[2,2-$^2H_2$]acetic acid are listed in Table 6.1.

Single crystal X-ray diffraction studies provide ^2H–C_{alpha}–C_{acid}–OH torsion angles for each of the two methylene sites in the singly substituted acetic acids. The torsion angles are listed in Table 6.1. The individual deuterium quadrupole coupling constants are

assigned to the two methylene sites by following the trend (described in equation 6.1) already established by the molecular orbital calculations for the acetic acid dimer and also by the observations noted above for [9,9-$^2H_2$]fluorene and 2,2-bis(4-chlorophenyl)[2-^{2}H]acetic acid. In summary, the closer a deuteron is to the hydroxyl oxygen site, the smaller is the value for the deuterium quadrupole coupling constant.

In Figure 6.8, the deuterium quadrupole coupling constants are plotted against ^{2}H–C$_{alpha}$–C$_{acid}$–OH torsion angle. The traces are Karplus-type relationships for the deuterium quadrupole coupling constant. With this expanded data set, both the *A* and *C* parameters of equation 6.1 can now be fitted. Because there is no data available for ^{2}H–C$_{alpha}$–C$_{acid}$–OH torsion angles greater than 100°, the *B* parameter, obtained from molecular orbital calculations of acetic acid dimer, will be retained. Thus, we now have

$$e^2q_{zz}Q/h\ (\text{kHz}) = 170.3(3) - 0.5491\cos(\theta) - 2.6(4)\cos(2\theta). \quad (6.2)$$

There is a correlation between the experimental numbers and the Karplus-type fits for (4-chlorophenyl)[2,2-$^2H_2$]acetic acid, (4–bromophenyl)[2,2–$^2H_2$]acetic acid, and 2,2-bis(4-chlorophenyl)[2-^{2}H]acetic acid. The values for (2-naphthyl)[2,2-$^2H_2$]acetic acid are reduced relative to the other compounds; this deviation may be due to a difference in the orientation of the aromatic rings with respect to the methylene deuterons. This ring effect was investigated and is the subject of the next Chapter.

6.4 Conclusions

In substituted acetic acids, deuterons bound to the *alpha*-carbon atom can have differing values for the deuterium quadrupole coupling constant. In spite of dipolar coupling between the deuterons, peak maxima in the single quantum ADLF spectra of partially-deuterated methylene sites correspond closely to the unperturbed ν_- and ν_+

transition frequencies. The value of the double transition frequency confirms that two different deuterium sites exist at the same carbon site. The values of the deuterium quadrupole coupling constants are correlated with the $^{2}H–C_{alpha}–C_{acid}–OH$ torsion angle. To our knowledge, this is the first relationship between the value of the deuterium quadrupole coupling constant in a $C–^{2}H$ bond and any feature of the molecular geometry. One goal of this project is to apply the Karplus-type relationship to measure structural features in amorphous systems.

Acknowledgement

The support of the Petroleum Research Fund, administered by the American Chemical Society, the LSU Center for Energy Studies, and the Louisiana Board of Regents' through the Louisiana Educational Quality Support Fund is gratefully ackowledged. We thank Professor John L. Ragle for his spectral simulation program.

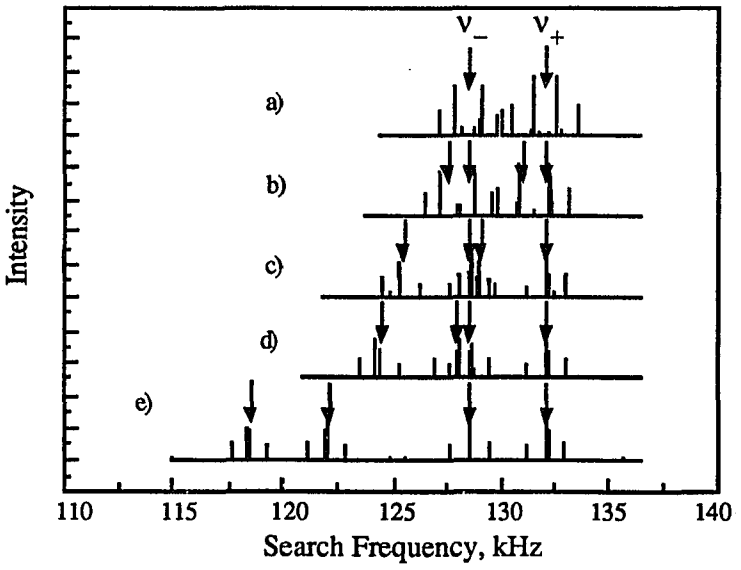

Figure 6.1 Simulated single quantum transitions for a C^2H_2 unit. The EFG orientations are taken from a molecular orbital calculation of the acetic acid dimer[10] for a conformer with ^2H–C_{alpha}–C_{acid}–OH equal to ±60°. Trace (a) corresponds to both sites having ν_- and ν_+ transition frequencies of 128.5 and 132.0 kHz, respectively. In traces (b)-(e), the transition frequencies for one site are reduced by the following amounts: (b) 1 kHz; (c) 3 kHz; (d) 4 kHz; (e) 10 kHz. Arrows indicate the unperturbed transition frequencies.

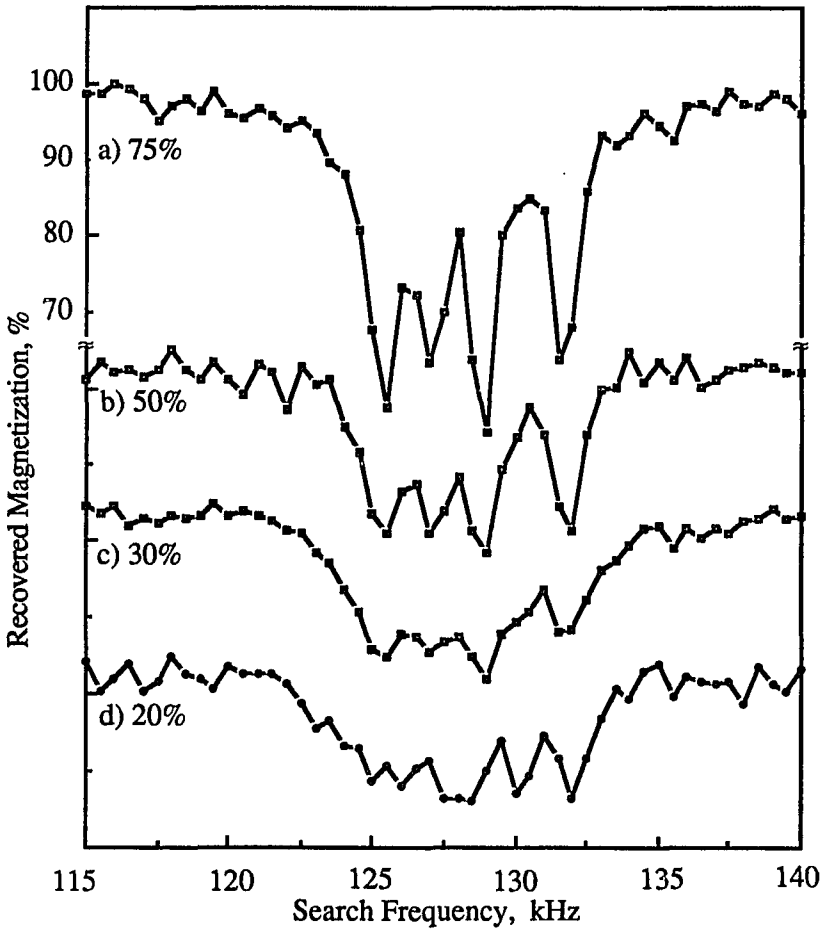

Figure 6.2 Single quantum ADLF spectra of (4-bromophenyl)[2,2-$^2H_2$]acetic acid for four different levels of deuteration. 100% deuteration corresponds to all molecules in the sample containing the C^2H_2 unit.

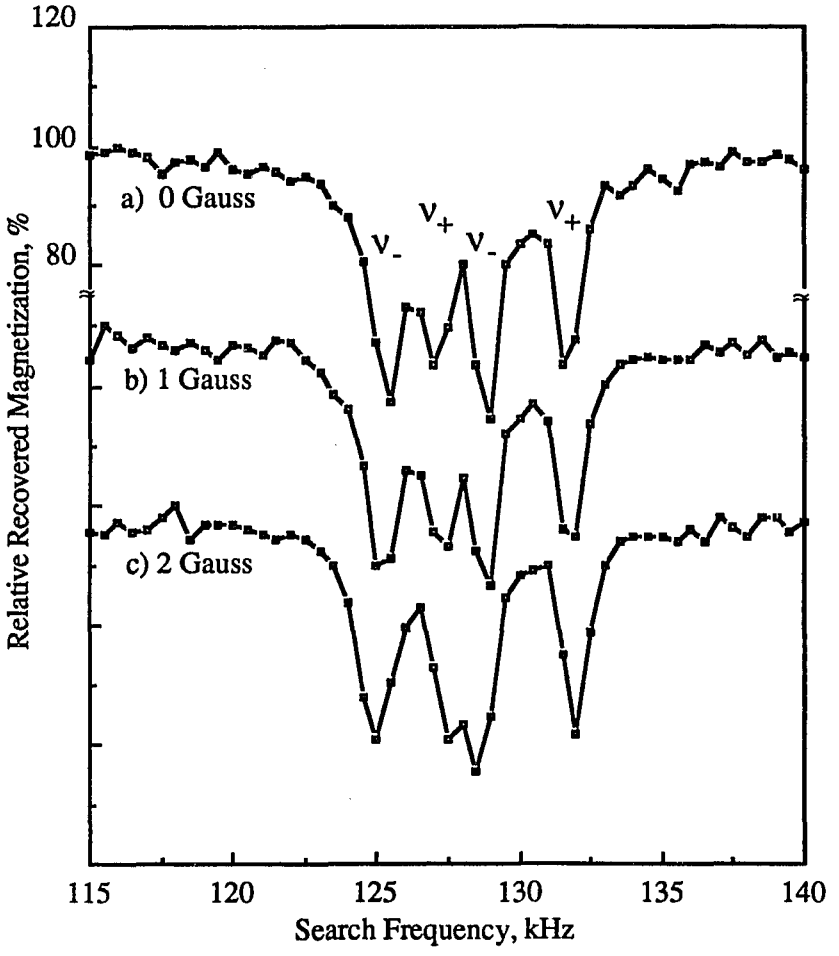

Figure 6.3 Single quantum ADLF spectra of (4-bromophenyl)[2,2-$^2H_2$]acetic acid for three applied magnetic fields. The deuteration level is 75%.

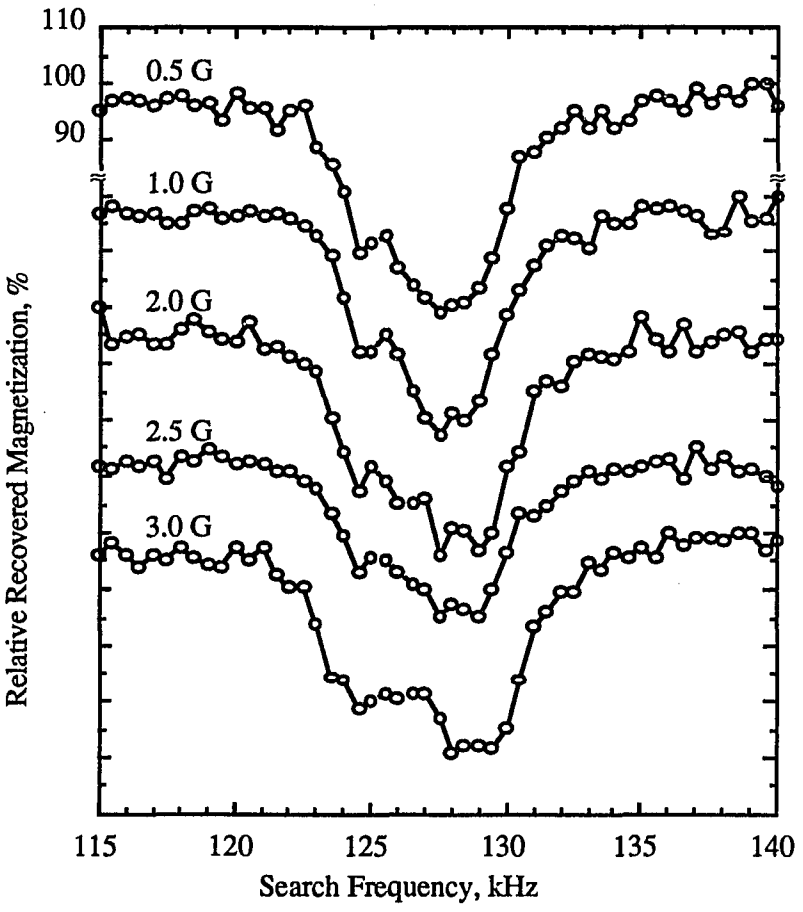

Figure 6.4 Single quantum ADLF spectra of (2-naphthyl)[2,2-$^2H_2$]acetic acid for five applied magnetic fields. The deuteration level is 40-50%.

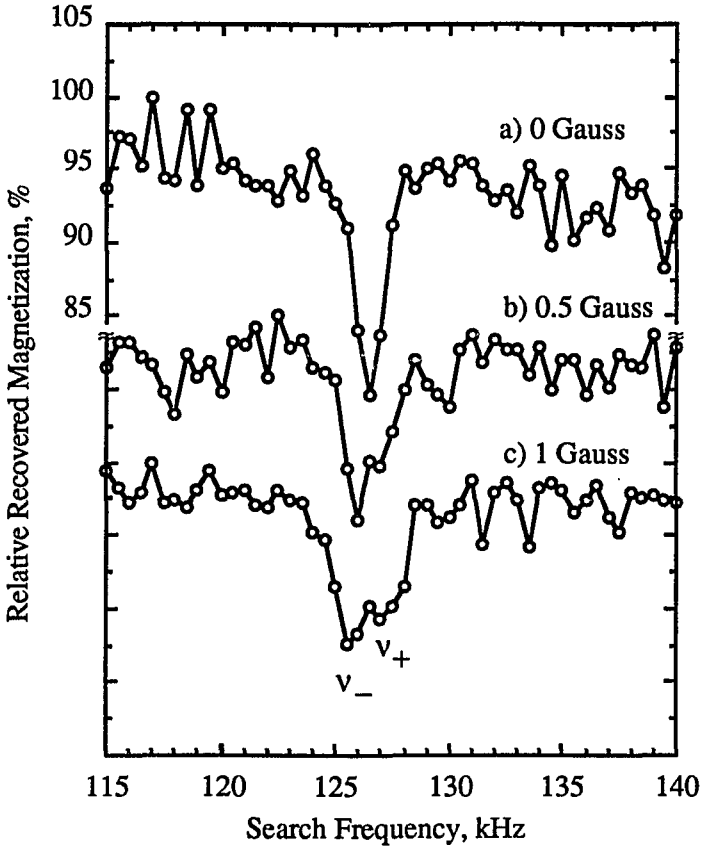

Figure 6.5 Single quantum ADLF spectra of 2,2–bis(4–chlorophenyl)[2–^{2}H]acetic acid acquired at 77 K and with applied magnetic fields of a) 0.0 Gauss, b) 0.5 Gauss, c) 1.0 Gauss. The deuteration level is 80%. The set of peaks labeled ν_+ and ν_- corresponds to single transitions of the deuteron bound to C_{alpha} in the methylene group.

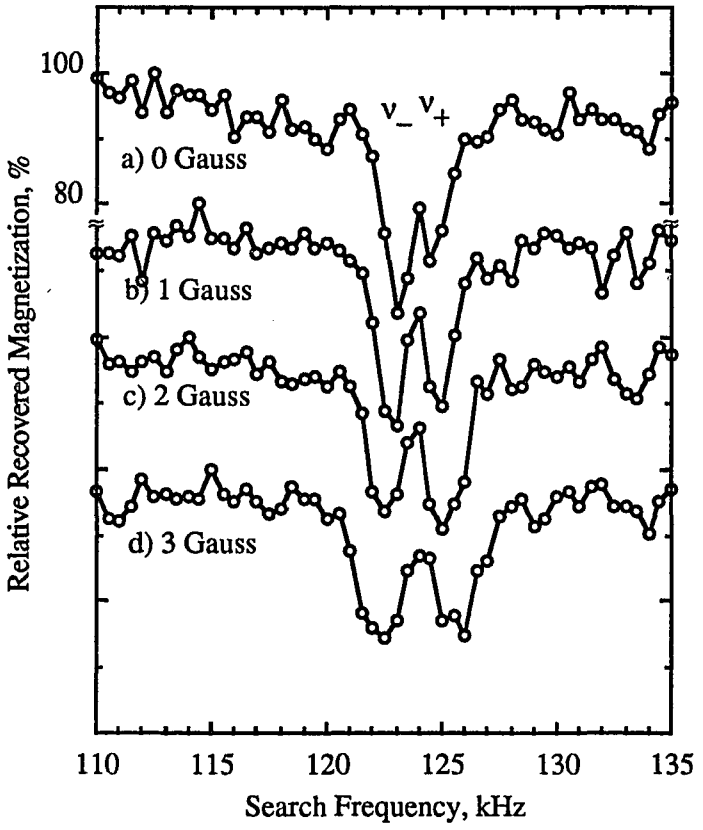

Figure 6.6 Single quantum ADLF spectra of (2,2-diphenyl)[2-^{2}H]acetic acid for four applied magnetic fields. The deuteration level is 40%. Some of these spectra were acquired by Dr. William L. Jarrett as a coorperative work. All deuteriated samples were prepared by Margo A. Jackisch.

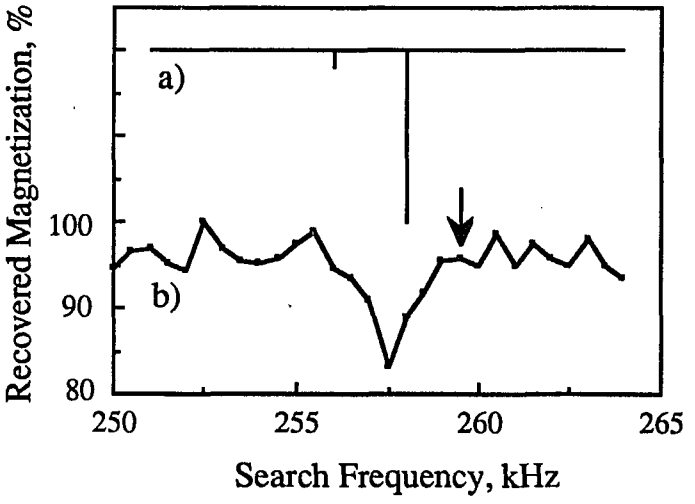

Figure 6.7 Double transition spectrum for (4-bromophenyl)[2,2-$^2H_2$]acetic acid. The deuteration level is 75%. Trace (a) is the simulated spectrum based on the experimental transition frequencies obtained from Figure 6.3 and listed in Table 6.1. The EFG orientations are the same as used in Figure 6.1. The slight frequency error between simulated and experimental transitions is ascribed to the relatively coarse 0.5 kHz rf search frequency increment. The arrow indicates the simple sum of the two ν_+ transition frequencies and is 1.5 kHz higher than the experimental double transition frequency.

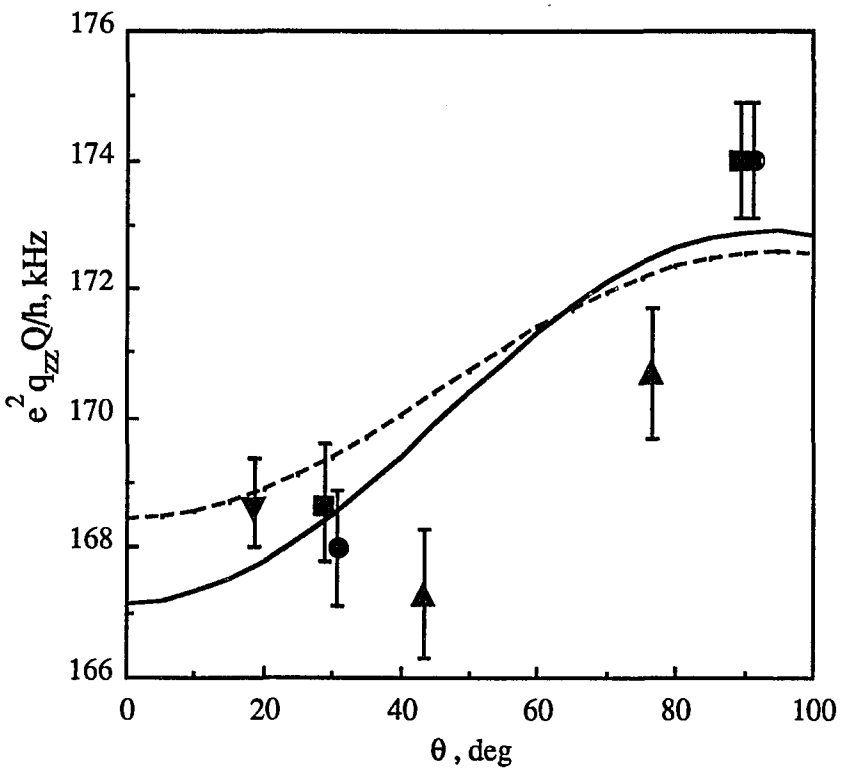

Figure 6.8 Correlation between the deuterium quadrupole coupling constant and the ^2H–C_{alpha}–C_{acid}–OH torsion angle. The dotted line is obtained from equation 6.1, the solid line is from equation 6.2. The compounds are: ●, (4-chlorophenyl)[2,2-$^2H_2$]acetic acid; ■, (4-bromophenyl)[2,2-$^2H_2$]acetic acid; ▲, (2-napthyl)[2,2-$^2H_2$]acetic acid; ▼, 2,2-bis(4-chlorophenyl)[2-^2H]acetic acid.

References

1 Chiba, T. *J. Chem. Phys.* **1964**, *41*, 1352-1358.

2 Butler, L. G.; Brown, T. L. *J. Am. Chem. Soc.* **1981**, *103*, 6541-6549.

3 Brown, T. L.; Butler, L. G.; Curtin, D. Y.; Hiyama, Y.; Paul, I. C.; Wilson, R. B. *J. Am. Chem. Soc.* **1982**, *104*, 1172-1177.

4 Keiter, E. A. Ph. D. Dissertation, University of Illinois, 1986.

5 Jarrett, W. L.; Farlee, R. D.; Butler, L. G. *Inorg. Chem.* **1987**, *26*, 1381-1383.

6 Guo, K.; Jarrett, W. L.; Butler, L. G. *Inorg. Chem.* **1987**, *26*, 3001-3004.

7 Altbach, M. I.; Hiyama, Y.; Gerson, D. J.; Butler, L. G. *J. Am. Chem. Soc.* **1987**, *109*, 5529-5531.

8 Hiyama, Y.; Roy, S.; Guo, K.; Butler, L. G.; Torchia, D. A. *J. Am. Chem. Soc.* **1987**, *109*, 2525-2526.

9. (a) Jackisch, M.; Jarrett, W. L.; Guo, K.; Fronczek, F.; Butler, L. G. *Polym. Prepr., Am. Chem. Soc., Div. Polym. Chem.* **1987**, *28(2)*, 298–299. (b) Jackisch, M.; Jarrett, W. L.; Guo, K.; Butler, L. G. *Polym. Prepr., Am. Chem. Soc., Div. Polym. Chem.* **1987**, *28(1)*, 204.

10 Jackisch, M. A.; Jarrett, W. L.; Guo, K.; Fronczek, F. R.; Butler, L. G. *J. Am. Chem. Soc.* **1988**, *110*, 343-347.

11 Karplus, M. *J. Chem. Phys.* **1959**, *30*, 11-15.

12 Colucci, W. J.; Gandour, R. D.; Mooberry, E. A. *J. Am. Chem. Soc.* **1986**, *108*, 7141-7147.

13 Schwartz, L. J.; Meirovitch, E.; Ripmeester, J. A.; Freed, J. H. *J. Phys. Chem.* **1983**, *87*, 4453-4461.

14 Jackisch, M. A.; Fronczek, F. R.; Guo, K.; Jarrett, W. L.; Park, Y. H.; Stauffer, M. T.; Watkins, S. F.; Butler, L. G. to be submitted to *Macromolecules.*

15 Shields, K. G.; Kennard, C. H. L. *J. Chem. Soc. Perkin II* **1977**, 463-465.

16 Edmonds, D. T. *Phys. Rep. C* **1977**, *29*, 233-290.

17 (a) Edmonds, D. T.; Hunt, M. J.; Mackay, A. L. *J. Magn. Reson.* **1975**, *20*, 505–514. (b) Edmonds, D. T.; White, A. A. L. *J. Magn. Reson.* **1978**, *31*, 149–159. (c) Edmonds, D. T.; Hunt, M. J.; Mackay, A. L. *J. Magn. Reson.* **1973**, *11*, 77–82. (d) d'Avignon, D. A.; Brown, T. L. *J. Phys. Chem.* **1981**, *85*, 4073–4079. (e) Day, R. O.; Hadipour, N.; Ragle, J. L. *J. Magn. Reson.* **1984**, *57*, 369–384.

18 Hadipour, N.; Ragle, J. L. *Z. Naturforsch. A: Phys., Phys. Chem., Kosmophys.* **1985**, *40A*, 355-360.

19 (a) Pross, A.; Radom, L. *J. Am. Chem. Soc.* **1978**, *100*, 6572-6575. (b) Nagaoka, S. I.; Hirota, N.; Matsushita, T.; Nishimoto, K. *Chem. Phys. Lett.* **1982**, *92*, 498-502.

20 Hunt, M. J.; Mackay, A. L. *J. Magn. Reson.* **1974**, *15*, 402-414.

21 Hunt, M. J.; Mackay, A. L. *J. Magn. Reson.* **1976**, *22*, 295-302.

22 Thayer, A. M.; Pines, A. *Accts. Chem. Res.* **1987**, *20*, 47-53.

23 Butler, L. G.; Brown, T. L. *J. Magn. Reson.* **1981**, *42*, 120-131.

(to be submitted to the *Macromolecules*, May, 1989)

CHAPTER SEVEN

A Karplus-Type Relationship for Deuterium Quadrupole Coupling Constants. III
The Origin of the Karplus-Type Relationship for Phenylacetic Acid.

Kermin Guo and Leslie G. Butler*

Contribution from the

Macromolecular Studies Group

Department of Chemistry

Louisiana State University, Baton Rouge, LA 70803

---

* To whom correspondence should be addressed.

Abstract

High-resolution solid-state zero-field deuterium spectra have revealed inequivalent deuterium sites in a series of monosubstituted arylacetic acids. The value of the deuterium quadrupole coupling constant is dependent upon the local molecular conformation about the C–^{2}H site. In this work, we consider the origin of the effects of the neighboring oxygen atoms and the aryl group upon the deuterium quadrupole coupling constants in alpha-deuterated arylacetic acids. Ab initio molecular orbital calculations have been performed on different conformations of acetic acid and phenylacetic acid in which the orientation of the alpha C–^{2}H bond vector is varied with respect to both the carboxyl oxygen atoms and the phenyl ring. The modulation of the deuterium quadrupole coupling constant in phenylacetic acid has been traced to: (a) the effective nuclear charge of the carbonyl and hydroxyl oxygen sites of the carboxyl group adjacent to the C^2H_2 unit, and (b) the partially unshielded nuclear charges of the ortho carbon and ortho hydrogen on the phenyl ring. The Mulliken atomic charge at the carbon alpha to the carboxylic acid group is not useful for predicting the value of the variation of the deuterium quadrupole coupling constant at the C–^{2}H site. Finally, correlation of the calculated deuterium quadrupole coupling constant with torsion angles describing the molecular conformation of phenylacetic acid is modeled by a modified Karplus-type equation.

7.1 Introduction

In the high-field solid-state deuterium NMR experiment, observed reductions in the apparent deuterium quadrupole coupling constant have been attributed to molecular motions that reorient the C–^{2}H bond with respect to the applied magnetic field. However, Hiyama *et al.* found that the deuterium powder pattern for a deuteriated methyl group in thymine–*methyl*–d_3 was affected by both a dynamic methyl group rotation factor and a nearby heavy atom factor due to an adjacent exocyclic oxygen atom.[1] Other occurrences of inequivalent C–^{2}H sites, bound to the same carbon atom, are to be found in succinic acid,[2] α-glycine,[3] and DL-serine;[4] all of these have at least two distinct values for the deuterium quadrupole coupling constant and all contain one or more oxygen atoms near a C^2H_2 unit.

Recently, we have used a high resolution rf excitation field-cycling NMR technique as a method for measuring the deuterium quadrupole coupling constants, and we have correlated the results with the torsion angles in polycrystalline samples of model organic compounds.[5] The Newman projection in Figure 7.1a illustrates the torsion angle for a ^{2}H–C_{alpha}–C_{acid}–OH unit. The NMR technique allows one to distinguish between two different deuterium sites with a resolution as high as 0.5 kHz. The experimental results show that inequivalent deuterium sites exist in a series of substituted arylacetic acids in which the carbon alpha to the carboxylic acid group has been deuteriated.[6] In the first report of this series,[7] the ^{2}H–C_{alpha}–C_{acid}–OH torsion angle, θ, and the deuterium quadrupole coupling constant, $e^2q_{zz}Q/h$, for these sites were correlated with a Karplus-type relationship.[8] In the second report, the technical details of the zero-field spectroscopy of the C^2H_2 unit were analyzed.[5] Herein, we report an analysis of the origin of the Karplus-type relationship for the deuterium quadrupole coupling constant in phenylacetic acid by using molecular orbital calculations. Two aspects of the phenylacetic acid molecular conformation that affect the deuterium quadrupole coupling constant will be

discussed: (a) the effective nuclear charge of oxygen atoms in the carbonyl and hydroxyl groups, and (b) the effective nuclear charge of the ortho carbon and ortho hydrogen atoms of the phenyl ring adjacent to the C^2H_2 unit. The charge variation on the methylene carbon due to a homoconjugation effect operative between the phenyl ring and the carboxyl group also has been investigated. Finally, the correlation of the calculated deuterium quadrupole coupling constant with the torsion angle for describing the molecular conformation of phenylacetic acid is modeled by a modified Karplus-type equation. The goal of this research project is the development of method for measuring torsion angles about selected sites in amorphorus materials, as shown in scheme I.

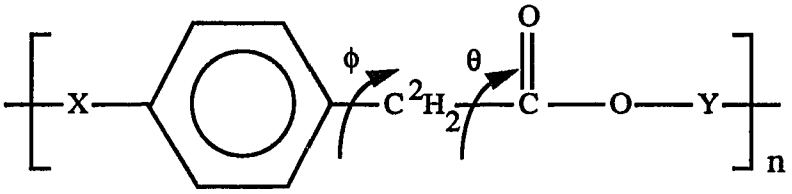

Scheme I

7.2 Theory

Solid-state deuterium nuclear magnetic resonance (NMR) methods are useful for the study of molecular structure,[7,9,10] bonding,[11] and dynamics.[12] There are two parameters that are measured in the solid-state deuterium NMR experiment: the deuterium quadrupole coupling constant, $e^2q_{zz}Q/h$, and the asymmetry parameter, η. The deuterium quadrupole coupling constant arises from the interaction between the deuterium nuclear electric quadrupole moment, Q, and the electric field gradient at the nuclear site. The electric field gradient is a sensitive function of molecular charge distribution in the close vicinity of the deuterium nucleus.[13] The asymmetry parameter, ranging from zero to one, is used to describe the shape of the electric field gradient. In the case of an sp^3 hybridized C–^{2}H bond in an organic compound, the major component of the electric field gradient

tensor is usually closely aligned with the C–^{2}H bond vector, the charge distribution around the deuterium atom is nearly axially symmetric, and we expect the asymmetry parameter to have a value close to zero. The electric field gradient, which is described by a 3x3 traceless tensor, has the units of esu/cm^3, and is the sum of the nuclear and electronic contributions,

$$eq_{zz} = \sum_n K_n \frac{3z_n^2 - r_n^2}{r_n^5} - e\left\langle \Psi^* \left| \sum_i \frac{3z_i^2 - r_i^2}{r_i^5} \right| \Psi \right\rangle \qquad (7.1)$$

where K_n is the nuclear charge for each nucleus in the molecule, e is the absolute value of the electronic charge, and the index i is over all electrons of the molecule.[14] Because the electronic contribution is derived only from the wavefunctions of occupied molecular orbitals, the calculations of quadrupole coupling constants are simpler than the similar calculations of chemical shielding and scalar coupling which often require evaluation of terms coupled to excited states.[15]

A point-charge model derived from the nuclear contribution term in equation 7.1 is used to estimate the unshielded nuclear charge contribution to the quadrupole coupling constant from the atoms near the C–^{2}H site. The nuclear contribution of the carboxyl oxygens to the electric field gradient at a carbon-bound deuterium site can be estimated by

$$\Delta eq_{zz}(\textit{unshielded nuclear}) = K'_{CO}\frac{3\cos^2\alpha_{CO} - 1}{r_{CO}^3} + K'_{OH}\frac{3\cos^2\alpha_{OH} - 1}{r_{OH}^3}, \qquad (7.2)$$

where K'_{CO} and K'_{OH} are the unshielded nuclear charges of the carbonyl and hydroxyl oxygen sites, respectively. The distances between the deuterium and the carbonyl and hydroxyl oxygens are r_{CO} and r_{OH}, respectively. Because the orientation of eq_{zz} is assumed to be collinear with the C–^{2}H bond vector, then α_{CO} and α_{OH} are the angles between the z axis of the principal axis system (the C–^{2}H bond vector) and the vector

along r_{CO} and r_{OH}, respectively. Because the observed value of the deuterium quadrupole coupling constant is perturbed by nearby charges and by the conformation of the phenylacetic acid molecules, equation 7.2 represents a new source for detailed structural information in the molecule.

In addition to the charge on neighboring oxygen atoms, the charge on the carbon to which the deuterium is bound will also affect the value of the deuterium quadrupole coupling constant. Since the contribution of electronic charge very close to the deuterium site cannot be simply modeled as a point charge, a more elaborate treatment is required. We can assume that changes in the charge on carbon reflect the occupancy of higher-lying carbon atomic orbitals that is affected rather than the core or low-lying valence orbitals. A model that predicts the change in the deuterium quadrupole coupling constant as a function of charge on carbon has been developed[16] and utilizes an expression similar to the following:

$$\Delta\, eq_{zz}\,(\textit{atomic charge}) = \left\langle \Psi^{*}_{2p} \left| \frac{3z^{2}_{2p} - r^{2}_{2p}}{r^{5}_{2p}} \right| \Psi_{2p} \right\rangle \Delta q, \qquad (7.3)$$

where Ψ_{2p} is a carbon 2p orbital and Δq is the signed change in the occupancy of the 2p orbital relative to a reference molecule. In a case where a particular orbital is identified with charge variation at carbon, a carbon 2p orbital orthogonal to the C–^{2}H bond, this model predicts a 70.2 kHz reduction in eq_{zz} for each one-electron increase in 2p orbital occupancy.[16] Herein, we will not attempt to assign the variation of Mulliken-derived atomic charges to any particular carbon atomic orbital. but rather we will investigate the correlation between the variation of charge on carbon and the deuterium quadrupole coupling constant.

7.3 Method

7.3.1 The assignment of torsion angles, θ and ϕ. There are no persistent rotational symmetry axes nor mirror planes of symmetry in the phenylacetic acid molecule in the solid state. Therefore, the two methylene hydrogens, H(A) and H(B), are not, in general, equivalent and will have differing values for their quadrupole coupling constants. Two torsion angles, θ and ϕ, are required to describe the molecular conformation, as shown in Figure 7.1. The orientation of the carboxyl group with respect to the methylene hydrogen site is described by the torsion angle θ(A), H(A)–C_{alpha}–C_{acid}–OH.[5,7] In this work, the sign of the torsion angles is important so as to distinguish among many molecular conformers. The sign of any torsion angle A–B–C–D is defined as positive if, when viewed along the B–C bond, atom A must be rotated clockwise to eclipse atom D.[17] The rotation of the phenyl ring with respect to the acid group is described by the torsion angle, ϕ(A), C_{ortho}(A)–C_{ring}–C_{alpha}–C_{acid}, where the C_{ortho}(A) is chosen so that the sign of ϕ(A) is positive; thus the range of ϕ(A) is from 0° to 180°.

There are two constraints upon these choices of torsion angles. First, specifying one methylene site as A and the other B has the effect of introducing unwanted chirality into the system. Labeling each site is necessary for reporting the deuterium quadrupole coupling constant as a function of a pair of torsion angles, θ and ϕ, but this asymmetry must be eliminated from the Karplus-type relationship we are seeking. Second, any Karplus–type relationship should be usable without prior determination of any aspect of the molecular conformation, i.e., the handedness of the molecule in the solid state.

Based on these constraints, the definitions of the two torsion angles for H(B) in each conformation are taken from the mirror images as shown in Figure 7.1. The torsion angle θ(B) is given by H(B)–C_{alpha}–C_{acid}–OH. The torsion angle ϕ(B) is defined as C_{ortho}(B)–C_{ring}–C_{alpha}–C_{acid} where C_{ortho}(B) is chosen from the mirror image of the molecule so as to give a positive sign for ϕ(B). Without application of a mirror plane symmetry operation, the torsion angles of the H(B) site are in an opposite sense relative to

those of H(A) site for the same molecule. But with the mirror operation applied to the molecule, the torsion angles for the H(B) site have the same sense as the torsion angles of the H(A) site. Thus the deuterium quadrupole coupling constant for both hydrogen sites can be described by the two torsion angles in the same equation.

While we use the label "Karplus-type" to describe the connection between the deuterium quadrupole coupling constant and the molecular geometry, the situation described herein is more complicated than encountered in solution ^{1}H NMR spectroscopy, as shown schematically below,

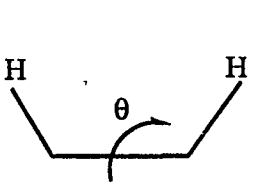

II

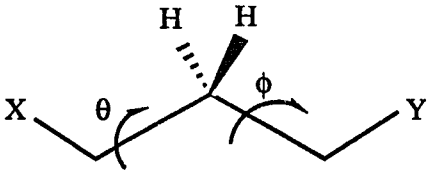

III

There is a single pairwise interaction in **II** versus four pairwise interactions in **III**. The notation in Figure 7.1 is complex, but it does offer advantages in the form of sum rules of the two torsion angles for the inequivalent H(A) and H(B) sites,

$$\theta(A) + \theta(B) = 120° \qquad (7.4)$$

$$\phi(A) + \phi(B) = 180° \qquad (7.5)$$

which are true for both positive and negative torsion angles. Note: the sum rules require that we assume a tetrahedral bonding geometry about C_{alpha}. There are several molecular conformations of the phenylacetic acid for which H(A) and H(B) are related by a mirror plane; these orientations correspond to $\theta(A) = -120°$, 60° or 240° and $\phi(A) = 0°$, 90°, or 180°.

7.3.2 Molecular orbital calculations. All calculated electric field gradients at the methyl hydrogen sites in acetic acid and the methylene hydrogen sites in phenylacetic acid were obtained from ab initio molecular orbital calculations with the Gaussian 82 program and the associated properties package[18] on an IBM 3090 computer at LSU and a Cray X-MP/48 at the Pittsburgh Supercomputer Center. For each structure, the restricted Hartree-Fock procedure was used with a 6–31G basis set[19] for all atoms including H. The bond lengths and angles in the acetic acid structure are assigned according to the literature data.[20] For phenylacetic acid, a methyl hydrogen was replaced with a phenyl ring of idealized geometry. To cover a variety of molecular conformations, the calculations were done with torsion angles ranging from $\theta = -120°$ to 240° and $\phi = 0°$ to 180°, in 30° steps for each angle, for a total of 38 unique molecular conformations. In this work, the convention of reporting the electric field gradient tensor elements is $|eq_{zz}| \geq |eq_{yy}| \geq |eq_{xx}|$.[21] The output of the GAUSSIAN 82 property package is eq in atomic units ($e = +1$). The deuterium nuclear electric quadrupole moment, Q, used herein for calculating the deuterium quadrupole coupling constant, is 0.00286×10^{-24} cm^2.[22] The conversion of the calculated electric field gradient to the nuclear quadrupole coupling constant is done by multiplying by a factor of $(-2.34965 \times 10^{29}) \times Q$ kHz/a.u.. No corrections for vibrational effects were made to the electric field gradient tensor calculations. In the cases where vibrational corrections have been applied, the general effect is to reduce the magnitude of the calculated electric field gradient tensor elements slightly.[23]

Due to the large number of atoms in the phenylacetic acid molecule, the monomeric form is studied with a 6–31G basis set in contrast to the 6–31G** basis set used for the previous acetic acid dimer calculations. While the less extensive basis set yields calculated values that are less accurate, trends due to changes in the molecular conformation are

preserved. As shown in Figure 7.2, a comparison of the calculated results for the acetic acid monomer with the 6–31G basis set and the dimer with the 6–31G** basis set[7] shows that the latter have deuterium quadrupole coupling constants closer to the experimental values, around 170 kHz, but both sets of calculations show similar changes in the deuterium quadrupole coupling constant as a function of the torsion angle θ.

7.4 Results and Discussion

All of the aliphatic C–^{2}H sites in acetic acid and phenylacetic acid have similar values for the calculated deuterium quadrupole coupling constant and asymmetry parameter at the 6–31G basis set level, typically 233 kHz and 0.05, respectively. At the 6–31G** basis set level, the acetic acid dimer has the values of $e^2q_{zz}Q/h$ = 217 kHz and η = 0.05 at θ = 60°.[7] In fluoromethane–d_3, with a double zeta basis set but augmented with d polarization functions on both carbon and fluorine and p polarization functions at the hydrogen, similar to the 6–31G** basis set, the values of $e^2q_{zz}Q/h$ = 202 kHz and η = 0.109 for the C–^{2}H site were reported.[24] For methane–d_4, $e^2q_{zz}Q/h$ = 200.4 kHz and η = 0 (as required by symmetry) were found with a basis set similar to that used for fluoromethane–d_3 plus an additional *d* polarization function at hydrogen.[25] For comparison, ADLF spectroscopy at 77 K shows that the two equivalent aliphatic C–^{2}H sites in [9,9-$^2H_2$]fluorene have a deuterium quadrupole coupling constant of 173(1) kHz and an asymmetry parameter of 0.02(1).[16a]

In all C–^{2}H sites studied here, the major axis of the electric field gradient tensor is closely aligned along the C–^{2}H bond vector. The maximum deviation of the *z* axis from the bond vector reported thus far is about 2° for one orientation of the methyl group in thymine-*methyl*-d_3.[1] In all cases, the sign of the deuterium quadrupole coupling constant is positive. Thus, according to equation 7.1, the largest contribution to eq_{zz} comes from the carbon nuclear charge. In fact, for a C–^{2}H bond length of 1.079 Å, the carbon

nuclear contribution to the deuterium quadrupole coupling constant is +950.6 kHz. The electronic contribution from the C–^{2}H bond orbital, the carbon core and other valence orbitals, and, to a much lesser extent, the rest of the molecular orbitals of the molecule, must therefore be on the order of –800 kHz.

The molecules studied by ab initio molecular orbital methods, methane, fluoromethane, thymine, acetic acid, and phenylacetic acid, have similar, though not identical, deuterium quadrupole coupling constants. It is the variation in the deuterium quadrupole coupling constant as a function of the conformation of these molecules that is important in this study.

7.4.1 Acetic acid. The calculated deuterium quadrupole coupling constant components from nuclear and electronic contributions are tabulated in Table 7.1 for the methyl group hydrogens of an acetic acid molecule together with the asymmetry parameters. The positive nuclear term is always larger than the negative electronic contribution. For the total electric field gradient tensor, the orientation of the z axis is always closely aligned (within 1°) with the C–^{2}H bond vector. While both the nuclear and electronic contribution are a function of the molecular conformation as described by the torsion angle θ, it is the nuclear contribution that has the larger range in values by about 3 kHz. Since the change in total electric field gradient is dominated by the nuclear contribution, we postulate that the variation in the deuterium quadrupole coupling constant is due to the two partially shielded oxygen nuclei. In Figure 7.3, we illustrate the oxygen nuclear contribution to the deuterium quadrupole coupling constant for the C–^{2}H site by placing a +1.0 e point charge at each oxygen site of the acetic acid molecule and evaluating equation 7.2 as a function of θ. The value of the deuterium quadrupole coupling constant is most affected when the C–^{2}H site is close to either oxygen nucleus. Because the angle C_{alpha}–C_{acid}–OH is more acute than the angle C_{alpha}–C_{acid}=O, $r_{OH}(\theta=0°)$ is generally smaller than $r_{CO}(\theta=180°)$. Therefore, the point charge model of equation 7.2 predicts a larger effect, i.e., a greater variation in the deuterium quadrupole coupling

constant, for the hydroxyl oxygen site than for the carbonyl site as is shown in Figures 7.2 and 7.3.

The middle trace in Figure 7.3 shows the sum of the contributions from the two point charges; the shape of this curve is very similar to that obtained for the total electric field gradient from a calculation of acetic acid at either the 6–31G level (this work) or the 6–31G** level.[7] The middle trace in Figure 7.3 can be fitted to an equation of the general form:

$$e^2q_{zz}Q/h \text{ (calc)} = A + B\cos(\theta) + C\cos(2\theta). \qquad (7.6)$$

This equation resembles the Karplus equations used in solution ^{1}H NMR spectroscopy.[8] In our studies, the A parameter is essentially the deuterium quadrupole coupling constant of the unperturbed C–^{2}H site. Based on Figure 7.3, the C parameter is a sum of the perturbation due to both hydroxyl and carbonyl oxygen sites. The B parameter reflects the difference in the values of r_{OH} and r_{CO}. Also, if the effective point charges, the unshielded nuclear charge, K'_{OH} and K'_{CO} associated with the oxygen sites differ, then this fact will also be incorporated into the B parameter.

7.4.2 Phenylacetic acid. The results for phenylacetic acids at the 6–31G basis set level are similar in many respect to the results obtained for acetic acids. The calculated deuterium quadrupole coupling constant and asymmetry parameter for phenylacetic acid over a full range of unique θ and ϕ are given in Table 7.2. The range in the values of the deuterium quadrupole coupling constant for phenylacetic acid is comparable to that for acetic acid, 4.9 kHz and 3.5 kHz, respectively. The asymmetry parameter, η, is always near zero, indicating nearly axial symmetry for the C–^{2}H bond. The z axis for the principal axis system of the electric field gradient is closely aligned with the C–^{2}H bond vector. The variation in the values of the deuterium quadrupole coupling constant as a

function of θ indicates that neighboring oxygen atoms are again a major source of perturbation of the electric field gradients at the C–^{2}H sites. That is, for a constant value of ϕ, the deuterium quadrupole coupling constants are at local minima for molecular conformations with θ of 0° and 180°. We attribute the slight decrease in the values of the deuterium quadrupole coupling constants at all molecular conformations of phenylacetic acid compared to acetic acid to the partially unshielded nuclear charges of the ortho carbon and ortho hydrogen that affect the C–^{2}H site in a manner similar to the hydroxyl and carbonyl oxygen sites, and are modeled with equation 7.2. At closest approach, corresponding to $\phi = \pm 60°$, the distance between a deuteron bond to C_{alpha} and an ortho hydrogen is 2.32 Å.

The effects of the ortho carbon and ortho hydrogen on the deuterium quadrupole coupling constantof the C–^{2}H site of C_{alpha} are apparent in two different calculations. First, a study of the methyl C–^{2}H sites of toluene showed a variation of 1.5 kHz in the deuterium quadrupole coupling constant as a function of methyl group rotation.[1] Second, for phenylacetic acids with molecular conformation at a constant value of θ, say 0°, changing the orientation of the phenyl ring, $\phi = 0°$ to 180°, modulates the value of the deuterium quadrupole coupling constant over a range of 1.2 kHz. This effect of the ortho carbon and ortho hydrogen can be modeled with a sin(2ϕ) function. The functional form of sin(2ϕ) was chosen based on the geometry of the possible orientations of the phenyl ring with respect to the C–^{2}H site. Because of the plane of symmetry for the aromatic ring, a sin(2ϕ + x) or equivalently, cos(π – 2ϕ – x) function will describe the effect of the through space interaction due to the ortho carbon and hydrogen nuclei upon the deuterium quadrupole coupling constant. The form sin(2ϕ) was chosen based on the best fit of the modified Karplus-type relation (*vida infra*) to the data given in Table 7.1.

Also noteworthy is that, relative to acetic acid, the Mulliken atomic charge on C_{alpha} in phenylacetic acid has a much larger variation with molecular conformation.

There is a variation in charge on the methylene C_{alpha} bridging the phenyl ring and the acid group as a function of molecular conformation. This is due to an interaction between the π orbitals of the phenyl ring and those of the carboxylic acid group, an interaction termed homoconjugation (or, for carbocations, the homoallylic interaction).[26] The extremes of the Mulliken atomic charge on C_{alpha} differ by 0.11 e. We investigated the electronic contribution on the deuterium quadrupole coupling constant from the charge buildup at C_{alpha} with equation 7.3. From the previous prediction of a 70.2 kHz reduction per unit electric charge for a carbon 2p orbital,[16] we would have expected a 7.8 kHz variation of the deuterium quadrupole coupling constant based on the carbon atomic charge variation. But, as shown in Table 7.2, we found that no correlation exists between the the Mulliken atomic charge at C_{alpha} and the variation of the deuterium quadrupole coupling constant at the C–^{2}H site. Also, as noted in equation 7.3, any increase in charge on carbon will monotonically reduce the value of the deuterium quadrupole coupling constant. The Mulliken atomic charge on C_{alpha} is more negative in acetic acid than in phenylacetic acid, this should have concomitantly reduced the deuterium quadrupole coupling constant in acetic acid . The fact that acetic acid has, at the 6–31G basis set level, a *larger* value of deuterium quadrupole coupling constant indicates to us that there are deficiencies at this basis set level in using the Mulliken atomic charge to access the charge on carbon.

To review, the value of the deuterium quadrupole coupling constant in a C–^{2}H site is determined mainly by the +6 nuclear charge of the carbon nucleus mitigated by the electronic charge of the carbon core and valence electrons and by the C–^{2}H bonding electrons. For phenylacetic acid, the partially unshielded nuclear charges of the hydroxyl and carbonyl oxygen sites as well as the ortho carbon and ortho hydrogen nuclei will, upon close approach as determined by the molecular conformation, also affect the value of the deuterium quadrupole coupling constant. Thus, we are led to a revised Karplus-type

relationship for phenylacetic acid that accounts for each factor modulating the deuterium quadrupole coupling constant,

$$e^2q_{ZZ}Q/h \text{ (calc)} = A + B\cos(\theta) + C\cos(2\theta) + D\sin(2\phi) \qquad (7.7)$$

where the A parameter is the unperturbed deuterium quadrupole coupling constant, B and C are due to the hydroxyl and carbonyl oxygen sites, and D is due to the ortho carbon and ortho hydrogen sites. The deuterium quadrupole coupling constants given in Table 7.2 can be fitted to equation 7.8 to yield

$$e^2q_{ZZ}Q/h \text{ (calc)} = 233.13 - 0.032\cos(\theta) - 1.71\cos(2\theta) - 0.628\sin(2\phi). \qquad (7.8)$$

A contour plot of the deuterium quadrupole coupling constant as a function of the torsion angles θ and ϕ is shown in Figure 7.4. The largest difference between any value listed in Table 7.2 and that calculated by equation 7.8 is 0.436 kHz. A symmetric molecular conformer with the torsion angles $\theta(A) = \theta(B) = 60°$ and $\phi(A) = \phi(B) = 90°$ is located at the center of the plot. Based on the sum rules of equations 7.4 and 7.5, any arbitrary conformer with torsion angles $\theta(A)$ and $\phi(A)$ at the H(A) site will have a companion H(B) site located on the contour plot at a point obtained by transforming through this symmetric center to give an site with torsion angles $\theta(B)$ and $\phi(B)$.

7.5 Conclusions

Ab initio molecular orbital calculations were performed on acetic acid and phenylacetic acid monomers with different molecular conformations. The major contribution to the change in the deuterium quadrupole coupling constants with different molecular conformations is due to surrounding atomic nuclei. The origin of the

Karplus–type relationship for deuterium quadrupole coupling constants in phenylacetic acid can be interpreted based on two considerations: (a) the partially unshielded nuclear charge of oxygen atoms at carbonyl and hydroxyl sites adjacent to the C–^{2}H site, (b) the partially unshielded nuclear charge of the ortho carbon and ortho hydrogen nuclei on the phenyl ring. A functional form is proposed for the use of the deuterium quadrupole coupling constant in the determination of molecular conformation about the methylene site in phenylacetic acid. Extensions of the function to the structural studies of arylacetic acids and to polymeric species as shown in Scheme **I** are anticipated.

An additional implication from this work is that the structural features may affect the value of the deuterium quadrupole coupling constant in a manner that resembles motional averaging. This point was first raised by Hiyama, *et al.*, in connection with the study of methyl group rotation in thymine-*methyl-d3*.[1] In thymine-*methyl-d3* case, a neighboring exocyclic oxygen atom affects the electric field gradient at the C–^{2}H site. In summary, we caution workers studying C–^{2}H sites in systems containing oxygen atoms that are close to (inter- or intramolecular) the C–^{2}H site. Based on the present work, it is no longer clear that a reduction of the value of the deuterium quadrupole coupling constant is strictly associated with molecular motion.

Acknowledgement

The support of the donors of the Petroleum Research Fund, administered by the American Chemical Society, the Louisiana Board of Regents, through the Louisiana Educational Quality Support Fund and, in part, the Pittsburgh Supercomputer Center, through their Workshop program, is gratefully acknowledged.

Table 7.1. Angular Dependence of Calculated Nuclear and Electronic Contributions to the Deuterium Quadrupole Coupling Constants and Asymmetry Parameters for Acetic Acid.

	$e^2q_{zz}Q/h$, kHz[a]					
θ,deg	Nuclear	Electronic	Total	η	δ, deg[b]	Mulliken Charge, e
0	1022.3	–793.1	232.7	0.043	0.911	–0.529
30	1030.0	–800.0	233.7	0.049	0.815	–0.521
60	1045.5	–813.8	235.5	0.057	0.672	–0.514
90	1055.8	–823.3	236.2	0.060	0.628	–0.521
120	1055.8	–824.0	235.4	0.056	0.625	–0.529
150	1049.7	–819.4	233.9	0.047	0.630	–0.521
180	1046.2	–816.6	233.1	0.040	0.642	–0.514

[a] Each component, nuclear, electronic, and total, is diagonalized in its own principal axis system. Because the orientation of each principal axis system is slightly different, the total deuterium quadrupole coupling constant is not exactly the sum of the nuclear and electronic components. [b] Angle between the *z* axis of the principal axis system of the total electric field gradient and the C–^{2}H bond vector. For the nuclear and electronic electric field gradient tensors, the angles lie within 6° and 7.6°, respectively.

Table 7.2. Calculated Deuterium Quadrupole Coupling Constants, Asymmetry Parameters, and Mulliken Charges on C_{alpha} for Phenylacetic Acid.

Deuterium Sites[a]								
Site (A)				Site (B)				Mulliken
θ, deg	ϕ, deg	$e^2q_{zz}Q/h$, kHz	η	θ, deg	ϕ, deg	$e^2q_{zz}Q/h$, kHz	η	Charge, e
60	180	234.15	0.054	60	0	234.15	0.054	-0.407
60	150	234.87	0.043	60	30	233.75	0.054	-0.419
60	120	234.74	0.030	60	60	233.87	0.043	-0.438
60	90	234.21	0.030	60	90	234.21	0.030	-0.450
60	60	233.87	0.043	60	120	234.74	0.030	-0.438
60	30	233.75	0.054	60	150	234.87	0.043	-0.419
90	180	234.90	0.058	30	0	232.28	0.046	-0.395
90	150	235.57	0.046	30	30	231.73	0.047	-0.412
90	120	235.46	0.035	30	60	231.92	0.037	-0.435
90	90	234.86	0.036	30	90	232.33	0.023	-0.444
90	60	234.47	0.052	30	120	232.82	0.025	-0.431
90	30	234.43	0.062	30	150	232.96	0.036	-0.407
120	180	233.94	0.060	0	0	231.33	0.046	-0.370
120	150	234.50	0.046	0	30	230.64	0.049	-0.380
120	120	234.39	0.036	0	60	230.71	0.041	-0.410
120	90	233.80	0.040	0	90	231.17	0.026	-0.423
120	60	233.35	0.056	0	120	231.69	0.025	-0.410
120	30	233.37	0.065	0	150	231.89	0.035	-0.384
150	180	232.42	0.053	-30	0	232.27	0.054	-0.348
150	150	232.90	0.041	-30	30	231.60	0.059	-0.360
150	120	232.73	0.031	-30	60	231.60	0.051	-0.386
150	90	232.20	0.035	-30	90	232.08	0.035	-0.400
150	60	231.76	0.051	-30	120	232.61	0.032	-0.385
150	30	231.80	0.059	-30	150	232.80	0.042	-0.355
180	180	231.67	0.043	-60	0	234.01	0.058	-0.349
180	150	232.19	0.032	-60	30	233.36	0.064	-0.365
180	120	232.00	0.022	-60	60	233.39	0.054	-0.396
180	90	231.47	0.025	-60	90	233.90	0.038	-0.410
180	60	231.02	0.040	-60	120	234.51	0.035	-0.399
180	30	230.98	0.047	-60	150	234.62	0.045	-0.364
210	180	232.31	0.044	-90	0	234.72	0.058	-0.386
210	150	232.95	0.033	-90	30	234.14	0.061	-0.396
210	120	232.80	0.022	-90	60	234.20	0.050	-0.426
210	90	232.28	0.021	-90	90	234.67	0.035	-0.443
210	60	231.87	0.035	-90	120	235.31	0.034	-0.439
210	30	231.75	0.045	-90	150	235.45	0.046	-0.410
240	180	233.88	0.055	-120	0	233.88	0.055	-0.416
240	150	234.55	0.041	-120	30	233.38	0.053	-0.433
240	120	234.41	0.029	-120	60	233.46	0.041	-0.450
240	90	233.86	0.027	-120	90	233.86	0.027	-0.462
240	60	233.46	0.041	-120	120	234.41	0.029	-0.450
240	30	233.38	0.053	-120	150	234.55	0.041	-0.433

[a] Any given trace for the phenylacetic acid in Figure 7.2 can be contructed from this data by plotting $e^2q_{zz}Q/h$ versus torsion angles θ for both sites at constant ϕ.

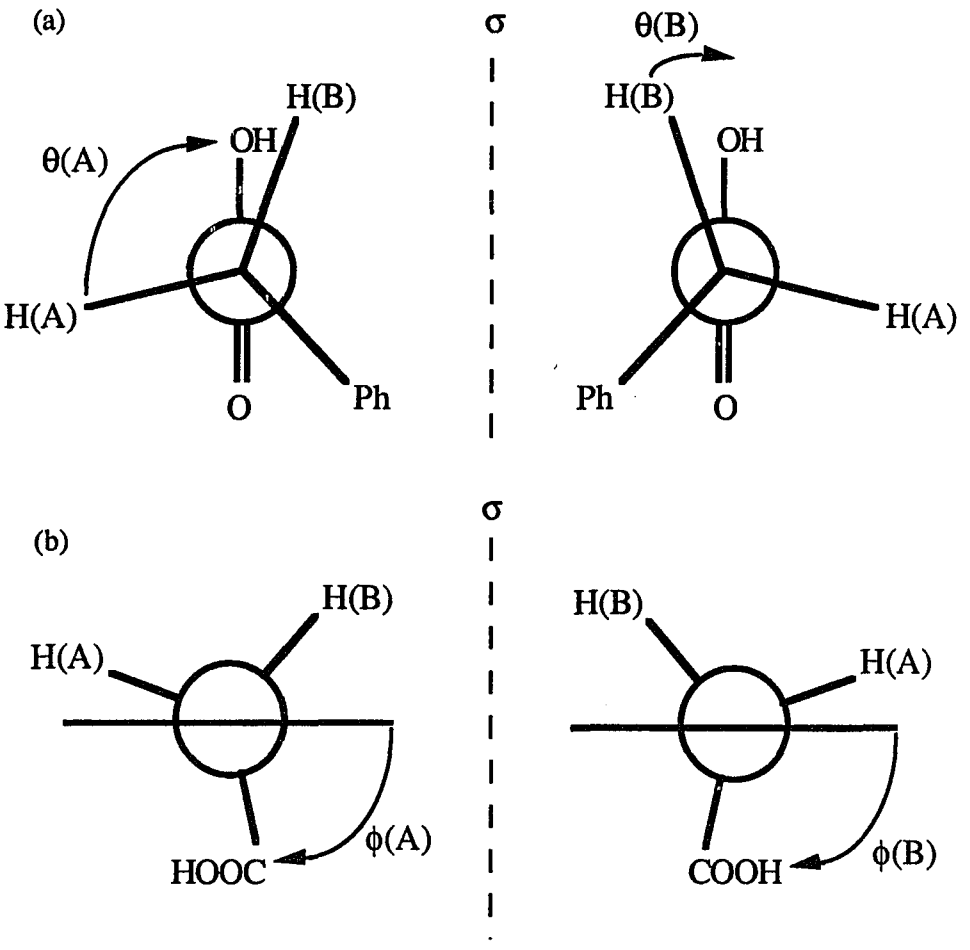

Figure 7.1. Newman projections for torsion angles (a) θ, ^{2}H–C_{alpha}–C_{acid}–OH, looking down the $C_{alpha}-C_{acid}$ bond, and (b) ϕ, C_{ortho}–C_{ring}–C_{alpha}–C_{acid}, looking down the C_{ring}–C_{alpha} bond. The horizontal bar in (b) indicates the phenyl ring. A mirror plane is denoted by σ.

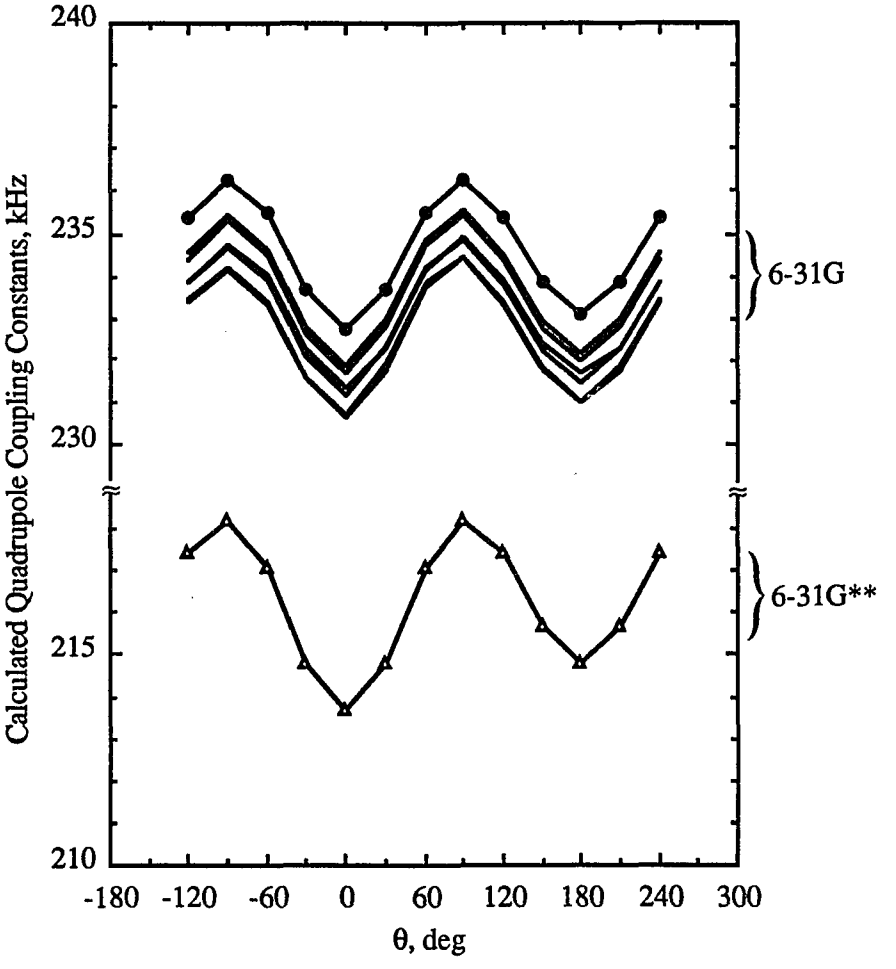

Figure 7.2. Calculated deuterium quadrupole coupling constants as a function of torsion angles θ at the 6–31G basis set level, for phenylacetic acid, – ; for acetic acid monomer, • ; and at the 6–31G** basis set level for acetic acid dimer, Δ. Torsion angle θ measured from hydroxyl oxygen: ^{2}H–C_{alpha}–C_{acid}–OH.

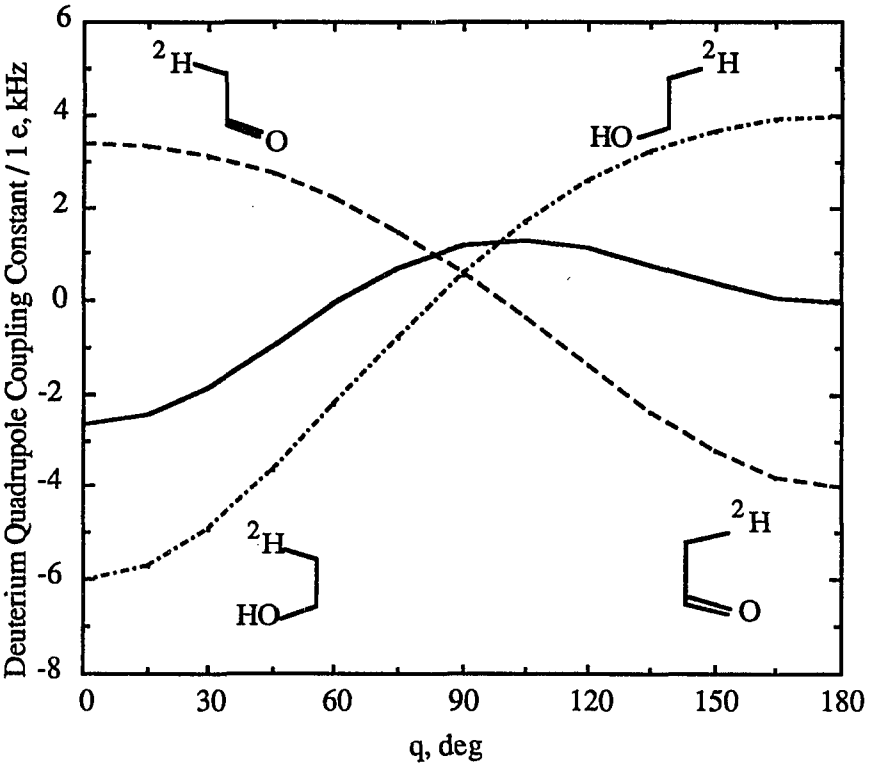

Figure 7.3. The effect on the deuterium quadrupole coupling constant due to partially shielded oxygen nuclei. Both the hydroxyl (– • –) and carbonyl (- - -) oxygen sites are modeled with a +1.0 e charge at the respective nuclear positions. The sum is shown by the solid trace. The effect on the deuterium quadrupole coupling constant is the projection of the electric field gradient from the point charge onto the C–^{2}H bond vector.

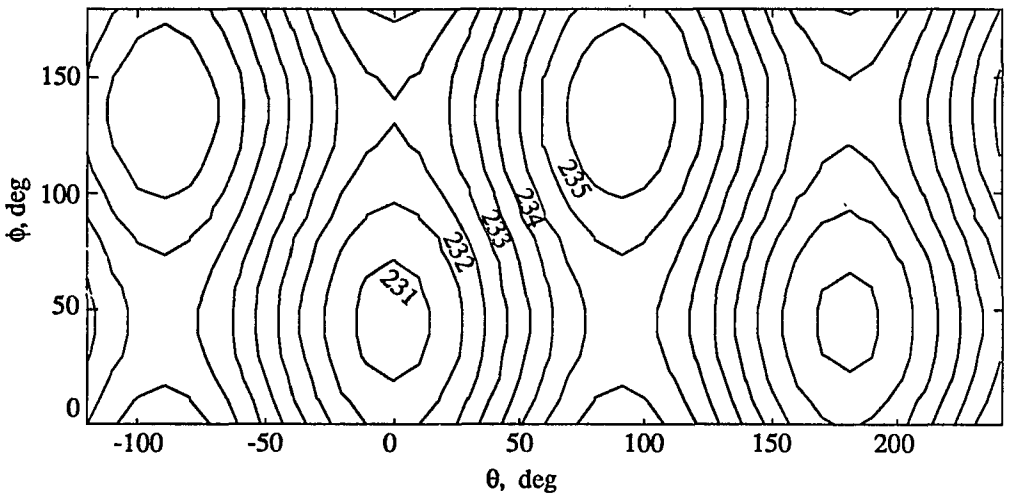

Figure 7.4. Contour plot, according to equation 7.8, of calculated deuterium quadrupole coupling constants of phenylacetic acid as a function of torsion angles θ and ϕ as determined from molecular orbital calculations at the 6–31G basis set level.

References

1. Hiyama, Y.; Roy, S.; Guo, K.; Butler, L. G.; Torchia, D. A. *J. Am. Chem. Soc.* **1987**, *109*, 2525-2526.
2. Boroske, E.; Mayas, L.; Möbius, K. *J. Magn. Reson.* **1979**, *35*, 231-246.
3. Weeding, T.; Kwiram, A. L.; Rawling, D. C.; Davidson, E. R. *J. Chem. Phys.* **1985**, *82*, 3516-3526.
4. Hartzell, C. J.; Kwiram, A. L. *J. Magn. Reson.* **1987**, *73*, 315-322.
5. Jarrett, W. L.; Guo, K.; Jackisch, M. A.; Butler, L. G. *J. Magn. Reson.* **1989**, *82*, 76-85.
6. Jackisch, M. A.; Fronczek, F.; Guo, K.; Jarrett, W. L., Jr.; Park, Y. H.; Stauffer, M. T.; Watkins, S. F.; Butler, L. G. *Macromolecules*, to be submitted.
7. Jackisch, M. A.; Jarrett, W. L.; Guo, K.; Fronczek, F. R.; Butler, L. G. *J. Am. Chem. Soc.* **1988**, *110*, 343-347.
8. (a) Karplus, M. *J. Chem. Phys.* **1959**, *30*, 11-15. (b) Colucci, W. J.; Gandour, R. D.; Mooberry, E. A. *J. Am. Chem. Soc.* **1986**, *108*, 7141-7147.
9. Brown, T. L.; Butler, L. G.; Curtin, D. Y.; Hiyama, Y.; Paul, I. C.; Wilson, R. G. *J. Am. Chem. Soc.* **1982**, *104*, 1172-1177.
10. Butler, L. G.; Brown, T. L. *J. Am. Chem. Soc.* **1981**, *103*, 6541-6549.
11. Jarrett, W. L.; Farlee, R. D.; Butler, L. G. *Inorg. Chem.* **1987**, *26*, 1381-1383.
12. (a) Spiess, H. W. *Adv. Polym. Sci.* **1985**, *66*, 23-58. (b) Jelinski, L. W. *Ann. Rev. Mater. Sci.* **1985**, *15*, 359-377. (c) Vold, R. R.; Brandes, R.; Tsang, P.; Kearns, D. R.; Vold, R. L., Rupprecht, A. *J. Am. Chem. Soc.* **1986**, *108*, 302-303 (d) Torchia, D. A. *Ann. Rev. Biophys. Bioeng.* **1984**, *13*, 125-144. (e) Frey, M. H.; DiVerdi, J. A.; Opella, S. J. *J. Am. Chem. Soc.* **1985**, *107*, 7311-7315. (f) Batchelder, L. S.; Niu, C. H.; Torchia, D. A. *J. Am. Chem. Soc.* **1983**, *105*, 2228–2231.

13. Barfield, M.; Gottlieb, H. P. W.; Doddrell, D. M. *J. Chem. Phys.* **1978**, *69*, 4504–4515.

14. Snyder, L. C. *J. Chem. Phys.* **1978**, *68*, 291-294.

15. Ando, I. and Webb, G. A. *Theory of NMR Parameters*; Academic: New York, 1983.

16. (a) Altbach, M. I.; Hiyama, Y.; Gerson, D. J.; Butler, L. G. *J. Am. Chem. Soc.* **1987**, *109*, 5529-5531. (b) Altbach, M. I.; Hubbard, J.; Morris, D.; Ellis, P. D.; Butler, L. G. *Organometallics* **1989** to be submitted.

17. *IUPAC-IUB Commission on Biochemical Nomenclature* in *J. Mol. Biol.* **1970**, *52*, 1-17.

18. GAUSSIAN 82 program was developed by Binkley, J. S.; Frisch, M. J.; DeFrees, D. J.; Raghavachari, K.; Whiteside, R. A.; Schlegel, H. B.; Fluder, E. M.; Pople, J. A. (Carnegie-Mellon University: Pittsburgh, PA, 1984).

19. 6–31G for Carbon and Oxygen: Hehre, W. J.; Ditchfield, R.; Pople, J. A. *J. Chem. Phys.* **1972**, *56*, 2257-2261. Polarization functions: Hariharan, P. C.; Pople, J. A. *Theor. Chim. Acta* **1973**, *28*, 213-222.

20. (a) Pross, A.; Radom, L. *J. Am. Chem. Soc.* **1978**, *100*, 6572-6575. (b) Nagaoka, S.–I.; Hirota, N.; Matsushita, T. Nishimoto, K. *Chem. Phys. Lett.* **1982**, *92*, 498–502.

21. (a) Abragam, A. *The Principles of Nuclear Magnetism*, Oxford: London, 1961, Chapter VII, p 232. (b) Cohen, M. H.; Reif, F. *Solid State Phys.* **1957**, *5*, 321-438.

22. Reid, R. V., Jr.; Vaida, M. L. *Phys. Rev. Lett.* **1975**, *34*, 1064. See also Reid, R. V., Jr.; Vaida, M. L. *Phys. Rev. A.* **1973**, *7*, 1841-1849.

23. (a) Kern, C. W.; Matcha, R. L. *J. Chem. Phys.* **1968** *49* 2081-2091. (b) Kim, H. W.; Hameka, H. F.; Zeroka, D. *J. Chem. Phys.* **1988**, *88*, 3159-3162.

24. Snyder, L. C. *J. Chem. Phys.* **1978**, *68*, 340-341.

25. Huber, H. *J. Chem. Phys.* **1985**, *83*, 4591-4598.

26. (a) McManus, S. P. and Pittman, Jr., C. U. *Bridged Carbonium Ions*; In *Organic Reactive Intermediates*; McManus, S. P., Ed.; Academic: New York, 1973; Chapter 4. (b) Barkhash, V. A. *Topics in. Curr. Chem.* **1984**, *116*, 1-265. (c) Simonetta, M.; Winstein, S. *J. Am. Chem. Soc.* **1954**, *76*, 18-21. (d) Olah, G. A.; Prakash, G. K. S.; Williams, R. E.; Field, L. D.; and Wade, K. *Hypercarbon Chemistry*; Wiley: New York, 1987.

CHAPTER EIGHT

Conclusions and Future Work

The deuterium quadrupole coupling constant, $e^2q_{zz}Q/h$, and asymmetry parameter, η, in different bonding environments were investigated. Different metal hydrogen bonding modes in transition metal hydride complexes have been represented by three models of alkali metal hydrides. Ab initio molecular orbital calculation results have shown that in terminal metal hydride systems, the metal core electrons effectively shielded the deuterium site from the metal nuclear charge. A lower limit for the deuterium quadrupole coupling constant in metal hydrides is 20 kHz. Also, the formation of bridging metal hydrides reduces the deuterium quadrupole coupling constant relative to the value found for terminal metal hydrides. In the case of dihydrogen addition, a rapid reduction of deuterium quadrupole coupling constant occurred as the H–H bond was being broken. For the deuterium at methyl group of acetic acid dimer, the deuterium quadrupole coupling constants changed as a function of the torsion angle about the carbon-carbon bond. The major source of the change in the deuterium quadrupole coupling constants with different molecular conformations is due to the nuclear charge at surrounding atoms. The electric field gradient tensors at the methyl hydrogen sites in acetic acid were obtained from ab initio molecular orbital calculations with the GAUSSIAN 82 program. Both the calculated quadrupole coupling constant and asymmetry parameter are fitted with a Karplus–type equation as a function of torsion angle. Adiabatic demagnetization in the laboratory frame spectroscopy at 77 K for substituted arylacetic acid showed that it is possible to detect inequivalent deuteron sites, on the basis of deuterium double transitions, even though two deuterium sites are bound to the same carbon atom. Single-crystal x-ray diffraction has been used to obtain the solid-state structure of arylacetic acids. A modified Karplus-type

relationship has been proposed to correlate the deuterium quadrupole coupling constants of substituted arylacetic acids with their solid-state structural features, that is, the torsion angles θ, ^2H–C_{alpha}–C_{acid}–OH, and ϕ, C_{ortho}–C_{ring}–C_{alpha}–C_{acid}.

To continue this work, the disubstituted arylacetic acid with two rings on the C_{alpha} position needs to be further investigated. Although the intermolecular interactions can be a source for the low values of the deuterium quadrupole coupling constant in some disubstituted arylacetic acids, the ADLF spectroscopic data of some other systems like ketones, aldehydes, or selected polymers in the polycrystalline state will be of great value. It is suggested that further investigation should include the effect of crystal packing forces, the possible phase changes at low temperature affecting the molecular crystal structure, and the intermolecular interactions with nearby molecules.

APPENDICES

Appendix 1 Program for the Energy Levels at Zero Field and the Transition Frequencies.

```
% HQ vs asymmetry parameter, according to Poole & Farach 2nd Ed.
% At zero field, Eo=-A; E±=(1/2)*A*(1±eta); where A=(1/2)e^2qQ
clg; clear
eta_axis = 0:0.01:1.0; % in Gauss
[m,X] = size(eta_axis);
e = 4.80325e-10;                    % in esu/e;
ao = 0.52917706e-8;                 % in cm/au
h = 6.626176e-27;                   % in erg-sec
qau = 0.25;                         % in atomic unit e/ao^3
% q = qau/(ao^3);                   % in e/cm3
Q = 2.86e-27;                       % in cm2
Factor = e^2*Q/(ao^3);              % in erg/au
% QCC = e^2*q*Q/(h*1000);           % in kHz
QCC = qau*Factor;                   % in erg
for n = 1:X
  Eo(n) = (-1/2)*QCC;
  Eplus(n) = (QCC/4)*(1+eta_axis(n));
  Eminus(n) = (QCC/4)*(1-eta_axis(n));
end
        Vo=(Eplus-Eminus)/(1e3*h);  % in kHz
        Vp=(Eplus-Eo)/(1e3*h);
        Vm=(Eminus-Eo)/(1e3*h);
subplot(211)
plot(eta_axis,Eo,'-',eta_axis,Eplus,'-',eta_axis,Eminus,'-')
%xlabel('Asymmetry Parameter')
%ylabel('Nuclear Quadrupole Energy Levels in erg');
plot(eta_axis,Vo,'-',eta_axis,Vp,'-',eta_axis,Vm,'-')
%xlabel('Asymmetry Parameter')
%ylabel('Transition Frequency in kHz');
```

Appendix 2 Program for the Energy Levels under Small Zeeman-Perturbation.

```
% HQ in small Zeeman perturbation, according to Poole & Farach 2nd Ed.
% At zero field, Eo=-A; E±=(1/2)*A*(1±eta);
% H0 applied magnetic field from z direction of PAS.
clg; clear
eta = 0.1;
H0_axis = 0:1:250;                          % in Gauss
[m,X] = size(H0_axis);
e = 4.80325e-10;                            % in esu/e;
ao = 0.52917715e-8;                         % in cm/au
h = 6.626176e-27;                           % in erg-sec
BetaN = 5.0505e-24;                         % nuclear Magneton in erg/Gauss
gN = 0.857387;                              % deuterium Lande factor
qau = 0.25;                                 % in atomic unit e/ao^3
q = qau/(ao^3);                             % in e/cm3
Q = 2.86e-27;                               % in cm2
Eo = zeros(1:X); Eplus = zeros(1:X); Eminus = zeros(1:X);
A = (1/2)*e^2*q*Q/(h*1000);                 % in kHz
K = (1/2)*A*eta;
for n = 1:X
 Eo(n) = -A;
 H_Zeeman = -H0_axis(n)*gN*BetaN/(h*10^3);  % in kHz
 Dev = sqrt(K^2 + H_Zeeman^2);
 Eplus(n) = A/2 + Dev;
 Eminus(n) = A/2 - Dev;
end
plot(H0_axis,Eo,'-',H0_axis,Eplus,'-',H0_axis,Eminus,'-')
%xlabel('Applied Field in Gauss')
%ylabel('Nuclear Quadrupole Energy levels in kHz');
```

Appendix 3 Program for the Transformation of Electric Field Gradient Tensor.

```
% EFG_tensor
% Program to diagonalize the calc traceless symmetric electric field gradient (efg) tensor
% from output of GAUSSIAN 82 molecular orbital calculation and print out
% the deuterium quadrupole coupling constant (QCC), asymmetry parameter (eta), and
% the angle between the C-D bond vector and the z axis of the efg tensor
% in principal axis system (PAS).
clear, clg, echo on;                    % input the Coords of C and D atom sites.
Csite = [0.0 0.0 0.0]';
Hasite = [0.0 0.0 1.079]';
Tstringa = ' For phenylacetic acid 6-31G basis set level, torsion angle theta=150';
Eqxxa =-0.497932; Eqyya =-0.699835; Eqzza = 1.197768;
Eqxya =-0.021750; Eqxza =-0.221490; Eqyza =-0.006985;
echo off                                % No more Input beyond this line;
Mat = [
Eqxx Eqxy Eqxz
Eqxy Eqyy Eqyz
Eqxz Eqyz Eqzz];
[Evct, Eval] = eig(Mat);                % diagonalize efg tensor to PAS
[e,m] = sort(abs(diag(Eval)));          % sort the absolute value of eqxx, eqyy, eqzz in PAS.
Evals = diag(Eval);                     % Evals is efg tensor components in PAS,
Evals = Evals(m)                        % sort in eqxx, eqyy, eqzz order.
eta = (Evals(1) – Evals(2))/Evals(3)    % eta is asymmetry parameter = (eqxx-eqyy)/eqzz.
QCC = -671.9994*Evals(3)                % print out the deuterium QCC in kHz.
Evcts = Evct(:,m)                       % sort the three PAS axes in Xpas, Ypas, Zpas order.
CHa = Hasite – Csite;
RCHa = sqrt(CHa'*CHa);
RZpas = sqrt(Evcts(:,3)'*Evcts(:,3));
PCHaZpas = CHa'*Evcts(:,3);
Sigma = (180/pi)*acos(PCHaZpas/(RCHa*RZpas))  % angle between C-D bond and eqzz
```

Appendix 4 Tree Chart for Zero-Field Cycling Program.

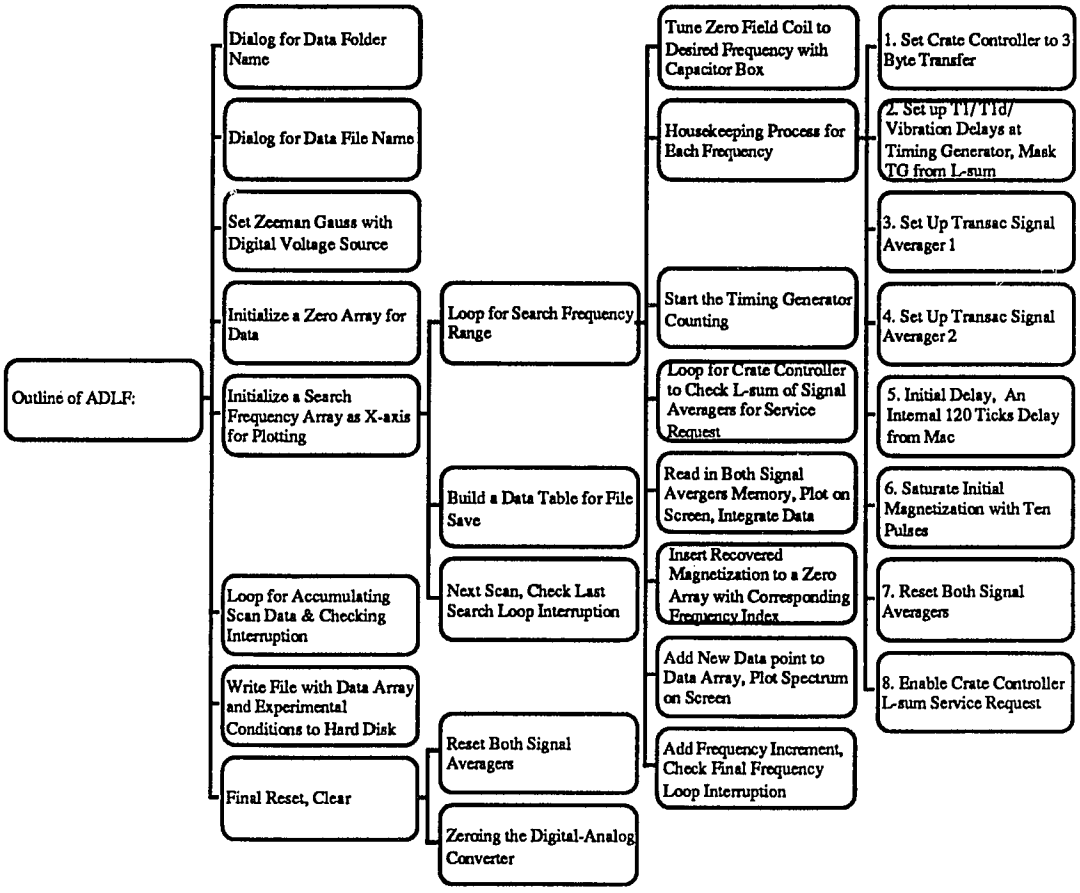

Appendix 5 Program for Fitting the Calculated QCC into a Karplus-type Equation.

```
% MatLab Program to Fit the calc QCC of HOAc Dimer into a Karplus-type Equation.
clear, clg, echo off, format short, Sm = 100;
Mat = [
  0      -0.317941      0.0393
 15      -0.318395      0.0406
 30      -0.319636      0.0437
 45      -0.321324      0.0472
 60      -0.322993      0.0502
 75      -0.324214      0.0521
 90      -0.324723      0.0527
105      -0.324467      0.0515
120      -0.323572      0.0486
135      -0.322295      0.0441
150      -0.320984      0.0389
165      -0.320007      0.0343
180      -0.319646      0.0324];   % Calculated eqzz of HOAc Dimer at 6-31G** level
The = Mat(:,1);                          % Torsion angle Ø
QCC = -671.9994*Mat(:,2);                % Convert eqzz to QCC
eta = Mat(:,3);                          % Asymmetry Parameter
[m n] = size(The);   ThetaR = (pi/180)*The;
Angle1 = cos(ThetaR);
Angle2 = cos(2*ThetaR);
Ang3 = zeros(m,3); ThetaQccQfitErr = zeros(m,4);
Ang3(:) = [ones(m,1) Angle1 Angle2];
Coeff = Ang3\QCC;
QCCfit = Ang3*Coeff;
dQCC = QCC-QCCfit;
S2Variance = (dQCC'*dQCC)/m^2            % Sample variance S2
ThetaQccQfitErr = [The QCC QCCfit dQCC]
TheSm = min(The):(max(The)-min(The))/(Sm-1):max(The);
ThetaRSm = (pi/180)*TheSm';
Angle1Sm = cos(ThetaRSm);
Angle2Sm = cos(2*ThetaRSm);
AngSm = zeros(Sm,3); QCCSm = zeros(Sm,1);
AngSm(:) = [ones(Sm,1) Angle1Sm Angle2Sm];
QCCSm = AngSm*Coeff;
plot(The,QCC,'+',TheSm,QCCSm);
```

Appendix 6 Program for Calculating the NQR Transitions of Dipolar Coupled Nuclei.

```
% DTQR_M
% This MatLab program adapted from Dr. Ragle's program to calculate
% intensities of allowed and forbidden NQR transitions for a
% pair of dipolar coupled nuclei, inputs are in following lines.
echo on, clear, clg, clc, format short,
vm1=125.5; vp1=126.5;                    % v-/v+ for site 1 in kHz
vm2=129.0; vp2=130.5;                    % v-/v+ for site 2 in kHz
qcc1 = (2/3)*(vp1+vm1); eta1 = (2/qcc1)*(vp1-vm1);
qcc2 = (2/3)*(vp2+vm2); eta2 = (2/qcc2)*(vp2-vm2);
EFG12 = [qcc1 eta1 qcc2 eta2],           % QCCs and etas for sites 1 & 2
R1=[3.389859  1.813886  0.880843]';      % coordinates of site 1
R2=[3.389859  1.813886 -0.880843]';      % coordinates of site 2
E1=[
-0.93538 -0.18422  0.30186
 0.31889 -0.80837  0.49481
 0.15286  0.55910  0.81489
]';                                      % Xpas/Ypas/Zpas for site 1
F2=[
 0.93538  0.18422  0.30186
 0.31889 -0.80837 -0.49481
 0.15286  0.55910 -0.81489
]';                                      % Xpas/Ypas/Zpas for site 2
echo off,                                % No more inputs beyond this line
i= sqrt(-1); h = 6.6261736e-27;          % in erg/Hz
gammaD = 0.41064e4;                      % H-2 gyromagnetic ratio in rad/gauss-sec
R = R2 - R1; R12 = sqrt(R'*R);           % internuclear separation in Å
R=R/R12;                                 % R as a unit vector from site 1 to site 2
S=zeros(1,3); Alpha=zeros(3,3); Beta=zeros(3,3);
H0=zeros(9,9)+i*zeros(9,9);
HD=H0; Hrfx1=H0; Hrfx2=H0; Hrfy1=H0; Hrfy2=H0; Hrfz1=H0; Hrfz2=H0;
E1 = orth(orth(orth(E1))); E2 = orth(orth(orth(E2))); m = [2 3 1];
E1 = E1(:,m); E2 = E2(:,m);              % Rearrange in X, Y, Z order
Alpha = E2'*E1;                          % Direct cos for PAS at site 2
for j = 1:3
  S(j) = E1(:,j)'*R;
end
for j = 1:3
 for k = 1:3
    if j==k, djk=1;
      else djk=0;
    end
    Beta(j,k) = 1.0*djk - 3.0*S(j)*S(k);
 end
end
DD = 2.84175/(R12^3);                    % (gammaD*h)^2/r^3
Beta = Beta.*DD;                         % Geometry of site 2 rel to z-axis at site 1
Gamma = Alpha*Beta;                      % Dipolar coupling matrix G
H0(3,3) = -(qcc1+qcc2)/2;                % unperturbed quadrupole energies in kHz
H0(9,9) = (1-eta1)*(qcc1/4) - (qcc2/2);  % Eoxz
```

```
H0(8,8) = (1-eta2)*(qcc2/4) - (qcc1/2);        % Eozx
H0(4,4) = (1+eta1)*(qcc1/4) - (qcc2/2);        % Eoyz
H0(5,5) = (1+eta2)*(qcc2/4) - (qcc1/2);        % Eozy
H0(1,1) = (1-eta1)*(qcc1/4) + (1-eta2)*(qcc2/4);     % Eoxx
H0(6,6) = (1-eta1)*(qcc1/4) + (1+eta2)*(qcc2/4);     % Eoxy
H0(7,7) = (1+eta1)*(qcc1/4) + (1-eta2)*(qcc2/4);     % Eoyx
H0(2,2) = (1+eta1)*(qcc1/4) + (1+eta2)*(qcc2/4);     % Eoyy
Eo = diag(H0);
Hrfx1(2,5)= 1; Hrfx1(3,4)= 1; Hrfx1(2,4)= 1;
Hrfx2(2,4)= 1; Hrfx2(3,5)= 1; Hrfx2(6,9)= 1;
Hrfy1(1,8)= -i; Hrfy1(3,9)= i; Hrfy1(5,6)= i;
Hrfy2(1,9)= -i; Hrfy2(3,8)= i; Hrfy2(4,7)= i;
Hrfz1(1,7)= 1; Hrfz1(2,6)= 1; Hrfz1(4,9)= i;
Hrfz2(1,6)= 1; Hrfz2(2,7)= 1; Hrfz2(5,8)= 1;
Hrfx1 = Hrfx1 + Hrfx1.'; Hrfx2 = Hrfx2 + Hrfx2.';
Hrfy1 = Hrfy1 + Hrfy1'; Hrfy2 = Hrfy2 + Hrfy2';
Hrfz1 = Hrfz1 + Hrfz1.'; Hrfz2 = Hrfz2 + Hrfz2.';
HD(1,2) = Gamma(3,3); HD(1,3) = -Gamma(2,2); HD(1,4) =-i*Gamma(2,3);
HD(1,5) =-i*Gamma(3,2); HD(2,3) = Gamma(1,1); HD(2,8) = Gamma(3,1);
HD(2,9) = Gamma(1,3); HD(3,6) = i*Gamma(1,2); HD(3,7) = i*Gamma(2,1);
HD(4,5) = Gamma(1,1); HD(4,6) = Gamma(1,3); HD(4,8) = i*Gamma(2,1);
HD(5,7) = Gamma(3,1); HD(5,9) = i*Gamma(1,2); HD(6,7) = Gamma(3,3);
HD(6,8) =-i*Gamma(3,2); HD(7,9) =-i*Gamma(2,3); HD(8,9) = Gamma(2,2);
HD = HD + HD'; % sum of upper array and its conjugate transpose
HT = H0 + HD - H0(3,3)*eye(9,9); % total Hamiltonian relative to lowest level
AR = real(HT); AI = imag(HT); % Zero-order Total Hamiltonian, in spin1 basis
[U,ET] = eig(HT);
[Energy,m] = sort(real(diag(ET)));U = U(:,m); U_conj = U';
Hrfx1 = U_conj*Hrfx1*U; Hrfy1 = U_conj*Hrfy1*U; Hrfz1 = U_conj*Hrfz1*U;
Hrfx2 = U_conj*Hrfx2*U; Hrfy2 = U_conj*Hrfy2*U; Hrfz2 = U_conj*Hrfz2*U;
CHrfx1=conj(Hrfx1).*Hrfx1; CHrfy1=conj(Hrfy1).*Hrfy1; CHrfz1=conj(Hrfz1).*Hrfz1;
CHrfx2=conj(Hrfx2).*Hrfx2; CHrfy2=conj(Hrfy2).*Hrfy2; CHrfz2=conj(Hrfz2).*Hrfz2;
Transition = zeros(3^2*(3^2-1)/2:4); m=0;
for j = 1:8
        for k = (j+1):9
        Freq(j,k) = Energy(k)-Energy(j);
        Ax1 = conj(Hrfx1(j,k)); Ay1 = conj(Hrfy1(j,k)); Az1=conj(Hrfz1(j,k));
        Ax2 = conj(Hrfx2(j,k)); Ay2 = conj(Hrfy2(j,k)); Az2=conj(Hrfz2(j,k));
A = CHrfx1(j,k)+CHrfy1(j,k)+CHrfz1(j,k)+CHrfx2(j,k)+CHrfy2(j,k)+CHrfz2(j,k);
B = Ax1*(Alpha(1,1)*Hrfx2(j,k)+Alpha(2,1)*Hrfy2(j,k)+Alpha(3,1)*Hrfz2(j,k));
C = Ay1*(Alpha(1,2)*Hrfx2(j,k)+Alpha(2,2)*Hrfy2(j,k)+Alpha(3,2)*Hrfz2(j,k));
D = Az1*(Alpha(1,3)*Hrfx2(j,k)+Alpha(2,3)*Hrfy2(j,k)+Alpha(3,3)*Hrfz2(j,k));
E = Ax2*(Alpha(1,1)*Hrfx1(j,k)+Alpha(1,2)*Hrfy1(j,k)+Alpha(1,3)*Hrfz1(j,k));
F = Ay2*(Alpha(2,2)*Hrfx1(j,k)+Alpha(2,2)*Hrfy1(j,k)+Alpha(2,3)*Hrfz1(j,k));
G = Az2*(Alpha(3,1)*Hrfx1(j,k)+Alpha(3,2)*Hrfy1(j,k)+Alpha(3,3)*Hrfz1(j,k));
        In(j,k) = real(A+B+C+D+E+F+G);
        m = m+1;
        Transition(m,:) = [j k Freq(j,k) In(j,k)];
        end
end
echo on % The following 4 columns are for j, k, Transition Freq(j,k) in kHz and Intensity
Transition
```

VITA

Kermin Guo was born in Taidon, Taiwan, Republic of China on July 25, 1956. He graduated from Hualien High School in Hualien, Taiwan in May of 1974. In October 1975 he enrolled in Fu-Jen Catholic University in Taipei, Taiwan, where he obtained his Bachelor of Science degree in Chemistry (June 1979). After graduation, he served in the ROC Army for 22 months. He came to the United States and began his graduate studies in August 1983. He obtained his Master of Science degree in Chemistry from Cleveland State University (December 1984) in Cleveland, Ohio. In January 1985, he entered the Ph.D program in Louisiana State University in Baton Rouge, Louisiana, where he worked for Dr. Leslie G. Butler.

He is a member of the American Chemical Society and Phi Lambda Upsilon, an honorary chemical society. He was elected and served as the Secretary of LSU's Chemistry Department Graduate Student Council for one year, and served as the Activities Coordinator of the Chinese Student Association in LSU for one year.

He married Yenping Fei Guo on June 1, 1985, and is presently, a candidate for the degree of Doctor of Philosophy at Louisiana State University. He will begin a postdoctoral research project in low temperature oxygen-17 NMR study with Professor Eric Oldfield at the University of Illinois at Urbana-Champaign in June, 1989.

DOCTORAL EXAMINATION AND DISSERTATION REPORT

Candidate: Kermin Guo

Major Field: Chemistry (Physical)

Title of Dissertation: Interpretation of the Solid-State Deuterium NMR Spectroscopy Parameters

Approved:

Major Professor and Chairman

Dean of the Graduate School

EXAMINING COMMITTEE:

Date of Examination:

April 24, 1989